THE ASTROPHYSICAL JOURNAL

An International Review of Spectroscopy and Astronomical Physics

FOUNDED IN 1895 BY GEORGE E. HALE AND JAMES E. KEELER

VOLUME 88

JULY–DECEMBER 1938

THE UNIVERSITY OF CHICAGO PRESS
CHICAGO, ILLINOIS

THE CAMBRIDGE UNIVERSITY PRESS, LONDON
THE MARUZEN COMPANY LIMITED, TOKYO
THE COMMERCIAL PRESS, LIMITED, SHANGHAI

PUBLISHED JULY, SEPTEMBER, OCTOBER, NOVEMBER, DECEMBER 1938

COMPOSED AND PRINTED BY THE UNIVERSITY OF CHICAGO PRESS
CHICAGO, ILLINOIS, U.S.A.

CONTENTS

NUMBER 1

PAGE

A PHOTOVISUAL INVESTIGATION OF THE BRIGHTNESS OF 59 AREAS ON THE MOON. Arthur L. Bennett 1

INVESTIGATIONS IN PROPER MOTIONS. Adriaan van Maanen 27

THE RADIAL VELOCITIES OF 600 STARS AND MEASURES OF 69 SPECTROSCOPIC BINARIES. William H. Christie and O. C. Wilson 34

PHYSICAL PROCESSES IN GASEOUS NEBULAE. III. THE BALMER DECREMENT. James G. Baker and Donald H. Menzel 52

A MULTIPLET CALIBRATION OF THE ARCTURUS SPECTRUM. Sidney G. Hacker 65

THE EXCITATION OF ABSORPTION LINES IN OUTER ATMOSPHERIC SHELLS OF STARS. O. Struve and K. Wurm 84

NOTE

A NEW FOURTH-MAGNITUDE ECLIPSING BINARY. W. W. Morgan and C. T. Elvey 110

REVIEWS 112

NUMBER 2

THE IMAGE-SLICER, A DEVICE FOR REDUCING LOSS OF LIGHT AT SLIT OF STELLAR SPECTROGRAPH. I. S. Bowen 113

FRAUNHOFER INTENSITIES IN THE INFRARED REGION λλ 8800–11830 A. C. W. Allen 125

THE THEORY OF CYCLICAL TRANSITIONS. L. G. Henyey 133

SODIUM IN THE UPPER ATMOSPHERE. J. Cabannes, J. Dufay, and J. Gauzit 164

ON THE INTENSITY DISTRIBUTION IN THE BANDS OF COMETARY SPECTRA. P. Swings and M. Nicolet 173

THE ANALYSIS OF THE INFRARED LIMIT OF ATMOSPHERIC TRANSMISSION. Arthur Adel and C. O. Lampland 182

FURTHER DETAIL IN THE ROCK-SALT PRISMATIC SOLAR SPECTRUM. Arthur Adel 186

NONRADIAL OSCILLATIONS OF STARS. C. L. Pekeris 189

NOTES PAGE

ORIGIN OF THE INFRARED TELLURIC ABSORPTION BAND q_2. Arthur Adel 200

A NEW SPECTRUM VARIABLE: 5 LACERTAE. J. A. Hynek 201

ERUPTIVE PROMINENCES AND IONOSPHERIC DISTURBANCES. R. G. Giovanelli 204

VARIABLE HYDROGEN EMISSION IN THE SPECTRUM OF γ URSAE MAJORIS. Ernest Cherrington, Jr. 205

REMARKS ON THE PAPER "THE SODIUM CONTENT OF THE HEAD OF THE GREAT DAYLIGHT COMET SKJELLERUP 1927K." Arthur Adel, V. M. Slipher, and R. Ladenburg 207

ERRATUM 208

NUMBER 3

THE GALACTIC STRUCTURE IN TAURUS. I. SURFACE DISTRIBUTION OF STARS. S. W. McCuskey 209

THE PRESENT SPECTRAL CHARACTERISTICS OF SIXTEEN OLD NOVAE. M. L. Humason 228

PROMINENCE STUDIES. Robert R. McMath and Edison Pettit 244

LINES OF IONIZED BARIUM IN STELLAR SPECTRA. Cora G. Burwell . . . 278

THE ABSOLUTE PHOTOGRAPHIC MAGNITUDE OF SUPERNOVAE. W. Baade . 285

A PHOTOELECTRIC LIGHT-CURVE OF EROS. F. E. Roach and Laurence G. Stoddard 305

PHYSICAL PROCESSES IN GASEOUS NEBULAE. IV. THE MECHANISTIC AND EQUILIBRIUM TREATMENT OF NEBULAR STATISTICS. Donald H. Menzel, Lawrence H. Aller, and James G. Baker 313

A RELATIONSHIP BETWEEN COLOR, SPECTRUM, AND ABSOLUTE MAGNITUDE FOR G-TYPE STARS. John S. Hall 319

SOME CHARACTERISTICS OF ASSOCIATED GALAXIES. I. A DENSITY RESTRICTION IN THE METAGALAXY. E. F. Carpenter 344

NOTES

THE SPECTROSCOPIC TRIPLE STAR 59 d SERPENTIS. Dean B. McLaughlin 356

A NOTE ON THE SPECTRUM AND RADIAL VELOCITY OF γ PERSEI. Dean B. McLaughlin 358

DIMENSIONS OF THE SOLAR GRANULES. Philip C. Keenan 360

EMISSION NEBULOSITIES IN CYGNUS AND CEPHEUS. Otto Struve and C. T. Elvey 364

REVIEWS 369

NUMBER 4

PAGE

THE MATHEMATICAL CHARACTERISTICS OF SUNSPOT VARIATIONS. John Q. Stewart and H. A. A. Panofsky 385

RADIAL VELOCITY-CURVE OF THE RR LYRAE VARIABLE W CANUM VENATICORUM. Alfred H. Joy 408

PHOTOGRAPHIC LIGHT-CURVES OF THE TWO SUPERNOVAE IN IC 4182 AND NGC 1003. W. Baade and F. Zwicky 411

PHYSICAL PROCESSES IN GASEOUS NEBULAE. V. ELECTRON TEMPERATURES. James G. Baker, Donald H. Menzel, and Lawrence H. Aller . 422

THE MAGNITUDE OF THE SUN, THE STELLAR TEMPERATURE SCALE, AND BOLOMETRIC CORRECTIONS. G. P. Kuiper 429

THE EMPIRICAL MASS-LUMINOSITY RELATION. G. P. Kuiper 472

TABLES FACILITATING THE CALCULATION OF LINE ABSORPTION COEFFICIENTS. F. Hjerting 508

ON THE INTEGRATION OF THE EQUATION OF RADIATIVE TRANSFER. P. Swings and L. Dor 516

NOTES

ON COLLAPSED NEUTRON STARS. F. Zwicky 522

SPECTRAL TYPES AND RADIOMETRIC OBSERVATIONS OF STARS OF LARGE INFRARED INDEX. Carl F. Rust 525

A METHOD FOR THE DETECTION OF SMALL OBJECTS HAVING EMISSION SPECTRA. Carl K. Seyfert 527

ERRATUM 528

NUMBER 5

ON THE FREQUENCY OF SUPERNOVAE. F. Zwicky 529

A SIMPLIFIED SPECTROHELIOSCOPE. G. A. Mitchell 542

LIMITING MAGNITUDES. Frank E. Ross 548

THE THEORY OF THE COLORS OF REFLECTION NEBULAE. L. G. Henyey and Jesse L. Greenstein 580

THE TEMPERATURES OF THE EXTRAGALACTIC NEBULAE AND THE RED-SHIFT CORRECTION. Jesse L. Greenstein 605

Fe III LINES IN STELLAR SPECTRA. P. Swings and B. Edlén 618

NOTES

RECENT CHANGES IN THE SPECTRUM OF PLEIONE. Dean B. McLaughlin 622

SOME CHANGES IN THE SPECTRA OF THE PLEIADES. Orren Mohler . 623

REVIEWS 624

INDEX 628

THE ASTROPHYSICAL JOURNAL

AN INTERNATIONAL REVIEW OF SPECTROSCOPY AND ASTRONOMICAL PHYSICS

VOLUME 88 JULY 1938 NUMBER 1

A PHOTOVISUAL INVESTIGATION OF THE BRIGHTNESS OF 59 AREAS ON THE MOON[1]

ARTHUR L. BENNETT

ABSTRACT

The brightness, on a uniform scale, of 59 areas on the surface of the moon, at eleven phase angles, was determined photovisually from plates taken at the Lowell Observatory. It was found that the variation of brightness is similar for all the areas and depends strongly on the angle of reflection as well as on the azimuth between the incident and the reflected rays. On the assumptions that the surface is pitted with spheroidal cups whose contribution to the brightness is proportional to the projected area of the visible illuminated surface, and that the surface between the cups is plane and that its brightness follows Lambert's law, it is possible to represent the observed variation for small angles of reflection. When the angle of reflection is great, the computed brightness is a maximum for normal incidence and not at full moon, as observed. There is, however, a large dependence of the brightness on the azimuth.

Early in 1928, when the author was research assistant at the Lowell Observatory, it was decided to undertake an investigation of the brightness of a number of regions on the moon's surface. During the spring of that year the technique was developed and the required apparatus constructed. By June the observational difficulties had been overcome, and about eighty photographs of the moon were taken during the lunation of June–July. The measurement of the plates was begun in Flagstaff but was completed the following summer at Princeton with the same densitometer.

[1] A dissertation presented to the faculty of Princeton University in candidacy for the degree of Doctor of Philosophy in 1932. It was originally planned that this should be published as a bulletin of the Lowell Observatory. It has now been agreed to present it here in somewhat condensed form.

METHOD

The method of photographic photometry employed in this work was based on the following principle. If two beams of light of the same wave length, acting on the plate for equal exposure times, give the same density, then the two beams are of equal intensity. This avoids all assumptions concerning the characteristics of the photographic plate, except only that the sensitivity and development are uniform over the plate.[2] Immediately after the moon was photographed, each plate was calibrated by exposing it to a wide range of intensities given by an optical wedge illuminated by a standard lamp. To determine the relative intensities of two areas on the moon, the two places on the wedge image having the same densities as the areas were found. The difference in distance of these places from the index at the end of the wedge image was then a measure of the relative intensities.

TELESCOPE AND CAMERA

The telescope used was the 24-inch Clark refractor, of 386 inches focal length. The aperture was reduced to 3 inches in order to make the exposure time long enough for accurate timing.

A double-slide camera equipped with a metal plateholder, taking a plate 5×7 inches, was available. A Graflex focal-plane shutter, for which an electric control was devised, was built into the camera. The shutter was adjusted so that it opened and closed rapidly, but without jarring the telescope. The timing was controlled from a seconds pendulum; a key was pressed to open the shutter, which then remained open for an integral number of seconds until the circuit was again closed. The yellow filter for adapting the telescope to photovisual work fitted into a slot in the camera about 4 cm from the plate. The range of wave length transmitted by the Wallace "C" filter was determined by taking a number of spectrograms of both the moon and the standard lamp; the same Iso Medium plates that were used for the moon photographs were employed. Dr. V. M. Slipher very kindly determined the effective transmission to be from about λ 4830 to λ 5900.

[2] Dobson, Griffith, and Harrison, *Photographic Photometry*, Oxford, 1926.

STANDARDIZATION OF THE PLATES

For the standardization of the plates a wooden box, shaped like a horizontal V, was built, each arm being 5 × 7 inches inside and about 30 inches long. Near the end of one of the arms the standard lamp, a gas-filled 6-volt, 36-watt lamp having a small coiled filament was mounted. Two pairs of leads were soldered to the base, one for the current supply and the other for the voltmeter. The lamp was seasoned before use and was operated at 5.6 volts to prolong its life and to prevent rapid blackening of the inside of the bulb. Near the lamp was a diaphragm with an aperture over which could be placed one of several Eastman neutral-tint optical filters, in order to make the range of intensities given by the wedge correspond to that of the moon's image. On the opposite side of the diaphragm an electrically controlled shutter was mounted, and near by was a slide for the same yellow filter used at the telescope. The flat bottom of the V was covered with a sheet of white blotting paper, serving as a diffuse reflector; except for this, the interior of the box was coated with flat black paint. The optical wedge was mounted on the outside of the other end of the V, so that the plateholder could be slipped into place, bringing the emulsion almost into contact with the wedge. Just beyond the dense end of the wedge a thin strip of brass was mounted in contact with the photographic plate, giving a sharp line at the end of the wedge image to serve as an index. Tests made with the wedge removed showed that the illumination over the area it normally covered was very uniform. An Eastman neutral tint optical wedge 1 cm wide and 10 cm long, varying in density from 0 to 2, was used, which gave an available range in intensity of somewhat less than 100 to 1.

DEVELOPMENT

For the development of the plates a deep wooden tray was constructed. The bottom was made of a sheet of plate glass on which strips of glass of the same thickness as the plates to be developed were arranged. This left a recess in which the plate fitted quite closely, bringing the emulsion flush with the surface surrounding it. During the development, the plate was steadily stroked with a wide, soft, camel's-hair brush. The developer used was sodium

paramidophenolate,[3] similar to Rodinal, which, in four minutes at 60° F., gave a contrast small enough that the whole range of intensities given by the optical wedge could be measured without having the maximum density inconveniently great.

All the plates were backed with a mixture of lampblack in caramel, thus preventing any halation. They were fixed in an acid fixing-bath. The washing was much prolonged, usually eight hours, to remove the last traces of the dye with which the plates were sensitized. They were dried in a cabinet equipped with an electric fan.

MEASUREMENT

The densitometer used for the measurement of the plates was designed by Fabry and Buisson and constructed by Jobin in Paris. It is similar to the Hartmann type but is superior to the former in that the Maxwellian view[4] is employed. With this system the appearance of the grain of the plate is eliminated and the brightness of two uniform surfaces is equalized. An Eastman wedge (density 0–2) was used in the instrument. The setting of the wedge was read to 0.1 mm. Ordinarily two settings, one in each direction, were taken unless they differed by more than 0.4 mm, in which case two more were added. The area of the plate measured was circular, 0.2 mm in diameter, equivalent to 4.5 seconds of arc or 5.2 miles at the center of the moon at mean distance.

THE WEDGE CONSTANT

The "wedge constant" is defined as the logarithm of the ratio of the intensities of the light transmitted by the optical wedge at two points separated by 1 mm. Although the wedge was calibrated by the manufacturer, it was necessary to determine the constant under the conditions of use. An optical bench was used to vary the intensity of a second standard lamp for comparison with the range of intensities given by the calibration wedge. All possible precautions were taken to avoid systematic errors. An image of the wedge was impressed on each end of a plate, and then six exposures were made at each of nine positions on the bench. Densitometer readings were

[3] Neblette, *Photography*, p. 312, New York, 1926.

[4] Walsh, *Photometry*, p. 109, London, 1926.

taken at 5-mm intervals along the wedge image, starting from the index. Plotting these readings against the distance from the index, y, a characteristic curve of the plate (on an arbitrary scale) was obtained. The mean photometer reading for the six exposures at one bench setting then gave, by means of this curve, the y corresponding to the intensity at that bench position, y_n.

The bench stops were numbered from 1 to 9 in order of increasing distance from the source, or of decreasing intensity, the spacing being such that

$$\frac{I_n}{I_{n+1}} = 1.585\,, \qquad \log \frac{I_n}{I_{n+1}} = 0.2\,,$$

where I_n is the intensity at position n.

The wedge constant, K, is, by definition,

$$K = \frac{\log \dfrac{I_2}{I_1}}{y_2 - y_1}\,.$$

Hence, if it is constant, K can be obtained from

$$n = -5Ky_n + C\,.$$

Table 1 contains the measures of the two plates, 275 and 276. In the first four columns are given: the bench position, the ratio of intensity to that at position 9, and the y for each of the plates. The bench position, n, was plotted against the values of y_n for the two plates. The points, with the exception of two end ones, fall satisfactorily along a straight line. The value of y read from this line is given in column "y_c," Table 1, and the residuals of the observed values from this line are in the succeeding columns. The points of large deviation are entitled to less weight, owing to the fact that they fall on the toe or shoulder of the characteristic curve. Furthermore, the manufacturer's calibration curve showed no indication of curvature, nor could it be detected in supplementary examinations of the wedge in the densitometer. The straight line, signifying a constant value of K along the wedge, was consequently adopted. The value of K derived was 0.0196, whereas that given by the manufacturer's calibration was 0.0202.

THE LUNAR PLATES

The data concerning the eleven lunar plates measured are given in Table 2. The columns contain: the number of the plate, the Greenwich Civil Time of mid-exposure, the exposure time, the zenith distance, the phase angle corrected for parallax, and the selenographic latitude and longitude of the observer.

TABLE 1

n	I_n/I_9	y_n		y_c	$y-y_c$	
		275	276		275	276
1	39.8	88.3	91.1	87.8	+0.5	+3.3
2	25.1	77.1	78.8	77.6	−0.5	+1.2
3	15.8	66.7	66.5	67.4	−0.7	−0.9
4	10.0	57.9	56.1	57.1	+0.8	−1.0
5	6.31	47.9	46.0	46.9	+1.0	−0.9
6	3.98	37.5	36.3	36.7	+0.8	−0.4
7	2.51	26.1	26.0	26.4	−0.3	−0.4
8	1.58	16.3	15.8	16.2	+0.1	−0.4
9	1.00	7.3	5.5	6.0	+1.3	−0.5

TABLE 2

Plate	G.C.T., 1928	E	z	g	λ'_E	β'_E
a 188	June $23^d\ 5^h15^m21^s$	14^s	69°.6	−109°.0	+7°.8	−6°.7
b 196	25 4 15 6	14	48.4	− 86.6	+6.4	−5.8
c 201	26 4 31 50	12	48.8	− 76.4	+5.3	−4.9
d 211	28 4 42 52	12	50.3	− 53.7	+2.5	−2.5
e 219	30 5 01 41	12	56.2	− 32.1	−0.6	+0.3
f 228	July 2 7 0 55	12	60.6	− 9.7	−3.2	+3.3
g 231	3 7 0 46	6	61.6	+ 4.1	−4.4	+4.6
h 246	5 9 41 47	12	57.5	+ 25.8	−5.6	+6.7
i 252	7 9 18 2	12	55.5	+ 50.0	−6.3	+7.3
j 261	9 10 49 40	14	45.9	+ 75.6	−5.6	+6.6
k 268	12 10 39 10	20	61.7	+114.3	−3.4	+2.9

The selenographic longitudes and latitudes of the earth (λ_E, β_E) and sun ($\lambda_\odot$, $\beta_\odot$) were interpolated from the American Ephemeris. The values for the earth were corrected for parallax as follows:

$$\Delta\lambda_E = \frac{\pi \sin z}{\cos \beta_E} \sin (q + C), \qquad \Delta\beta_E = \pi \sin z \cos (q + C),$$

$$\lambda'_E = \lambda_E + \Delta\lambda_E, \qquad \beta'_E = \beta_E + \Delta\beta_E,$$

where q is the parallactic angle given by

$$\sin q = \frac{\sin t \cos \phi}{\sin z}$$

and C is the position angle of the moon's axis, interpolated from the American Ephemeris.

The phase angle, g, corrected for parallax, was then determined from

$$\cos g = \sin \beta'_E \sin \beta_\odot + \cos \beta'_E \cos \beta_\odot \cos (\lambda_\odot - \lambda'_E) .$$

MEASUREMENT AND REDUCTION

The measurement of the lunar plates was carried out in a manner similar to that for the determination of the wedge constant. Photometer readings were taken at 2-mm intervals along each of the two wedge images on a plate, and were plotted together against y. From this characteristic curve any photometer setting on the image of the moon could then be reduced to a value of y, and thence to an intensity, by the equation

$$\log I = Ky + \text{const} ,$$

or by a corresponding table.

"Brightness" is defined as luminous intensity per unit area. This scale of relative intensity is, therefore, a scale of relative brightness, inasmuch as the area of the image measured on the densitometer was constant.

In order to combine the measures on the different plates, it was necessary to transform the relative scale for each plate to one uniform scale of brightness. The mean surface brightness of each lunar image, $\bar{B}$, was determined from the average of a large number of readings at regular intervals over the whole of the illuminated portion of the moon. On the plate nearest full moon the brightness of 643 areas was determined, at 3-mm intervals in each co-ordinate. In order to compensate for the greater range and irregularity in brightness of the images of greatest phase angle, the spacing was decreased to 2 mm in one co-ordinate and 1 mm in the other, so that the number of areas was increased to more than one thousand.

The plates taken at large phase angles were underexposed along the terminator because the exposure time was adjusted to keep the density of the brightest areas within measurable limits. Large charts, $\frac{1}{5}$ inch to 1 mm on the plate, were constructed, and the limb was plotted from numerous settings taken during the measurement of the plates. The position of the terminator was computed, and, when it had been drawn in, the brightness of the unmeasurable portion was estimated. The possible error thus introduced was well

TABLE 3

Plate	g	$\bar{h}$	$\bar{B}$	F	E	FE	Filter (Per Cent)
a.....	−109.0	15.8	14.3	1.10	1.28	1.41	25
b.....	− 86.6	24.6	26.1	0.943	1.07	1.01	25
c.....	− 76.4	29.3	30.7	0.954	1.07	1.02	25
d.....	− 53.7	40.8	22.4	1.82	1.07	1.95	50
e.....	− 32.1	55.9	30.0	1.86	1.11	2.03	50
f.....	− 9.7	82.9	48.0	1.73	1.14	1.97	50
g.....	+ 4.1	92.7	28.5	3.25	1.16	3.77	100
h.....	+ 25.8	59.2	34.1	1.74	1.12	1.95	50
i.....	+ 50.0	36.3	20.9	1.74	1.11	1.93	50
j.....	+ 75.6	24.7	13.4	1.84	1.06	1.95	50
k.....	+114.3	14.0	9.08	1.54	1.16	1.79	50

under 1 per cent for all of the plates except the first and the last, for which it may amount to somewhat more.

The visual mean surface brightness is given by Russell[5] in magnitudes for 10° intervals of phase angle. These data were converted to a scale of brightness such that the full moon had the value 100, and were plotted against the phase angle. The visual mean surface brightness, $\bar{h}$, at the phase angle of each of the plates was read from the curve. The ratio of $\bar{h}$ to $\bar{B}$ for each plate was called F. Each measurement on a plate was then multiplied by the factor F for that plate and was thus converted into the uniform scale for all the plates.

Table 3 gives for each plate: the phase angle, g; the mean brightness read from the phase curve, $\bar{h}$; the mean brightness on the arbitrary scale, $\bar{B}$; the factor, F; the extinction correction, E (taken

[5] *Ap. J.*, **43**, 114, 1916.

PLATE I

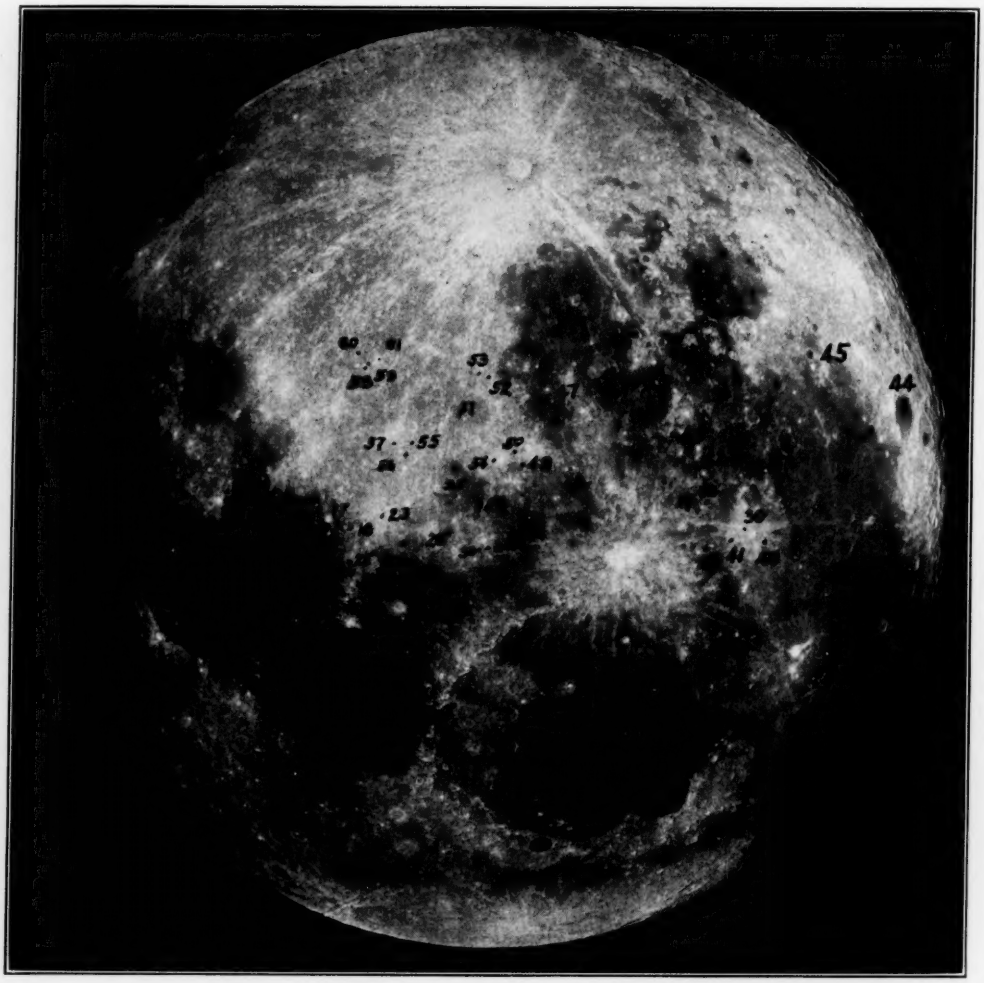

THE LOCATION OF THE AREAS MEASURED

from the table given by Müller for Santis[6]); the product *FE;* and the approximate transmission of the neutral filter used at the standard lamp.

The constancy of the values of *FE* is a check on the accuracy of the method of reducing the plates to a uniform scale, assuming that the light of the standard lamp and the transparency of the atmosphere remained constant. The transmission of the neutral filters was not determined under the conditions of use; consequently, only the plates calibrated with the same filter are directly comparable. The large deviation of *FE* for plate *a* remains unaccounted for, but the low value for plate *k* was due to a slightly hazy sky. It should be noted that these deviations do not affect the result, but rather indicate what errors might have been incurred if the zero-point of each plate had not been established by the method used.

THE LUNAR AREAS

The areas on the surface of the moon chosen for investigation were, for the most part, apparently smooth and free from large irregularities. The second qualification was that they should be easily identified under all conditions of illumination. This requirement was best satisfied by locating the area relative to near-by small craters. The selection was made by reference to the map and the description of the surface given by Neison.[7] Plate I indicates the location of the areas. They were classified under general types according to the nature of the surface, as follows:

Maria: 2, 3, 4, 5, 11, 15, 19, 20, 21, 22, 29, 30, 32, 35, 35A, 36, 42, 43, 47, 48
Dark crater floors: 1, 6, 8, 9, 12, 24, 25, 26, 27, 44, 45, 46
Highlands:[8] 16, 17, 18, 23, 28, 33, 34, 49, 50, 51, 53, 54, 55, 56, 57, 58, 59, 60
Rays: 7, 37, 38 Nimbi: 39, 40, 41 Miscellaneous: 52, 61

THE INDEPENDENT VARIABLES

The brightness of a diffusely reflecting surface can be expressed as a function of the reflecting power, the angle of incidence, the angle of emission, and the azimuth. The last is the angle between the planes

[6] *Photometrie der Gestirne*, p. 515, Leipzig, 1897.

[7] *The Moon*, London, 1876.

[8] It should be noted that the classification "highlands" usually denotes relatively smooth surfaces in a generally mountainous portion of the moon.

through the normal and the incident ray, and through the normal and the emergent ray. These angles were computed in the manner outlined in the following paragraphs.

When the specific areas were measured on the densitometer, the carriage scales were read, making it possible to plot the areas on the large charts already referred to. With the exception of the plates too near full moon, the image was oriented by means of the "horns," so that the line joining them was parallel to one motion and the illumination equator parallel to the other. For the remaining plates the selenographic co-ordinates of a number of the specific regions were taken from Neison, and the position of the illumination equator was computed relative to these.

For the plates oriented by means of the horns, a simple translation gave the positions of the areas in rectangular co-ordinates with the center of the moon as origin and the positive x-axis in the direction of the sun. For the other plates the transformation was made graphically, the co-ordinates being read from the charts.

Let Q' be a point on the photograph or chart representing the point Q on the moon at a distance r from the center. Then

$$r = \sqrt{x^2 + y^2}, \qquad \sin \theta = \frac{y}{r},$$

where θ is the angle between x and r.

In the plane triangle formed by the observer O, the moon's center C', and the observed point Q, the angle of emission, ϵ, is the external angle at Q, while r is the internal angle at O. Hence $(\sin \epsilon)/(\sin r) = OC'/QC'$. But $QC' = OC' \sin R$, where R is the moon's apparent radius (which was found from the charts). To a sufficient degree of approximation, therefore,

$$\sin \epsilon = \frac{r}{R}.$$

Consider, now, the spherical triangle on the moon's surface formed by the apparent center C, the subsolar point S, and the point Q. The side QC equals the angle of emission, ϵ; QS is the angle of incidence, ι; and CS is the phase angle, g. The angle SCQ is the same

as θ, defined above, while SQC is the azimuth, A, of the emitted rays. It follows that

$$\cos \iota = \cos \epsilon \cos g + \sin \epsilon \sin g \cos \theta$$

$$\sin A = \frac{\sin \theta \sin g}{\sin \iota}.$$

THE OBSERVATIONS

The observed brightness and the computed values of the variables on which it depends are brought together for each area in Table 4. The columns contain, in order, the number of the area and the interpolated brightness at full moon, the letter designating the plate, the angle of emission, the angle of incidence, the azimuth, and the ratio (times 100) of each observed brightness to the brightness at full moon.

DISCUSSION OF THE DATA

The first step in the examination of the results was to plot the brightness of each of the areas against the phase angle at which the observation was made. Several illustrative examples are given in Figure 1. The phase-curve for the mean brightness of area 4, on Mare Crisium near the west limb of the moon, rises slowly to maximum near full moon and then drops very rapidly. Conversely, the brightness of area 45, Billy, near the east limb, rises abruptly to a maximum near full and then falls gradually. The curve for area 35A, Sinus Medii, is much more symmetrical, as would be expected from its central location on the moon. These curves show well the striking phenomenon, already pointed out by Wirtz[9] and Barabascheff,[10] that each of the elements of the lunar surface has its maximum brightness very near the time of full moon.

It is noteworthy that the curves for area 4 before full moon and for area 45 afterward follow the slope of the mean phase-curve rather closely at distances greater than 40° or 50° from full moon. When the parts of these curves opposite full moon are examined, it is seen that the slope is fully as steep as that of the mean curve very close to full moon. The slope of the curve for area 35A is of an intermediate value. If the ordinates of these three curves are combined,

[9] *A.N.*, **201**, p. 289, 1915.

[10] *Ibid.*, **217**, p. 445, 1922.

TABLE 4

Area/h_0	Plate	ϵ	ι	A	h/h_0	Area/h_0	Plate	ϵ	ι	A	h/h_0
1	a	59°	52°	163°	24	7	a	45°	71°	147°	18
71	b	60	29	156	39	140	b	46	49	139	40
	c	59	19	123	46		c	46	39	133	45
	d	62	10	36	53		d	47	18	96	70
	e	64	32	6	76		e	48	21	31	85
	f	67	58	4	93		f	50	42	8	96
	g	67	70	4	86		g	50	53	4	96
							h	51	77	3	32
2	a	52	78	156	22						
68	b	52	40	144	43	8	a	47	71	142	17
	c	52	30	137	46	92	b	48	50	131	38
	d	54	12	90	58		c	48	41	125	47
	e	55	25	18	75		d	49	22	90	66
	f	58	51	6	93		e	49	23	36	87
	g	58	61	4	87		f	51	44	9	96
	h	59	85	1	12		g	51	54	3	100
							h	52	77	6	10
3	a	52	78	152	23						
73	b	53	41	140	40	9	a	38	81	137	8
	c	53	32	132	48	66	b	38	59	130	27
	d	55	15	81	61		c	38	49	126	36
	e	55	26	22	76		d	39	27	107	53
	f	58	50	7	92		e	39	18	56	74
	g	58	61	3	89		f	41	34	11	92
	h	59	85	3	13		g	41	44	4	94
							h	42	67	6	43
4	a	52	78	151	23						
68	b	53	42	138	38	11	b	36	65	125	20
	c	53	33	129	47	54	c	36	54	120	31
	d	54	17	83	59		d	36	32	105	46
	e	55	27	23	77		e	36	20	65	65
	f	58	50	7	92		f	36	33	13	92
	g	58	61	3	89		h	38	63	8	41
	h	59	85	3	14		i	37	86	16	10
5	a	65	50	151	30	12	a	41	85	127	5
62	b	66	29	132	43	62	b	41	65	118	24
	c	66	22	115	52		c	40	56	112	35
	d	69	22	42	57		d	40	35	95	52
	e	69	38	14	83		e	40	25	56	71
	f	71	63	6	95		f	40	35	14	91
	g	71	74	3	87		g	40	43	3	96
							h	40	64	12	44
6	a	39	75	148	15		i	40	86	21	10
68	b	40	52	143	28						
	c	40	43	140	38	15	b	18	72	146	14
	d	41	20	121	52	61	c	18	61	150	26
	e	42	15	39	75		d	19	35	157	43
	f	44	37	8	93		e	21	11	159	69
	g	45	48	4	90		f	24	14	11	90
	h	46	72	2	36		g	25	27	8	93
							h	27	52	7	52
							i	26	76	9	16

TABLE 4—*Continued*

Area/h_0	Plate	ϵ	ι	A	h/h_0	Area/h_0	Plate	ϵ	ι	A	h/h_0
16	b	15°	75°	141°	13	22	b	31°	65°	132°	21
72	c	15	64	144	26	61	c	30	55	129	31
	d	16	38	155	44		d	31	30	123	47
	e	18	15	162	70		e	32	14	80	68
	f	22	13	12	91		f	33	26	15	89
	g	22	24	9	97		g	34	37	5	96
	h	24	49	8	58		h	35	60	4	47
	i	23	73	11	21		i	34	84	8	10
17	b	14	76	139	12	23	b	10	82	121	10
84	c	14	65	143	24	125	c	9	71	126	23
	d	15	39	155	44		d	10	45	146	47
	e	17	16	163	71		e	11	22	163	71
	f	19	10	14	90		f	14	5	25	90
	g	20	22	10	94		g	15	17	14	96
	h	22	48	9	57		h	16	41	14	64
	i	22	72	12	18		i	17	66	17	30
18	b	13	78	132	11	24	b	18	77	120	9
89	c	13	67	136	24	68	c	18	67	121	19
	d	14	41	150	45		d	18	41	126	39
	e	15	18	159	73		e	18	19	123	62
	f	18	9	19	91		f	19	12	27	87
	g	19	21	11	97		g	20	23	8	93
	h	20	46	9	61		h	21	47	3	50
	i	21	70	11	25		i	21	71	2	22
19	b	22	73	126	13	25	b	17	77	123	10
57	c	22	62	127	23	90	c	17	67	124	22
	d	22	37	129	41		d	17	41	132	41
	e	23	16	113	66		e	17	19	128	77
	f	24	17	19	88		f	18	11	27	89
	g	25	28	7	96		g	19	22	9	93
	h	26	52	2	49		h	21	46	1	63
	i	25	75	5	17		i	21	71	0	23
20	b	25	70	131	14	26	c	16	70	109	18
59	c	25	59	130	25	63	d	15	45	118	38
	d	25	34	129	42		e	15	22	119	64
	e	26	14	106	69		f	16	10	39	90
	f	27	20	16	90		g	16	19	9	93
	g	28	31	6	93		h	18	43	5	56
	h	29	54	2	47		i	17	67	4	24
	i	29	78	5	15						
						27	b	16	81	110	7
21	b	30	61	146	24	75	c	15	71	110	20
58	c	30	50	145	35		d	15	45	118	41
	d	31	25	141	50		e	14	22	119	65
	e	33	8	90	73		f	15	10	39	91
	f	35	26	9	92		g	16	19	9	92
	g	36	38	5	97		h	17	43	1	56
	h	37	63	1	47		i	16	66	3	24

TABLE 4—*Continued*

Area/h_0	Plate	ϵ	ι	A	h/h_0	Area/h_0	Plate	ϵ	ι	A	h/h_0
28	c	11°	81°	66°	12	35	c	7°	80°	57°	10
68	d	8	54	88	43	76	d	4	55	72	36
	e	6	30	102	67		e	1	31	146	65
	f	6	6	103	94		f	5	5	157	97
	g	6	9	21	95		g	6	7	4	98
	h	8	33	11	66		h	9	32	36	66
	i	8	57	17	36		i	9	56	43	36
	j	7	83	9	9		j	8	81	45	10
29	c	17	72	103	16	35A	c	8	83	41	8
70	d	16	47	107	38	70	d	5	57	48	33
	e	15	25	105	63		e	1	33	47	66
	f	14	10	45	87		f	3	7	176	92
	g	16	19	7	93		g	5	6	43	99
	h	16	42	8	56		h	7	30	46	64
	i	16	65	11	25		i	8	54	55	35
							j	7	79	59	11
30	c	18	73	100	17						
67	d	16	48	101	38	36	e	33	64	12	45
	e	15	26	100	63	71	f	28	38	1	83
	f	15	12	41	88		g	27	27	9	95
	g	15	19	6	93		h	25	8	90	72
	h	16	41	11	58		i	25	26	158	53
	i	16	65	14	26		j	26	48	168	35
31	c	19	76	95	15	37	d	33	86	12	6
65	d	17	51	90	38	78	e	31	62	7	45
	e	15	28	90	66		f	27	37	3	82
	f	14	13	41	91		g	26	25	9	95
	g	14	18	5	94		h	24	3	90	67
	h	14	39	17	64		i	24	26	179	51
	i	13	62	22	30		j	25	50	177	31
32	c	19	78	96	15	38	d	34	87	11	5
65	d	17	52	90	37	86	e	32	64	6	38
	e	15	31	83	65		f	28	37	3	82
	f	13	14	43	89		g	27	26	9	95
	g	13	17	4	94		h	26	4	90	64
	h	13	37	22	61		i	26	24	178	49
	i	12	61	28	31		j	27	49	175	32
							k	30	85	180	4
33	c	14	83	60	8						
80	d	11	58	67	34	39	e	38	69	8	38
	e	8	34	68	64	105	f	34	44	1	82
	f	5	11	62	90		g	33	32	7	94
	h	4	30	9	71		h	31	8	45	69
	i	4	54	2	39		i	31	19	163	56
	j	3	79	18	12		j	32	44	174	39
							k	35	80	174	9
34	c	14	84	57	8						
85	d	11	59	61	36	40	e	41	73	9	32
	e	8	35	61	67	92	f	37	43	1	82
	f	5	11	57	91		g	36	35	7	95
	h	3	29	13	70		h	34	11	36	68
	i	3	53	3	37		i	34	17	151	57
	j	2	78	26	12		j	35	41	169	38
							k	38	76	172	11

TABLE 4—*Continued*

Area/h_0	Plate	ϵ	ι	A	h/h_0	Area/h_0	Plate	ϵ	ι	A	h/h_0
41	e	36°	67°	10°	36	48	d	16°	69°	5°	24
100	f	32	42	3	84	84	e	14	46	4	60
	g	31	30	8	95		f	11	20	18	86
	h	29	8	57	71		g	11	9	15	97
	i	29	22	159	54		h	11	18	123	68
	j	30	46	170	37		i	12	42	128	46
	k	33	81	172	6		j	12	67	135	22
42	d	32	86	4	6	49	d	10	64	3	31
68	e	30	62	0	42	81	e	8	40	14	61
	f	27	37	6	84		f	7	14	37	86
	g	26	24	8	95		g	8	4	2	98
	h	25	3	90	71		h	8	24	96	64
	i	26	25	158	53		i	10	48	97	44
	j	26	50	162	32		j	10	73	106	16
43	d	31	85	1	7	50	d	9	63	5	31
67	e	30	62	2	42	95	e	8	39	25	63
	f	27	36	7	83		f	8	14	42	88
	g	26	24	8	95		g	9	5	7	97
	h	25	5	90	69		h	10	25	84	67
	i	26	26	150	47		i	11	49	97	44
	j	27	51	155	30		j	11	74	99	20
44	f	66	75	4	66	51	c	6	81	39	9
60	g	64	62	4	98	94	d	7	56	66	35
	h	63	38	1	83		e	9	34	74	62
	i	64	15	18	65		f	13	12	45	88
	j	64	15	139	48		g	14	12	14	93
	k	66	49	166	31		h	16	33	52	67
							i	17	56	64	39
45	e	52	83	8	15		j	16	81	71	10
65	f	50	58	7	76						
	g	49	46	4	95	52	d	13	61	52	31
	h	49	25	16	69	78	e	15	39	53	66
	i	49	15	90	53		f	17	18	32	91
	j	49	34	135	36		g	18	15	7	91
	k	51	67	157	16		h	20	31	57	63
							i	21	53	75	42
46	d	30	80	24	14		j	20	77	84	11
82	e	30	59	22	45						
	f	30	35	15	83	53	c	12	84	50	6
	g	30	26	2	95	110	d	13	60	57	31
	h	30	21	73	69		e	15	38	57	58
	i	31	36	99	49		f	17	17	33	90
	j	31	59	96	27		g	19	15	8	91
							h	21	32	54	62
47	d	16	68	25	24		i	22	54	71	37
71	e	16	46	29	57		j	21	78	82	12
	f	16	21	26	85						
	g	17	13	0	98						
	h	18	23	76	69						
	i	19	45	97	40						
	j	19	69	106	18						

TABLE 4—*Continued*

Area/h_0	Plate	ϵ	ι	A	h/h_0	Area/h_0	Plate	ϵ	ι	A	h/h_0
54	c	9°	85°	9°	6	58	b	12°	81°	118°	8
101	d	6	59	4	33	115	c	13	70	116	21
	e	5	36	34	62		d	17	46	109	44
	f	7	11	58	89		e	20	27	90	65
	g	8	6	27	93		f	25	18	20	88
	h	10	28	68	64		g	26	25	9	97
	i	11	51	79	41		h	29	47	31	60
	j	10	77	86	13		i	29	69	44	28
55	b	1	86	123	3	59	b	12	81	116	9
115	c	2	75	129	17	113	c	13	70	114	22
	d	5	50	130	37		d	17	47	106	45
	e	9	27	114	64		e	20	27	85	71
	f	13	7	48	90		f	25	18	21	90
	g	15	14	16	94		g	26	25	9	96
	h	17	38	35	60		h	29	46	32	60
	i	18	62	45	33		i	29	68	45	27
	j	17	86	48	4						
						60	b	14	80	119	9
56	d	5	49	148	36	118	c	15	69	116	22
109	e	8	26	130	64		d	19	46	105	42
	f	13	6	33	87		e	22	27	83	65
	g	14	14	16	98		f	27	20	18	91
	h	16	38	31	62		g	28	27	8	93
	i	17	62	41	34		h	31	48	31	56
	j	16	87	43	5		i	31	69	45	25
57	b	3	84	171	3	61	b	12	82	112	5
128	c	4	73	155	15	216	c	13	72	108	16
	d	8	47	147	38		d	16	48	101	40
	e	10	25	126	59		e	20	28	84	65
	f	15	7	33	88		f	24	18	21	74
	g	17	16	14	.93		g	26	24	9	90
	h	19	41	31	56		h	28	45	34	60
	i	19	64	41	33		i	29	67	47	28

the resulting curve will be a rough approximation to the mean curve for the whole moon, exhibiting the same steep rise to maximum at full moon. It seems probable that the combination of a large number of areas over the whole surface of the moon, similar in behavior to the three examples shown, would represent the observed mean phase-curve. In other words, it is possible to conclude that the variation of the areas represented is typical. This conclusion is strengthened by a study of all the phase-curves together. Even the curve for area 7, on the bright ray northeast of Proclus, shown in Figure 1, agrees quite closely with the curve of the neighboring dark

area 4, when its brightness at every point is decreased by a constant factor. This appears to be the case, likewise, for the other areas located on rays and nimbi.

The phase-curve for any area, as has been already pointed out, depends to a very large extent on its location on the surface of the moon. The true nature of the surface will be more readily apparent

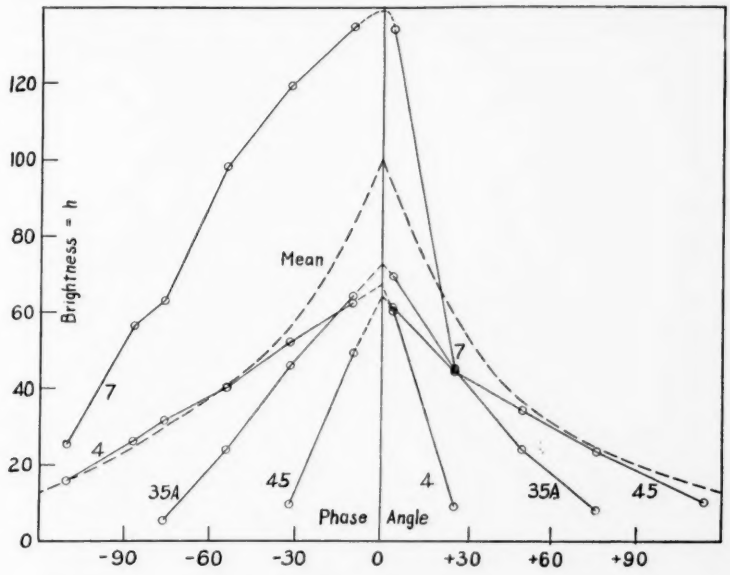

FIG. 1.—The variation of brightness with phase angle

if the surface is considered as a physical unit and the variables on which the brightness depends are referred to the surface itself. The angle of incidence, ι, and the angle of reflection, ϵ, are the variables in customary use.

The laws of diffuse reflection which have been used in astronomy are functions of ι, ϵ, and the reflecting-power. Of the three laws, that of Lommel and Seeliger has the advantage of a theoretical basis, although the assumptions are not too secure. This law represents the appearance of the full moon, in that it gives a uniformly bright surface when $\iota = \epsilon$. Under other conditions of illumination, however, it agrees very poorly with observation.

Öpik[11] and Fessenkoff[12] have derived empirical relations for the brightness of the lunar surface, introducing a function of the phase angle, without a satisfactory representation of the observations. The extensive work of Schoenberg[13] indicated that an approach to an understanding of the true nature of the surface would be found through the introduction of the azimuth as the fourth variable.

The values of the brightness for areas 4, 35A, and 45 are plotted against cos ι in Figure 2. The study of the phase-curves has already shown that the maximum brightness of every region is attained very nearly at the time of full moon, when the angle of incidence is equal to the angle of emission, and not, in general, when the angle of incidence is a minimum. Following the points of area 4, in order of increasing phase angle (Table 3), the brightness increases gradually with decreasing angle of incidence (Table 4) until the sun is nearly over the surface. As the angle of incidence increases again, the brightness continues to increase slowly until the angle of incidence becomes equal to the angle of emission. From this point the brightness rapidly decreases to zero as the sun sinks to the horizon of the area. The variation of area 45 is of the same form, except that the order of the changes is reversed because the minimum value of the angle of incidence is reached after full moon. The variation of area 35A is much simpler, since the minimum value of ι is reached very nearly at the time of full moon.

The observing conditions limit the range of measurements that can be made on any given area, owing to the fact that ϵ remains almost constant. In order to investigate the effect of this angle, it is necessary to transfer from one area to another. It is seen that the change in the form of the "curves" follows the change in ϵ; for areas 4, 35A, and 45, ϵ is around 55°, 5°, and 50°, respectively. Furthermore, the wide loops obtained for the areas of large ϵ follow the variation in the azimuth. When the azimuth is large, the brightness is much decreased, relative to the values for small azimuths. The loop has practically disappeared for area 35A. The gap between the

[11] "Photometric Measures of the Moon," *Pub. Tartu (Dorpat)*, **26**, No. 1, 1924.

[12] "Photometry of the Moon," *Pub. de l'Inst. astrophysique de Russie*, **4**, 1, 1928.

[13] "Untersuchung zur Theorie der Beleuchtung des Mondes," *Acta societatis scientiarum Fennicae (Finska Vetenskaps)*, **50**, No. 9, 1925.

two types is filled by a continuous sequence among the other areas observed, as ϵ varies between these limits.

It is immediately apparent from the graphs that no expression for the brightness which is single-valued in terms of ι and ϵ can represent the observed variation.

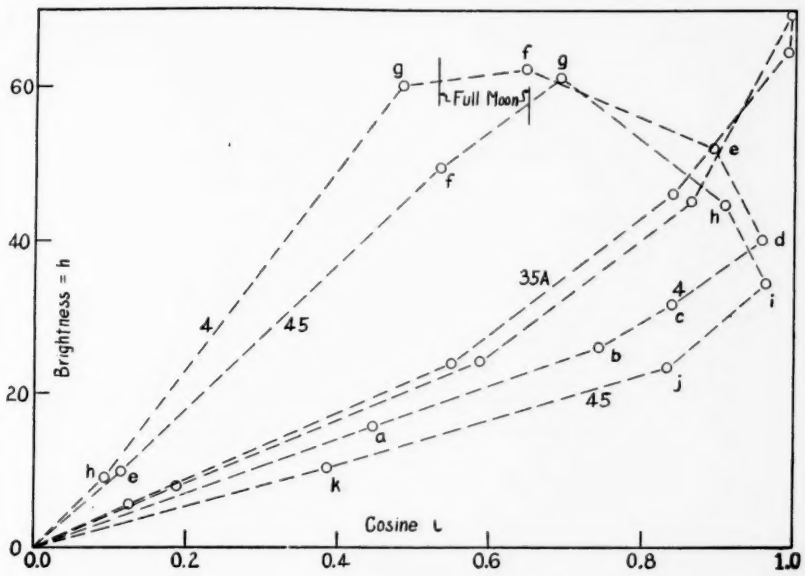

FIG. 2.—The variation of brightness with cos ι

The behavior of the lunar surface, as shown above, brings out very strongly the fact, recognized since Zöllner's time from the form of the mean phase-curve, that the surface must be very rough. As Russell has pointed out,[14] the effect is too great to be accounted for by the visible mountains. It is here shown that the areas which appear smooth show the phenomenon. The variation is so dissimilar to the behavior of smooth, diffusely reflecting substances that it is very likely due to the formation of shadows much too small to be visible. When the surface is seen from directly above, a change in the azimuth can have no effect, because the shadows cast by the irregularities move around without their size or proportion of the

[14] *Ap. J.*, **43**, 192, 1916.

total area varying. If, however, the surface is seen from an angle, the shadows will be hidden by the irregularities when the azimuth is small. As this angle increases, the shadows will come more and more into view.

THEORETICAL FORM OF THE SURFACE

From the work of Schoenberg[13] it appeared that the form of the irregularities of the surface most likely to represent the observations was that of circular pits or cups, similar to the porous surface of pumice stone. Inasmuch as the surface of the interior of the cups is undoubtedly rough, being more or less a repetition of the original surface on a smaller scale, it seemed that the simplest assumption might be as good as a more complicated expression for the quantity of light reflected. It was assumed, therefore, that the brightness would vary directly with the fraction of the visible area of the inner surface which was illuminated. For the plane surface between the cups the brightness was assumed to follow Lambert's law, $h_1 = h_0 \cos \iota$, where h_0 is the brightness for normal incidence. The complete expression then becomes

$$h = h_0\{C \cos \iota + (1 - C)V\} ,$$

where h_0 is the brightness for $\iota = \epsilon = 0$, C is the fraction of the surface which is plane, and V is the fraction of the area occupied by the cups which is at the same time visible and illuminated.

For the derivation of the fraction V in terms of ι, ϵ, and A, a sphere of unit radius was taken whose center was at the origin of a three-dimensional co-ordinate system, the lower half of the sphere being the cup. The z-axis was taken along the emitted ray, the y-axis in the plane of the surface, and the x-axis at the angle ϵ with the surface. The projection of the edge of the cup on the xy-plane was then the apparent boundary of the cup, an ellipse whose equation is

$$\frac{1}{\cos^2 \epsilon} x^2 + y^2 = 1 ,$$

or, putting T for $1/\cos^2 \epsilon$,

$$Tx^2 + y^2 - 1 = 0 . \qquad \text{(A)}$$

The boundary between the illuminated portion of the interior surface of the cup and the portion in shadow is half of a great circle which makes an angle 2ι with the edge of the cup. A portion of the sphere is shown in Figure 3; DE is the edge of the cup, DF the trace of the xy-plane on the sphere. The points K and P are the poles of the edge of the cup and of the shadow boundary, respectively. Then arc $KG = \epsilon$; arc $KP = 2\iota$; arc $EB = A$; arc KE = arc KB = arc $KD = 90°$.

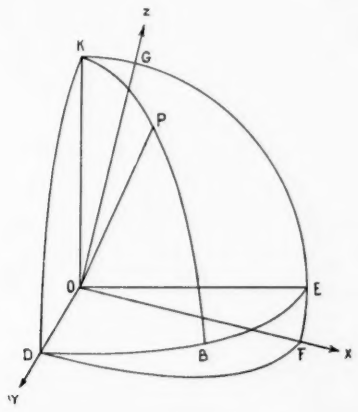

FIG. 3

The equation of the plane containing the shadow boundary was then derived in the normal form:

$$x \cos \alpha + y \cos \beta + z \cos \gamma = 0 . \qquad \text{(B)}$$

The arcs FP, DP, and GP measure the direction angles α, β, and γ of the line OP; and the solution of the spherical triangle FKP gives

$$\begin{aligned}
\cos \alpha &= \cos PF = \cos FK \cos KP + \sin FK \sin KP \cos FKP \\
&= \cos (90° + \epsilon) \cos 2\iota + \sin (90° + \epsilon) \sin 2\iota \cos A \\
&= -\sin \epsilon \cos 2\iota + \cos \epsilon \sin 2\iota \cos A , \\
\cos \beta &= \sin 2\iota \sin A , \\
\cos \gamma &= \cos \epsilon \cos 2\iota + \sin \epsilon \sin 2\iota \cos A .
\end{aligned}$$

The equation of the sphere is

$$x^2 + y^2 + z^2 = 1 . \tag{C}$$

When z is eliminated between (B) and (C), the equation of the projection of the shadow boundary on the xy-plane is obtained:

$$x^2\left(\frac{\cos^2\alpha}{\cos^2\gamma} + 1\right) + 2xy\left(\frac{\cos\alpha\cos\beta}{\cos^2\gamma}\right) + y^2\left(\frac{\cos^2\beta}{\cos^2\gamma} + 1\right) - 1 = 0,$$

or

$$Kx^2 + 2Lxy + My^2 - 1 = 0 . \tag{D}$$

The area S, inside of ellipse (A) and outside of ellipse (D), is the apparent area of the interior of the cup that is in shadow when $\cos\gamma > 0$ and the area illuminated when $\cos\gamma < 0$.

The x-co-ordinate was expanded to transform equation (A) to that of a circle by the substitution $\sqrt{T}x = x'$, so that equation (A) becomes

$$(x')^2 + y^2 - 1 = 0 \tag{E}$$

and (D) is converted to

$$\frac{K}{T}(x')^2 + 2\frac{L}{\sqrt{T}}x'y + My^2 - 1 = 0 ,$$

or

$$K'(x')^2 + 2L'x'y + M'y^2 - 1 = 0 . \tag{F}$$

The axes were then rotated by the substitution

$$\begin{aligned} x' &= \xi\cos\psi - \eta\sin\psi , \\ y &= \xi\sin\psi + \eta\cos\psi , \end{aligned} \qquad \tan\psi = \frac{2L'}{K' - M'} ,$$

so that (E) and (F) become

$$\begin{aligned} &\xi^2 + \eta^2 - 1 = 0 , \\ &P\xi + Q\eta^2 - 1 = 0 , \qquad Q > P , \end{aligned}$$

where

$$P = \frac{K' + M'}{2} \pm \left[\frac{K' - M'}{2} \cos 2\psi + L' \sin 2\psi\right],$$

$$Q = \frac{K' + M'}{2} \mp \left[\frac{K' - M'}{2} \cos 2\psi + L' \sin 2\psi\right].$$

The area S is now twice that between the η axis and the point of intersection of the two ellipses, where $\xi_1 = \sqrt{(1 - Q)/(P - Q)}$. That is,

$$S = 2\int_0^{\xi_1} \left(\sqrt{1 - \xi^2} - \frac{1}{\sqrt{Q}} \sqrt{1 - P\xi^2}\right) d\xi,$$

whence

$$S = \arcsin \xi_1 - \frac{1}{\sqrt{PQ}} \arcsin \sqrt{P}\, \xi_1.$$

From equation (A) the projected area of the cup is $\pi \cos \epsilon$. Therefore, when $\cos \gamma > 0$,

$$V = \frac{\pi \cos \epsilon - S}{\pi \cos \epsilon} = 1 - \frac{S}{\pi \cos \epsilon};$$

and when $\cos \gamma < 0$,

$$V = \frac{S}{\pi \cos \epsilon}.$$

COMPARISON WITH OBSERVATION

The application of these assumptions was first tried near the center of the moon, for which $\epsilon = 0$, approximately. In this special case the derivation of V was greatly simplified. The cup now appears to be a circle of radius one, and the shadow boundary an ellipse whose minor axis is $\cos 2\iota$. The projection of the area illuminated is

$$\frac{\pi}{2} + \frac{\pi}{2} \cos 2\iota = \pi \cos^2 \iota$$

and

$$V = \frac{\pi \cos^2 \iota}{\pi} = \cos^2 \iota.$$

Then

$$\frac{h}{h_0} = C \cos \iota + (1 - C) \cos^2 \iota.$$

Nearly all of the observations of areas 28, 33, 34, 35, and 35A were taken when the value of ϵ was less than 10°. The brightness at full moon, h_0, was interpolated from the phase-curves, and the ratio h/h_0 was obtained for each measurement, as given in Table 4. These values were then plotted, and the theoretical curve was compared with the observed values. It was immediately apparent that the theoretical curve gave too slow a decrease in brightness as cos ι decreased. It was then found that the curve could be greatly steepened by increasing the depth of the pits so that they became spheroidal in form. The effect of this change is seen in Figure 4. Every point on the hemisphere is moved downward parallel to the z-axis, so that the z-co-ordinate is numerically increased by the factor b. The point E moves to the position F, both points projecting into the same point D. The projection of the shadow boundary will be properly represented by the use of an angle ι' in place of ι in the derived expression for S, such that

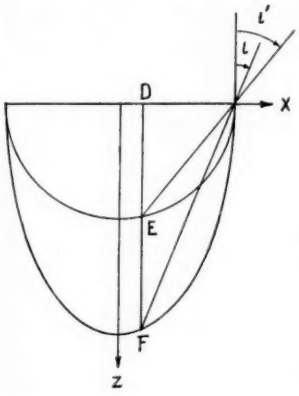

FIG. 4

$$\tan \iota' = b \tan \iota ,$$

where b is the ratio of the polar and equatorial axes of the spheroid.

By trial and error it was found that $b = 1.8$ and $C = 0.55$ gave a very satisfactory representation of the observations. The brightness of the surface, viewed normally, is then given by

$$\frac{h}{h_0} = 0.55 \cos \iota + 0.45 \cos^2 \iota' .$$

The observed points are plotted in Figure 5. The theoretical expression is represented by the curve.

Area 44 was then chosen for a trial of the general expression, in the form

$$\frac{h}{h_0} = 0.55 \cos \iota + 0.45V .$$

The value of b found above was used in the computation of S. The interpolated value of the brightness at full moon, when $\iota = \epsilon \neq 0$, was used for h_0. The data are given in Table 5.

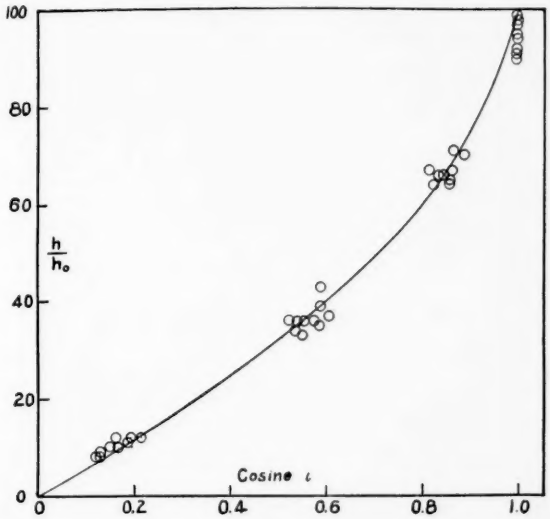

FIG. 5.—The observed variation of brightness of several areas near the center of the moon ($\epsilon < 10°$) is shown by circles. The theoretical variation for $\epsilon = 0$ is given by the curve.

TABLE 5

PLATE	ϵ	A	ι	ι'	S	V	h/h_0	
							Comp.	Obs.
f.....	66°	4°	75°	81°	0.45	0.35	0.30	0.66
g.....	64	4	62	74	.48	0.64	.55	.98
h.....	63	1	38	54	.00	1.00	.89	.83
i.....	64	18	15	24	.00	1.00	.98	.65
j.....	64	139	15	25	.33	0.24	.64	.48
k.....	66	166	49	64	0.01	0.01	0.36	0.31

The observed and computed values are plotted in Figure 6. It is at once evident from the figure that the present analysis is a step in the right direction in that the brightness depends strongly on the azimuth. It does fail, however, to give the maximum brightness at full moon, indicating that a considerable modification will have to

be made in the assumptions before a satisfactory representation of the observations can be obtained.

It does not seem worth while to carry the theoretical investigation farther at the present time. The data on the behavior of the lunar surface here presented are more extensive than similar obser-

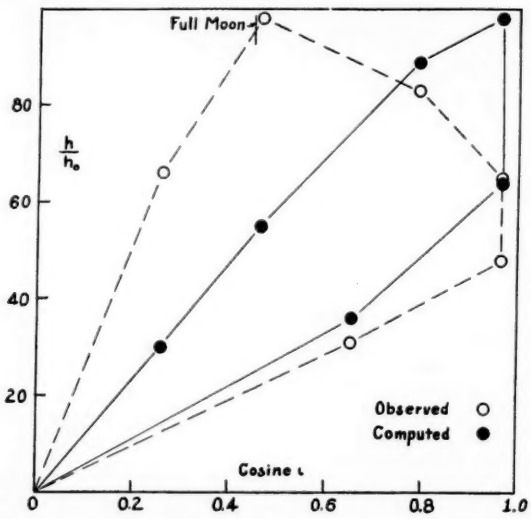

FIG. 6.—Comparison of the observed and the theoretical variation of brightness for area 44 (Grimaldi).

vations of terrestrial substances. As soon as the latter become available, it should be possible to identify the structure corresponding to the lunar surface.

The author is indebted to Professor Russell and Professor Dugan for much valuable advice and criticism; to the Lowell Observatory for the opportunity of obtaining the observational material and to the members of the staff for many helpful suggestions; and finally to Professor Schlesinger, who made it possible for him to complete this work after his appointment to the staff of the Yale Observatory in October, 1931.

YALE OBSERVATORY
January 1938

INVESTIGATIONS IN PROPER MOTION*

TWENTIETH PAPER: PROPER MOTIONS IN FIELDS OF STARS WITH LARGE MOTION

ADRIAAN VAN MAANEN

ABSTRACT

By superposing photographs, taken at intervals ranging from ten to twenty-three years, 105 stars showing a decided proper motion were found in 223 fields in which the central stars had a motion of about 0".5 or more annually. Sixteen of these stars are companions of the central stars; for all these the parallax is known. The distances from the central stars range from 100 to 10,000 astronomical units, the absolute photographic magnitudes from +10.1 to +14.0 with a maximum frequency at about +12.

When I started the parallax program at the 80-foot Cassegrain arrangement of the 60-inch Mount Wilson reflector, many plates were taken during the middle of the night, when the parallax factors are small, for the investigation of several problems in proper motion. One of these was the discovery of faint companions of stars whose proper motions were known to be large ($\geqq$ 0".500 per year.)[1] These plates have now been duplicated after an interval ranging from ten to twenty-three years. For 223 fields the photographs have now been examined for stars of large proper motion by simply superposing the old and the new plates. The plates are not suitable for blinking in the stereocomparator on account of the large scale and the corresponding scarcity of stars per square inch and also on account of the considerable difference in scale between many of the old and new plates. As will be seen later, however, the simple superposition seems quite efficient if we are concerned only with the larger motions.

One hundred and five stars were found which showed a decided proper motion; these stars were subsequently measured in the stereocomparator, by van Maanen, Karpov, or Miss Lowen, using three or four comparison stars. Of these, 16 are companions of the central stars with large proper motion; only two others have motions exceeding 0".5 of arc annually.

* *Contributions from the Mount Wilson Observatory, Carnegie Institution of Washington*, No. 592.

[1] As the fields were taken from a list compiled in 1915, several of the stars included were found later to have motions smaller than this limit.

Table 1 gives the stars for which motions were derived, while the companions are listed in Table 2. In the first table the successive columns show the current number, the name of the central star, the co-ordinates of the new proper-motion star, the photographic magnitude, right ascension and declination for 1900.0, the μ_α, μ_δ, and total μ, and, finally, the interval in years between the old and the new plates.

The limiting magnitude is 15.8, but in general the plates show stars only as faint as 15.0 or 15.5. Comparing the number of stars found on the 46.5 square degrees investigated with the number of stars of the same magnitude discovered by van Maanen, Willis, and Oosterhoff in the 135 Selected Areas taken at the Newtonian focus of the 60-inch reflector by blinking the plates in the stereocomparator, we find the number of stars per square degree with motions exceeding $0''.2$ annually to be practically the same. For the smaller motions the relative number found here is about one-half, a ratio which decreases rapidly for the stars of fourteenth and fifteenth magnitude, since the superposition of the plates yields only 20 per cent of the number found by blinking. As the purpose, however, was principally the discovery of companions, the method employed here was sufficient.

The companions were measured in two different ways: for the closer ones the distances $\Delta\alpha$ and $\Delta\delta$ from the principal stars were measured on the old and on the new plates; for the more distant companions, μ_α and μ_δ were measured for the central stars as well as for the companions. In no case was enough difference found to indicate any orbital motion. In Table 2, which lists the 16 companions that were unknown previous to their discovery on the plates, the successive columns give the current number; the name, the proper motion, and the parallax of the principal star; the distance and position angle; the right ascension and declination for 1900; the photographic magnitude; and, finally, the photographic absolute magnitude of the companion.

The photographic magnitudes in both Tables 1 and 2 were derived from counts of stars of equal or brighter magnitude and are based on Table 4, *Groningen Publications*, No. 27.

It was satisfactory to find that parallaxes are available for all the principal stars for which companions were found. The wide range in

TABLE 1

STARS FOUND TO HAVE PROPER MOTION

No.	Central Star	x	y	Phot. Mag.	α 1900	δ 1900	μ_α	μ_δ	μ	Interval
1.....	Fur 2	− 3′.4	+ 7′.4	10.2	$0^h11^m29^s$	+40° 30′	+0″.209	+0″.033	0″.212	16
2.....	54 Piscium	+11.8	+ 4.7	14.3	0 35 1	20 48	+0.056	−0.072	0.091	22
3.....	Lal 1299	+11.1	+ 8.9	12.9	0 43 52	4 55	+1.264	−2.739	3.017	11*
4.....	AG Hels 914	− 9.2	−12.3	9.8	0 59 0	63 12	+0.239	−0.157	0.286	17
5.....	WB 1^h 262	− 3.3	−11.3	11.7	1 15 35	30 38	−0.060	−0.016	.062	22
6.....	Lal 2450	− 5.8	+ 1.6	10.9	1 16 28	18 12	+0.053	−0.022	.057	22†
7.....	Lal 2450	− 5.7	+ 1.4	15.7	1 16 28	18 11	+0.053	−0.024	.058	22†
8.....	Lal 3022	− 7.5	− 8.7	13.8	1 33 22	27 27	−0.050	−0.119	.129	22
9.....	Lal 2966	+ 3.2	− 2.6	12.0	1 34 42	66 22	+0.020	−0.049	.053	17
10.....	Lal 3054	−10.5	+ 3.2	11.9	1 34 45	42 10	−0.134	+0.013	.135	16
11.....	Lal 4855	+12.8	+ 3.9	13.9	2 33 34	30 28	−0.036	−0.100	.106	20
12.....	WB 3^h 113	− 7.2	+ 8.6	13.1	3 8 53	8 46	+0.289	−0.068	.297	17
13.....	Lal 7443	+ 5.6	+ 3.6	12.9	3 56 59	35 6	+0.046	−0.050	.068	19
14.....	AG Berl B 1366	− 0.6	+ 5.6	7.3	4 8 33	22 12	+0.070	−0.014	.071	20
15.....	Lal 9012	−15.1	+ 8.3	11.9	4 42 56	45 49	+0.190	−0.222	.292	16
16.....	Lal 9599	+ 2.7	+ 2.9	10.7	5 1 43	18 34	+0.045	−0.010	.046	20
17.....	Wolf 232	− 2.5	− 4.9	11.4	5 6 46	19 32	+0.268	+0.246	.364	17
18.....	Wolf 232	+ 1.6	+ 7.3	11.4	5 7 4	19 44	+0.010	−0.091	.092	17
19.....	λ Aurigae	+ 4.2	− 8.9	13.6	5 12 28	39 52	+0.062	−0.052	.081	20
20.....	Lal 13427	− 5.7	− 2.1	13.8	6 53 26	48 30	+0.010	−0.084	.085	20
21.....	β Geminorum	−12.6	− 4.4	11.6	7 38 15	28 12	−0.111	−0.098	.148	20
22.....	Lal 15565	− 1.0	−13.4	12.8	7 54 16	29 18	−0.024	−0.352	.353	19‡
23.....	BD+33°1694	+ 0.8	+ 3.7	13.1	8 19 0	33 2	+0.009	−0.076	.077	16
24.....	Wolf 308	− 3.7	− 9.5	12.9	8 22 10	46 6	+0.168	−0.008	.168	15
25.....	Wolf 320	+12.2	+ 7.4	11.5	8 36 57	45 0	−0.045	−0.050	0.067	17

* Van Maanen's star. † Pair, $\Delta = 12''$ in $p = 158°$. ‡ This is Wolf 1059; Wolf gives $\mu = 0''.58$ but states that the measures are poor.

TABLE 1—*Continued*

No.	Central Star	x	y	Phot. Mag.	α 1900	δ 1900	μ_α	μ_δ	μ	Interval
26.....	Lal 18286	− 2′.7	+ 0′.3	14.1	$9^h11^m45^s$	+29° 0′	−0″.039	−0″.005	0″.039	18
27.....	Lal 18286	− 2.6	− 0.9	15.1	9 11 45	28 59	− .196	− .075	.210	18§
28.....	Lal 18286	− 2.5	− 1.0	15.5	9 11 46	28 59	− .195	− .068	.207	18§
29.....	Lal 18812	− 3.5	+ 4.9	12.4	9 29 23	36 21	− .082	− .105	.212	14
30.....	Lal 20881	+ 2.5	+ 9.3	13.6	10 46 18	20 58	− .094	− .028	.098	20
31.....	83′ Leonis	− 9.6	−11.7	12.6	11 21 4	3 22	− .036	− .067	.076	22
32.....	Lal 22069	+13.8	+ 0.8	14.2	11 34 49	45 41	− .101	+ .032	.106	19
33.....	WB 11^h 920	− 3.9	−10.8	12.2	11 49 12	19 48	− .138	− .084	.162	20
34.....	Lal 22632	−10.8	− 3.2	12.2	11 56 25	43 36	+ .080	− .013	.081	18
35.....	Lal 22632	− 6.0	+ 8.4	14.0	11 56 52	43 47	+ .243	− .416	.482	18
36.....	Lal 23243	+ 1.5	− 6.0	12.3	12 20 29	32 19	+ .061	− .160	.171	20
37.....	Lal 23498	− 4.7	− 0.4	12.2	12 28 35	41 54	− .274	− .070	.283	17
38.....	Lal 23808	+11.1	+10.0	12.8	12 42 3	10 16	− .102	+ .060	.118	15
39.....	Lal 23808	+11.2	+ 8.4	14.6	12 42 3	10 14	+ .044	− .116	.124	15
40.....	Lal 24504	+ 9.5	− 5.8	14.2	13 7 4	10 3	− .125	− .021	.127	17
41.....	Lal 25426	+ 7.8	−12.4	11.3	13 43 4	17 45	+ .104	− .089	.137	18
42.....	Lal 26294	+ 1.7	+ 8.9	13.1	14 17 47	30 15	− .058	+ .054	.079	19
43.....	WB 14^h 847	− 9.9	+ 8.8	13.6	14 41 2	17 5	− .080	.000	.080	18
44.....	WB 14^h 847	− 7.9	+11.0	11.2	14 41 10	17 8	− .216	− .057	.223	18
45.....	Lal 27137	−11.4	− 4.7	11.2	14 48 3	19 28	− .018	− .076	.078	14
46.....	Lal 27958	− 4.2	+ 4.8	11.2	15 14 26	26 9	− .140	− .072	.157	17
47.....	Lal 28992	+ 6.0	+ 1.1	12.6	15 49 46	42 45	+ .056	− .022	.060	19‖
48.....	Lal 28992	+ 6.0	+ 1.1	12.6	15 49 46	42 45	+ .056	− .022	.060	19‖
49.....	Lal 29213	−15.4	+ 2.1	12.4	15 55 59	33 38	− .027	− .037	.046	19
50.....	Lal 29439	+ 5.5	+ 6.7	13.0	16 3 22	+39 2	−0.018	+0.074	0.076	16

§ Pair, $\Delta = 6''$ in $p = 120°$. ‖ Pair, $\Delta = 1''.7$ in $p = 6°$.

TABLE 1—*Continued*

No.	Central Star	x	y	Phot. Mag.	α 1900	δ 1900	μ_α	μ_δ	μ	Interval
51	Lal 29439	+11′.8	+ 8′.2	13.7	$16^h\ 3^m55^s$	+39° 3′	−0″.008	−0″.038	0″.039	16
52	Lal 31132	+14.3	+ 2.5	10.7	17 1 11	47 14	+ .002	+ .108	.108	15
53	Ci 20, 1050	+ 7.1	− 0.4	10.0	17 33 54	18 37	− .190	− .192	.270	20
54	Ci 20, 1050	+13.0	− 0.3	10.4	17 34 19	18 37	+ .052	− .094	.107	20
55	Lal 32519	+15.6	+ 3.2	10.4	17 43 44	27 50	− .114	− .193	.224	19
56	PM 2164′	− 7.6	− 9.4	12.7	18 40 40	59 20	− .082	− .052	.097	20
57	Lal 36245	−11.2	+ 6.5	13.2	19 8 21	49 46	+ .073	+ .260	.270	18
58	Lal 36647	−13.2	+12.0	11.0	19 19 18	11 56	− .018	+ .064	.066	19
59	σ Draconis	−11.7	− 9.2	12.2	19 30 19	69 20	+ .046	+ .060	.076	20
60	Groom 2875	+ 9.5	− 7.3	14.2	19 30 40	58 16	− .002	+ .062	.062	21
61	Groom 2875	+10.5	+ 5.8	12.6	19 30 48	58 29	+ .018	+ .070	.072	21
62	Lal 38287	− 8.8	−10.2	12.4	19 57 24	15 10	+ .006	− .065	.065	20
63	Lal 38287	+11.5	+ 8.5	11.8	19 58 47	15 28	− .072	− .112	.133	20
64	b′ Cygni	+ 5.2	+ 9.8	11.0	20 3 3	35 52	+ .012	− .086	.087	16
65	Fed 3562	+ 0.7	− 6.1	11.3	20 38 52	75 8	− .052	− .052	.074	20
66	Fed 3562	+13.7	− 3.3	11.3	20 42 13	75 11	+ .036	+ .041	.055	20
67	BD+61°2068	−11.1	+ 9.3	13.7	20 49 42	61 57	+ .064	+ .072	.096	21
68	BD+61°2068	− 9.6	+ 0.8	11.4	20 49 54	61 49	+ .085	+ .117	.145	21
69	Fur 54	− 1.0	+10.6	7.1	20 56 7	39 52	+ .222	+ .214	.308	14
70	Fur 54	+ 0.8	+ 7.7	11.3	20 56 16	39 49	+ .078	− .004	.078	14¶
71	Fur 54	+ 0.9	+ 7.8	11.7	20 56 17	39 49	+ .074	− .004	.074	14¶
72	WB 21^h 97	+ 3.6	−11.2	15.3	21 7 36	17 10	− .528	− .352	.635	10
73	WB 21^h 594	− 3.3	− 1.6	14.0	21 25 41	45 25	+ .060	+ .018	.063	19
74	Wolf 1014	+ 5.0	0.0	15.0	22 7 57	8 5	− .049	− .048	.069	18
75	Wolf 1014	+ 5.2	− 3.0	11.5	22 7 58	+ 8 2	+0.008	−0.062	0.063	18

¶ Pair, $\Delta = 9''$ in $p = 38°$.

TABLE 1—*Continued*

No.	Central Star	x	y	Phot. Mag.	α 1900	δ 1900	μ_α	μ_δ	μ	Interval
76.....	Wolf 1014	+ 9'.1	− 4'.9	13.0	$22^h\ 8^m14^s$	+ 8° 0′	+0″.067	−0″.008	0″.067	18
77.....	Lal 43492	+ 5.9	+10.7	14.3	22 12 39	12 35	− .016	− .069	.071	14
78.....	Kli 6256	−14.6	+ 5.4	11.7	22 29 34	4 57	+ .005	− .160	.160	20
79.....	Kli 6256	−10.3	+ 9.4	13.2	22 29 51	5 1	− .038	− .037	.053	20
80.....	Kli 6256	−10.1	+ 0.9	14.1	22 29 52	4 53	+ .042	+ .002	.042	20
81.....	Lal 44739	− 1.7	−10.5	11.7	22 47 13	9 8	+ .144	+ .060	.156	19
82.....	Fur 60	−14.7	− 3.7	14.1	23 20 27	44 43	+ .106	+ .035	.112	18
83.....	Lal 46221	− 1.9	+ 8.5	13.1	23 30 19	30 36	+ .106	+ .012	.107	13
84.....	Lal 46221	− 0.4	+ 8.6	11.3	23 30 26	30 36	+ .048	+ .005	.048	13
85.....	Lal 46221	+ 0.7	+ 9.6	10.5	23 30 31	30 37	− .184	− .278	.333	13
86.....	Lal 46351	−12.8	−10.9	11.1	23 33 57	4 54	+ .077	+ .132	.153	18
87.....	Lal 46495	+13.7	+12.0	10.6	23 40 15	57 43	− .066	− .078	.102	19
88.....	Lal 46650	+ 4.5	− 9.4	12.6	23 44 17	1 43	+ .001	− .047	.047	22
89.....	Lal 46650	+12.1	− 1.9	11.2	23 44 47	+ 1 50	+0.074	−0.142	0.160	22

the distances is quite interesting; they vary from 2".7 to 732", or from about 100 to over 10,000 astronomical units. The apparent photographic magnitudes range from 11.5 to 15.8, the photographic absolute magnitudes from +10.1 to +14.0 with a maximum frequency at about +12.

TABLE 2

PHYSICAL COMPANIONS OF STARS WITH LARGE PROPER MOTION

No.	Name	μ‖	π	Δ	p	α 1900	δ 1900	Phot. Mag.	M Phot.
1....	Lal 1964	0".52	+0".046	10"	74°	1h 2m15s	+22°26′	15.2	+13.5
2....	WB 1h 262....	0.50	.032	11	291	1 15 49	30 49	15.2	12.7
3....	Pi 2h 123.....	2.32	.144	165	109	2 30 46	6 24	13.2	14.0
4....	Lal 5490	0.98	.036	266	65	2 56 31	61 22	13.3	11.1
5....	Fur 16*	0.65	.025	2.7	268	5 7 43	44 26	15.2	12.2
6....	Pi 5h 146†	0.54	.096	97	70	5 33 24	53 27	11.5	11.4
7....	AG Berl A 1866	0.91	.024	7	224	5 57 16	19 23	14.0	10.9
8....	AG Bonn 5621	0.44	.037	37	6	6 49 30	40 13	12.3	10.1
9....	ρ′ Cancri	0.53	.064	85	129	8 46 44	28 42	14.5	13.5
10....	Groom 1646‡	0.90	.040	5	15	10 21 54	49 19	13.6	11.6
11....	BD+10°2703	0.54	.038	72	86	14 28 45	9 47	15.8	13.7
12....	Lal 27958	0.58	.018	4	185	15 14 45	26 4	14.4	10.7
13....	Lal 32324§	0.56	.072	732	162	17 34 29	61 45	11.8	11.1
14....	ε Cygni	0.49	.036	78	266	20 42 4	33 36	14.8	12.6
15....	Lal 44739	0.52	.039	248	20	22 47 26	9 22	14.8	12.8
16....	Lal 46221	0.59	+0.026	8	110	23 30 29	+30 27	14.8	+11.9

* Espin gives Δ = 1".9 in p = 262°, 1915.

† This companion is also given in *Pub. Cincinnati Obs.*, No. 20, 1930.

‡ This companion was also found independently by G. P. Kuiper, *Pub. A.S.P.*, **47**, 98, 1935.

§ The principal star is ADS 10660.

‖ μ taken from *Pub. Cincinnati Obs.*, No. 20, 1930.

For completeness it may be added that the number of companions which were already known in the 223 fields was investigated. These companions belong to 4 triple systems and 34 double stars. One of the new companions, No. 13, makes Lalande 32324 a triple system. Including the new companions in Table 2, we find that one in every four or five of the stars in question is a double or a multiple system.

CARNEGIE INSTITUTION OF WASHINGTON
MOUNT WILSON OBSERVATORY
March 1938

THE RADIAL VELOCITIES OF 600 STARS AND MEASURES OF 69 SPECTROSCOPIC BINARIES*

WILLIAM H. CHRISTIE AND O. C. WILSON

ABSTRACT

The radial velocities of 600 stars observed with the 60- and 100-inch reflectors are given. This list is in no way homogeneous and contains stars from several observing lists made up for various investigations.

In addition, measures are given for 69 variable-velocity stars, some of which have been observed elsewhere.

The radial velocities of the stars contained in the following tables have been derived from a rather heterogeneous mass of material, for they are, in part, the result of an effort to clean up a number of stars left over from earlier observing-lists. It invariably happens that some stars from such a list are not included in a publication because of lack of sufficient observations or because of the poor quality of the plates or spectra. In most of these cases we have obtained additional observations, with the result that the velocities may now be published with some confidence.

A large number of measures by other members of the staff were available to us. In fact, nearly all those engaged in spectroscopic work are here represented, as are practically all the various combinations of spectrographs and cameras that have been used since observations were first commenced at Mount Wilson, with the exception of the coudé and nebular spectrographs. But since the writers have been more or less responsible for the completion of these velocities, it has fallen to their lot to be responsible also for their publication.

In order to make the results as homogeneous as possible, it was necessary for us to weight the measures according to the quality and the dispersion of the individual plates. This was done after all measuring had been completed, thus making the system of weights consistent throughout.

* *Contributions from the Mount Wilson Observatory, Carnegie Institution of Washington*, No. 593.

The several columns in the accompanying tables need but little explanation. Unless indicated otherwise, the designation in the second column is that of Boss's *Preliminary General Catalogue. Bonner Durchmusterung* stars are given with the initials omitted. In the "HD" column we have included designations which may prove helpful to those interested. In Table 1, stars which were included in the Selected Area lists are designated by an asterisk; those which were selected because of large proper motion, by a dagger; stars whose velocity may be variable are indicated by a double dagger. The familiar formula,

$$\text{P.E.} = 0.6745\sqrt{\frac{\Sigma pvv}{n(n-1)}}$$

has been used in computing the probable errors given in the eighth column.

TABLE 1

THE RADIAL VELOCITIES OF 600 STARS

HD	Star	α (1900)	δ (1900)	Mag.	Sp.	Vel.	P.E.	No.
315.....	Boss 7	$0^h\ 2^m6$	− 3°06′	6.3	Aon	+ 13.2	1.7	5
448.....	13	0 3.9	+17 39	5.7	G9	− 23.9	1.2	3
545.....	17	0 4.8	− 3 07	7.2	M2	+ 18.5	1.2	4
587.....	20	0 5.2	− 5 48	6.0	G9	+ 24.3	0.6	3
919*.....	+75°4	0 8.5	+75 28	7.6	M4	− 0.2	0.4	5
947*.....	+75°5	0 8.8	+75 28	7.9	G4	− 16.4	1.4	3
1061B.....	35B	0 9.8	+08 16	7.8	A9s	+ 8.3	0.8	3
1195*.....	−15°38	0 11.2	−15 02	8.6	F5	+ 22.0	1.9	3
1227.....	39	0 11.4	+07 41	6.2	G6	+ 0.8	0.6	5
1317B.....	45B	0 12.3	+ 8 19	8.0	A9s	+ 39.3	0.8	3
1352*.....	48	0 12.6	+15 47	7.4	F5	+ 7.4	1.1	6
1367.....	49	0 12.7	+ 1 08	6.4	G6	− 9.5	0.7	3
1563*.....	54	0 14.8	+15 42	6.8	G8	+ 21.3	0.1	3
2023.....	69	0 19.4	− 2 46	6.3	K1	+ 14.4	1.1	3
2035.....	70	0 19.5	+13 46	6.8	Ko	− 15.3	1.8	4
2114.....	73A	0 20.3	+ 1 23	6.0	G5	− 5.3	0.2	3
2273.....	79	0 21.5	− 0 36	6.4	G4	− 23.2	1.6	3
2313*.....	+30°59	0 21.9	+30 37	7.6	M1	+ 30.5	0.1	3
2410.....	80	0 22.8	+18 58	6.7	G7	+ 10.7	1.7	4
3512.....	129A	0 33.0	− 1 03	6.9	K3	− 55.3	1.5	4
3989*.....	+45°181	0 37.4	+45 21	7.4	Mo	− 18.7	0.9	4
4301.....	156	0 40.3	− 5 11	6.4	Mo	+ 7.5	1.2	3
4406*.....	+45°199	0 41.3	+45 49	7.6	G3	+ 0.2	1.6	3
4482.....	162	0 41.8	+11 26	5.7	G9	− 0.3	1.0	3
4928.....	188	0 46.2	+ 2 51	6.5	G7	+ 6.8	0.2	3
5098.....	190A	0 47.8	−24 33	5.9	K2	+ 39.5	0.4	3
5268‡.....	194	0 49.2	−09 17	6.4	G3	+ 44.2	2.4	3
5437.....	202	0 51.0	−11 48	5.5	K5	− 29.1	0.9	3
5722.....	211	0 53.7	−11 55	5.8	G7	− 18.1	1.2	3
5747*.....	+59°161	0 54.0	+59 59	7.2	G8	+ 16.7	1.3	3
5780.....	215A	0 54.3	+ 0 15	7.8	Mo	−103.0	1.1	5
5802†.....	+13°143	0 54.5	+14 04	9.0	Fo	+ 6.8	0.9	3
6130*.....	ADS 868A	0 57.4	+60 32	5.9	A9s	− 1.8	1.6	3
6203.....	228	0 58.0	− 5 22	5.7	K1	+ 15.8	0.4	3
6319.....	232	0 59.1	+86 37	6.4	K2	− 4.8	0.7	4
6482.....	237	1 0.6	−10 31	6.4	G8	+ 12.8	1.2	3
6473.....	239	1 0.7	+79 29	6.4	G6	− 27.5	1.3	4
6476.....	241A	1 0.7	+31 39	6.6	K2	+ 28.2	1.7	5
6680.....	248	1 2.5	+31 29	6.3	A7n	+ 17.6	1.7	5
6706.....	250	1 2.7	−10 19	5.9	F3	+ 21.4	1.1	3

* Selected Area star. † Proper-motion star. ‡ Velocity may be variable.

TABLE 1—*Continued*

HD	Star	α (1900)	δ (1900)	Mag.	Sp.	Vel.	P.E.	No.
7010*.....	+59°199	1h 5m.4	+59°58′	7.9	K0	+ 12.6	1.7	3
7147.....	273	1 6.6	− 2 47	6.2	K4	− 8.4	0.4	3
7238.....	276	1 7.7	+79 23	6.4	F5	− 43.1	1.0	3
7268.....	278	1 7.8	−07 19	6.9	G8	− 10.9	1.7	3
7439.....	285A	1 9.4	− 8 28	5.2	F2	+ 19.6	1.5	3
8036.....	302A	1 14.7	− 1 02	6.0	G3	+ 17.6	0.2	3
8110*.....	+14°204	1 15.4	+15 11	7.5	G6	+ 8.1	2.1	3
8248*.....	+15°198	1 16.7	+15 17	7.5	F4	+ 3.0	0.9	3
8829.....	322	1 21.9	−13 35	5.7	F1	+ 9.9	0.4	3
8875.....	324AB	1 22.5	+ 4 50	7.9	G0	− 15.1	1.1	3
8941.....	326	1 23.1	+16 34	6.8	F8	+ 8.5	0.2	3
9024.....	328	1 23.8	+ 6 47	6.7	F0	− 8.9	2.3	5
9856.....	351	1 31.1	−15 55	5.5	K1	+ 25.2	1.3	3
9919.....	356	1 31.8	+11 38	5.6	A5n	+ 3.0	2.8	4
10072.....	360	1 33.3	+43 53	5.5	G5	+ 9.1	0.8	3
10086*.....	+45°404	1 33.5	+45 23	6.7	G4	+ 4.8	1.1	3
10135.....	362	1 33.9	+13 47	6.9	K0	− 2.4	0.6	3
10204.....	368	1 34.7	+42 48	5.5	A0n	+ 24.9	1.4	3
10453B.....	381B	1 36.8	−11 49	7.4	F3	− 21.9	0.1	3
10486*.....	+44°354	1 37.2	+44 48	6.5	K2	+ 12.7	0.9	3
10597*.....	+45°432	1 38.3	+45 39	6.5	K5	− 17.4	0.8	3
10824.....	397	1 41.0	− 6 14	5.5	K4	+ 11.3	0.9	3
10975.....	402	1 42.7	+37 27	6.0	G7	+ 37.2	0.6	3
10995.....	404	1 42.9	+16 31	7.3	G0	+ 12.0	2.3	4
11131.....	408	1 44.5	−11 12	6.8	G1	− 3.0	2.0	6
11949.....	439	1 52.2	+48 43	5.8	G7	− 1.1	1.0	3
12641.....	473A	1 58.7	− 0 49	6.0	G5	+ 24.4	0.8	3
13228.....	485	2 04.1	− 2 48	7.1	F5	− 11.9	0.7	3
13555.....	501	2 07.2	+20 44	5.4	F4	+ 7.9	1.1	3
14044‡.....	516A	2 11.3	−10 17	7.5	G2	+ 31.0	2.7	5
14691.....	541	2 17.1	−11 14	5.6	A8n	+ 11.2	2.6	4
14770.....	542	2 17.8	+49 33	5.5	G5	− 12.2	1.1	3
15257.....	559	2 22.3	+29 13	5.4	A7n	− 24.8	1.3	3
15550.....	566	2 25.0	+19 25	6.1	A4n	+ 23.5	2.7	5
15634.....	569	2 25.7	−25 38	6.5	A9n	+ 24.5	1.3	3
15788*‡.....	+29°434	2 27.2	+29 31	7.8	G7	+ 11.8	2.4	3
15814.....	576	2 27.4	+14 36	6.4	F7	− 3.3	0.2	3
16042*.....	+30°414	2 29.5	+30 14	8.5	G4	− 14.7	1.6	3
16397*.....	+30°421	2 32.6	+30 24	7.2	G0	−100.8	0.9	4
16446.....	598	2 33.2	−23 26	6.9	G9	+ 24.8	1.3	3
16505.....	600	2 33.8	+67 38	7.8	K3	− 69.4	1.4	3
16784†.....	C 345	2 36.3	−30 34	8.1	F9	+ 33.9	2.2	3
17017.....	624	2 38.7	+17 20	6.5	K2	− 30.8	0.8	3
18145*.....	−0°450	2 49.7	− 0 28	6.7	G6	+ 6.4	1.8	3
18200.....	+51°657	2 50.3	+52 06	8.0	G6	− 40.5	1.0	3

TABLE 1—*Continued*

HD	Star	α (1900)	δ (1900)	Mag.	Sp.	Vel.	P.E.	No.
18262.....	662	$2^h50^m.9$	+ 7° 59′	6.1	F7	+ 28.8	1.2	5
18535.....	676	2 53.6	−24 00	6.0	K2	+ 7.9	0.5	4
18766*.....	+59°588	2 56.0	+59 55	7.2	F4	− 50.9	2.2	3
19270‡.....	704	3 00.9	+12 48	5.8	Ko	− 16.0	1.7	3
19305†.....	+1°543	3 01.2	+ 1 36	8.9	Mo	− 21.4	1.4	4
19968*.....	+60°651	3 07.5	+60 45	8.0	B5s	− 7.1	4.3	3
20084.....	726	3 08.6	+84 33	6.1	G4	+ 31.9	0.9	3
20290.....	736	3 10.7	− 9 08	6.8	K2	+ 15.0	0.2	3
20395.....	743	3 11.7	− 9 31	6.2	F4	− 5.8	0.8	3
20512*.....	+14°550	3 12.9	+14 49	7.7	G4	+ 10.4	0.6	3
20610.....	750A	3 13.9	−22 53	5.0	G6	+ 21.8	1.2	4
20618.....	751	3 14.0	+26 43	5.9	G5	− 0.5	1.9	3
20709.....	760	3 15.1	+72 51	7.3	K2	− 19.7	1.8	4
20791.....	763	3 15.9	+ 3 19	5.8	G8	+ 11.7	1.5	4
21467‡.....	792A	3 22.6	+22 28	6.1	G6	+ 44.2	2.3	4
21530.....	794	3 23.2	−11 38	5.8	K2	− 1.3	1.3	6
21834*.....	+29°571	3 26.1	+29 39	8.0	A5n	+ 2.5	2.3	3
22409.....	822	3 31.2	−11 32	5.7	G7	+ 37.0	1.9	4
22701.....	830	3 33.9	+86 20	5.8	F1	− 4.7	1.2	3
22796.....	835	3 34.6	+ 2 44	5.8	G6	+ 21.2	1.0	3
23082*.....	+44°782	3 37.2	+44 34	7.8	cK5	+ 8.2	1.4	4
24546.....	900A	3 49.2	+50 24	6.0	F4	+ 25.3	0.7	3
24740.....	908	3 51.0	+22 11	5.8	F3	+ 28.6	0.2	3
25102.....	+9°524	3 54.2	+10 02	6.4	F3	+ 39.8	2.0	3
25165.....	916	3 54.8	−12.51	5.9	K5	− 4.6	0.9	3
25230.....	921	3 55.3	+19 55	6.8	G4	+ 20.7	0.9	4
25723.....	942	3 59.7	−13 04	5.7	Ko	+ 32.4	2.0	3
25867.....	944	4 00.8	+28 44	5.3	F1	+ 7.6	1.5	3
26380*.....	+15°592	4 05.2	+15 41	7.2	Aon	+ 10.5	0.5	3
26659.....	968	4 08.0	+83 06	5.7	G4	− 38.2	0.3	3
26755.....	973	4 08.8	+57 37	5.8	K2	− 40.9	0.5	3
27497.....	1008	4 15.4	+05 54	5.9	G6	+ 7.4	1.2	6
27518.....	1009	4 15.5	−25 16	6.9	K5	− 28.8	1.2	3
27524.....	+20°740	4 15.6	+20 49	6.9	F2	+ 36.6	0.4	3
27971.....	1030	4 19.7	+31 13	5.3	G6	+ 26.7	2.2	3
28139.....	1037A	4 21.2	+18 54	7.7	F5	+ 40.8	2.0	3
28446B.....	1050B	4 24.1	+53 42	.....	B3s	+ 4.2	2.6	4
28556.....	1056	4 25.0	+13 30	5.5	F1	+ 37.9	1.3	3
28693‡.....	1060	4 26.3	+42 49	6.8	A8s	+ 0.8	2.3	5
29038†‡.....	C 593	4 29.2	+16 47	7.7	K4	+ 43.4	2.0	6
29737‡.....	1104	4 36.0	−24 41	5.9	G6	− 14.1	1.8	4
29859.....	1109	4 37.2	+23 54	6.2	F6	+ 5.8	0.8	6
30557.....	1134	4 43.6	+48 34	5.8	Ko	+ 29.5	1.0	3
30606.....	1137	4 44.0	−16 30	6.0	F6	+ 34.9	0.6	3
30604†.....	C 618	4 44.1	+70 28	8.6	G1	+ 44.6	2.5	3

TABLE 1—*Continued*

HD	Star	α (1900)	δ (1900)	Mag.	Sp.	Vel.	P.E.	No.
30812*	−0°785	4^h45^m7	−00° 16′	7.4	Ko	− 8.3	1.1	3
31296	1162	4 49.4	+ 7 37	5.5	K1	− 4.5	0.4	3
31444	1170	4 50.8	−16 35	5.8	G4	+ 31.8	1.9	3
31539	1174	4 51.6	+17 00	5.7	K1	+ 25.3	1.4	3
31647	1178B	4 52.5	+37 44	8.9	F9	+ 6.4	0.4	5
32008	1188	4 55.1	−10 25	5.7	G4	− 12.6	2.5	5
32503	1200	4 58.5	−22 56	5.8	K1	+ 33.0	0.6	3
34255	1255	5 11.0	+62 33	5.9	cK4	− 5.3	1.2	4
34531	1264	5 13.1	+78 13	6.8	F4	+ 15.0	1.3	6
34538	1263	5 13.1	−13 38	5.7	G9	+ 75.8	0.4	3
35067	1286	5 16.8	+ 3 28	7.7	M1	+ 51.4	0.8	3
35601*	+29°897	5 20.8	+29 50	8.0	Mo	− 0.7	1.1	3
35850	1319	5 22.4	−11 59	6.4	F7	+ 18.3	1.2	3
35984*	+29°909	5 23.4	+29 07	6.2	F2	+ 11.0	2.2	4
36044*	+29°911	5 23.8	+29 29	7.2	G6	+ 47.2	1.0	3
36719	1350	5 28.7	+47 39	6.0	Fo	+ 13.1	1.7	3
36947	+43°1315	5 30.1	+44 01	7.4	Go	− 18.7	1.7	5
37981	1406	5 37.3	+14 08	6.9	K1	+ 63.2	1.7	4
38182	1415A	5 38.8	+15 01	7.5	Go	+ 46.0	0.8	3
39099	1450	5 45.2	+14 01	6.8	Ko	− 47.1	0.8	3
41074	1506	5 57.9	+42 59	5.9	A8n	+ 33.6	1.6	3
41927	1530	6 02.8	+65 44	5.4	K2	+ 3.8	0.9	5
42341	1540	6 05.0	−14 34	5.7	K2	+ 31.6	0.7	3
42633	1552	6 06.7	+60 02	5.6	K4	+ 10.4	1.2	3
43624	1583	6 12.1	+27 15	6.7	Ko	− 53.4	1.4	3
44033*	1596	6 14.4	+14 42	6.0	Mo	+ 35.0	0.5	4
44974	1615	6 19.7	+21 42	6.6	G6	− 23.1	0.5	3
45352	1623A	6 21.8	+20 51	6.6	K2	− 29.6	1.9	4
45433	1630	6 22.1	− 0 13	5.8	K5	+ 39.3	1.3	3
45784*	+29°1248	6 24.4	+29 53	8.1	F2	+ 34.3	1.0	3
47174	1694	6 32.2	+42 35	5.1	K2	+ 16.8	0.4	3
47977	1712A	6 36.0	+59 33	8.3	F4	− 40.6	0.2	3
48410*	+44°1528	6 38.2	+44 20	7.8	Go	+ 4.6	0.2	3
48766	1727A	6 39.9	+55 49	6.3	F4	+ 8.8	2.0	3
48781	1728	6 40.0	+48 54	5.3	Ko	+ 0.9	1.3	3
49380	1745	6 43.2	+32 43	5.8	K4	− 15.5	1.0	3
51440	1794	6 52.2	+38 11	6.2	Ko	+ 27.1	1.4	5
51530	1796	6 52.6	+26 13	6.1	F4	+ 3.8	0.4	3
53633	1824	7 0.7	+60 57	6.7	K1	+ 1.8	0.6	3
54079	1832	7 2.4	+ 7 38	5.9	Ko	+ 24.4	0.8	4
54099*	+59°1053	7 2.5	+59 13	7.6	G7	+ 12.3	1.5	3
54131	1835A	7 2.6	+16 05	5.6	G8	− 15.2	1.6	3
56243*	1881	7 11.2	+59 26	6.9	K5	+ 8.6	1.6	5
56578	1888	7 12.4	−23 08	7.0	Fo	+ 36.4	0.9	4
57044	1900A	7 14.5	+73 16	7.1	A7n	− 33.1	1.8	3

TABLE 1—*Continued*

HD	Star	α (1900)	δ (1900)	Mag.	Sp.	Vel.	P.E.	No.
57478.....	1915	7^h16^m4	−14° 10′	5.7	G5	+ 13.7	0.3	3
58746*.....	+29°1535	7 21.9	+29 37	7.4	A8n	+ 13.4	0.3	3
60294.....	1980	7 28.6	+55 59	6.0	K2	+ 2.2	1.2	7
60341.....	1982	7 28.9	−19 12	5.8	K3	+ 16.9	1.6	5
60584‡.....	1989	7 30.1	−23 15	5.9	F4	− 5.7	2.4	3
60585.....	1990	7 30.1	−23 15	6.0	F5	− 6.6	1.5	3
60986.....	1997A	7 32.0	+35 16	5.6	G5	− 35.0	1.8	3
65158*.....	−0°1864	7 52.3	− 0 21	7.0	A2s	+ 31.9	1.1	3
65301.....	2101	7 53.0	+59 19	5.8	F2	− 40.3	0.8	4
67402.....	2149A	8 2.7	+27 46	6.8	G9	+ 14.4	1.5	3
67483.....	2152	8 3.1	+13 56	6.3	F5	− 14.1	1.9	3
67690.....	2156	8 4.2	+26 08	6.7	K3	+ 5.7	0.7	4
68771.....	2182	8 8.7	+59 30	6.7	K2	− 28.4	1.4	3
69054*.....	+75°334	8 10.1	+75 08	6.5	K1	− 31.2	2.0	3
69994.....	2205	8 14.5	+21 04	5.9	K1	− 12.7	1.1	3
70523.....	2215	8 17.4	−17 16	5.8	K0	+ 68.2	0.9	3
70673.....	2221	8 18.1	−12 44	6.3	G7	− 16.0	0.5	3
71152.....	2238A	8 20.7	+24 52	7.1	F1	+ 13.2	0.9	3
71704.....	2256	8 23.7	+67 38	7.8	G7	+ 6.2	0.7	3
72041.....	2263	8 25.6	+24 25	5.7	A9n	+ 18.2	2.1	4
72146*.....	+29°1772	8 26.2	+29 39	7.1	G6	+ 2.6	1.1	3
72673.....	2279	8 29.0	−31 11	6.4	G8	+ 18.5	1.3	4
72905.....	2284	8 30.3	+65 22	5.7	G0	− 14.1	1.5	3
72946.....	2286B	8 30.5	+ 6 58	7.2	G5	+ 27.2	1.1	4
72968.....	2287	8 30.6	− 7 38	5.6	A4sp	+ 24.0	0.3	3
73508.....	2304	8 33.7	+33 05	6.9	K0	+ 14.1	0.9	3
73593.....	2306	8 34.1	+46 11	5.5	G6	− 38.1	0.9	3
74576†.....	C 1026	8 39.6	−38 32	6.6	K5	+ 18.9	2.7	5
74688.....	2346A	8 40.3	− 2 14	6.7	F5	− 18.7	0.9	5
74794.....	2351	8 41.0	− 1 41	5.8	K0	+ 10.7	1.2	3
75117*.....	+45°1641	8 43.0	+45 20	7.6	F4	+ 19.6	1.4	3
75628.....	2369	8 45.5	+15 43	6.3	G2	+ 44.7	0.2	3
76291.....	2392	8 50.1	+46 01	5.9	K2	+ 56.1	0.2	3
76572.....	2401	8 51.9	+30 37	6.2	F3	+ 7.8	0.8	4
76813.....	2409A	8 53.4	+32 48	5.6	G9	+ 23.8	0.6	3
77570.....	2430	8 58.3	+51 13	6.7	F4	+ 13.1	0.8	3
77818*.....	+59°1218	8 59.7	+59 17	7.6	K0	− 38.6	0.5	3
78249*.....	+59°1221	9 2.1	+59 32	7.2	K2	+ 47.0	1.4	3
78391.....	ADS 7198A	9 3.9	− 6 44	8.4	F9	− 3.1	1.2	3
78479.....	2448	9 3.4	+17 52	7.4	K4	+ 77.0	1.9	3
79181.....	2466	9 7.4	−19 20	5.8	G9	− 0.2	1.6	3
79554.....	2480	9 9.7	+15 21	5.6	K1	+ 25.0	0.1	3
80290.....	2502A	9 13.8	+51 41	6.1	F3	− 8.2	0.7	3
80956.....	2518	9 17.7	+25 37	6.5	G2	− 1.6	1.4	3
81192.....	2527	9 19.1	+20 13	6.7	G5	+135.8	0.1	3

TABLE 1—*Continued*

HD	Star	α (1900)	δ (1900)	Mag.	Sp.	Vel.	P.E.	No.
81873	2539A	9^h23^m2	+ 8° 37′	5.9	K0	+ 22.7	1.6	5
81964†	+34°1998	9 23.9	+34 00	7.8	K3	− 57.5	0.5	3
82205	2548A	9 25.5	−26 09	5.7	K3	+ 12.3	1.1	4
82870	2572	9 29.6	− 5 28	5.7	K1	+ 13.1	1.7	4
83273	2583	9 32.1	+25 07	6.6	F8	+ 30.9	1.0	3
83332	2585	9 32.5	−24 51	5.9	K1	+30 .5	0.2	3
83343	2586	9 32.6	+14 48	6.6	F2	+ 26.1	2.0	3
83698	2597A	9 35.2	+39 24	7.3	G2	+ 4.5	0.8	3
84722	2624	9 42.1	+12 02	6.4	A3n	− 1.2	0.9	3
85217	2636	9 45.3	+ 4 49	6.7	F6	+ 19.6	1.4	5
85762	2654	9 48.9	+ 5 25	7.0	M0	+ 27.7	1.5	3
86322	2668	9 52.6	+75 14	7.1	K0	+ 6.9	1.1	5
87141	2684	9 58.0	+54 23	5.7	F4	− 16.6	0.3	3
87682	2693	10 1.6	+ 6 06	6.3	G6	+ 17.2	1.0	5
88048	2700	10 4.0	+ 6 40	6.8	K4	+ 26.8	1.5	6
88333	2708	10 6.0	− 7 56	5.8	K2	+ 0.7	1.7	4
88355	2711A	10 6.3	+13 51	6.8	F3	− 15.7	0.8	3
89024	+26°2064	10 11.1	+25 53	6.0	K0	+ 34.6	0.3	4
89376	ADS 7721A	10 13.7	+21 04	9.3	K5	+ 23.6	1.5	4
89396*	+15°2188	10 13.9	+15 10	8.5	K5	+ 54.2	1.7	3
90040	2761	10 18.4	+34 13	5.8	K1	− 24.2	1.2	3
90043	2759	10 18.4	− 0 24	6.6	K0	+ 0.5	2.1	3
90250	2765	10 20.0	+35 56	6.6	K0	+ 11.9	0.7	3
90485‡	2774	10 21.7	− 3 53	6.6	G7	+ 6.5	1.9	5
90717*	+30°2021	10 23.4	+30 15	6.7	K1	+ 2.6	0.9	3
90718	2782	10 23.5	+14 51	7.1	G5	+ 38.4	0.6	3
91011	2793	10 25.3	+ 2 40	7.1	K0	− 0.2	0.2	3
91163*	+30°2031	10 26.4	+30 14	7.8	F8	− 20.9	0.5	3
91256‡	2801	10 27.1	+ 5 10	7.2	G9	+ 7.7	2.8	5
92095	2828	10 32.9	+54 11	5.7	K3	+ 45.2	1.1	4
92196	2832	10 33.5	+16 39	6.6	F2	− 13.2	1.2	3
92354	2838	10 34.7	+68 58	5.9	K3	+ 3.8	1.3	3
92538†	C 1290	10 35.9	+66 32	8.7	G0	+ 2.5	0.4	3
92620	2847	10 36.6	+32 13	6.3	M5	+ 19.0	1.2	4
92749	2851A	10 37.5	+ 4 06	6.8	F5	+ 18.3	0.2	3
92841B	2858B	10 38.2	+ 5 16	7.1	G7	− 2.5	1.5	4
93013*	+45°1860	10 39.4	+45 30	8.2	G7	+ 13.1	1.3	3
93102	2864	10 40.0	+ 3 01	6.6	K4	+ 13.8	1.8	3
93213*	+44°2012	10 40.7	+44 38	8.0	F4	+ 25.5	1.4	3
93859	2890	10 45.0	+57 07	5.8	K1	+ 15.6	0.7	3
93875	2891	10 45.1	+59 51	5.7	K2	− 20.2	0.5	3
94084	2896	10 46.5	+53 02	6.6	K0	− 0.1	1.0	4
94480†	2904	10 49.3	+26 01	6.2	A5n	+ 5.1	2.5	6
94497	2907	10 49.4	+34 34	5.9	G7	− 27.4	1.4	3
94672‡	2913A	10 50.6	+ 1 16	6.0	F3	+ 8.2	1.7	5

TABLE 1—*Continued*

HD	Star	α (1900)	δ (1900)	Mag.	Sp.	Vel.	P.E.	No.
94738.....	2916A	10h51m0	+ 0° 58′	6.9	K3	− 27.1	0.2	3
†.....	+42°2163	10 51.4	+42 25	9.6	K3	− 25.6	2.2	4
94864*.....	+ 0°2718	10 52.0	+ 0 14	6.9	F4	+ 3.0	2.5	3
95808.....	2937A	10 58.3	−10 46	5.6	G6	− 8.0	1.5	4
95955†.....	C 1347	10 59.0	+66 21	8.5	K4	− 29.0	1.3	3
96813.....	+37°2162	11 3.9	+36 51	6.0	Mb	+ 22.7	0.7	3
97855.....	2977A	11 10.3	+53 19	6.3	F2	− 38.2	0.1	3
98354*.....	+15°2321	11 13.8	+14 49	6.9	F7	+ 24.2	1.6	3
98366.....	2988	11 13.8	+ 2 12	6.0	Ko	+ 5.7	1.5	3
98824.....	2994	11 17.3	+17 59	7.0	K2	+ 5.8	1.1	3
99055.....	3000	11 18.9	+ 1 57	5.5	G7	− 9.6	1.2	3
99285.....	3008A	11 20.4	+17 00	5.6	F2	+ 19.3	1.5	4
99564.....	3017	11 22.1	−11 48	6.0	F4	+ 5.2	0.9	3
100255*.....	+29°2179	11 27.2	+29 36	7.8	F2	+ 13.2	0.8	3
100470.....	+37°2195	11 28.6	+37 23	6.3	Ko	+ 22.0	0.5	3
100949.....	3059	11 32.0	−22 24	6.7	Ko	+ 22.1	1.5	3
101154.....	3066A	11 33.3	− 1 53	6.2	K1	− 14.5	1.2	3
101198.....	3070	11 33.6	−12 39	5.6	F5	− 24.3	1.0	3
101585*.....	+45°1955	11 36.3	+44 45	7.8	M3	+ 0.1	1.7	3
103327.....	3118	11 48.8	− 3 13	7.3	G6	+ 26.2	2.5	3
103462.....	3119	11 49.6	−25 10	5.5	G4	− 10.9	1.4	3
103932†.....	−26°8883	11 53.0	−27 08	7.2	K6	+ 57.0	0.7	4
104075.....	ADS 8374A	11 54.1	+33 43	6.0	Ko	− 0.2	1.3	3
104356.....	3140	11 55.9	− 1 13	6.4	G8	+ 36.1	0.9	4
104710*.....	+30°2217	11 58.4	+30 14	7.7	M5	− 3.7	0.8	3
104827B.....	3150B	11 59.2	+22 01	7.5	F2	+ 11.8	1.5	3
105089.....	3158	12 0.9	− 2 34	6.5	G8	+ 17.1	1.2	3
106574.....	3189	12 10.4	+70 45	5.9	K2	− 10.9	0.7	4
106798.....	3196A	12 11.9	+80 41	7.3	A8n	− 10.6	2.7	4
106888*.....	+15°2441	12 12.5	+15 00	8.1	F8	− 0.2	2.3	3
106975§.....	3201B	12 13.0	− 3 24	7.0	F5	+ 0.1	0.9	3
106976§.....	3201A	12 13.0	− 3 24	6.6	F4	− 1.1	....	2
107161.....	3205A	12 14.2	− 8 22	7.0	Ko	− 11.2	0.5	3
107170*.....	+15°2445	12 14.3	+15 07	6.7	G9	+ 25.9	1.3	3
107288*.....	+14°2489	12 15.0	+14 25	6.9	Ko	+ 9.2	0.8	3
107705.....	3223A	12 17.4	+05 52	6.5	F7	+ 4.6	0.4	3
107815.....	3226	12 18.1	−24 17	5.8	K1	− 1.8	0.8	3
108421.....	ADS 8553A	12 22.2	+27 35	9.2	K5	− 0.8	0.9	3
108477.....	3246	12 22.6	−16 05	6.5	G4	− 8.8	1.0	3
108877.....	ADS 8576A	12 25.5	+ 4 04	7.4	G7	− 4.3	1.5	3
108954.....	3267	12 26.1	+53 37	6.2	F7	− 19.7	1.2	3
109014.....	3270	12 26.5	− 4 30	6.3	G9	+ 2.7	1.1	3
109213*.....	+75°473	12 28.0	+75 22	7.5	G9	− 29.2	0.8	4
109272.....	3275	12 28.4	−12 17	5.8	G8	− 15.5	1.4	4
109519.....	+22°2490	12 30.2	+22 26	6.1	Ko	− 14.0	0.8	3

§ Combined velocity, −0.4 ± 0.6.

TABLE 1—*Continued*

HD	Star	α (1900)	δ (1900)	Mag.	Sp.	Vel.	P.E.	No.
109551.....	3287	12^h30^m5	+70° 34′	5.5	K2	+ 4.6	0.5	4
110646.....	3317	12 38.5	−01 02	6.1	G5	+ 0.2	0.4	4
110666.....	3318	12 38.7	−27 47	5.7	K4	+ 7.6	1.8	4
111199.....	3330	12 42.4	− 5 45	6.3	F5	+ 12.9	0.2	3
111631†.....	C 1633	12 45.6	− 0 13	8.7	Mo	+ 4.1	3.0	3
111892.....	3350B	12 47.4	+17 39	6.9	F5	+ 8.2	1.0	6
112374.....	3368	12 51.1	−25 55	6.8	cF6	− 22.0	1.1	5
112992.....	3378A	12 55.4	− 2 50	6.1	K2	+ 23.5	1.4	4
113337.....	3385	12 57.9	+64 09	6.0	F4	− 11.3	0.9	4
113459.....	3388	12 58.8	−03 08	7.2	A7n	+ 0.6	3.8	5
113847‡.....	3396A	13 01.4	+45 48	5.7	K2	− 19.2	1.5	5
113865*.....	+29°2365	13 01.4	+29 34	6.4	A3n	+ 2.0	1.6	4
114113‡.....	3404	13 03.3	−08 27	5.7	K3	+ 16.8	2.3	3
114493.....	ADS 8810A	13 05.8	+13 51	7.3	K2	− 17.8	1.8	4
114674.....	3423	13 06.9	+41 19	7.3	G6	− 1.6	1.5	3
115004.....	3432	13 09.2	+45 41	5.0	G9	− 19.9	1.1	3
115046.....	3434A	13 09.5	+11 52	5.8	Mo	+ 12.2	1.4	5
115136.....	+68°720	13 10.1	+67 49	6.8	Ko	+ 4.7	0.5	3
115466.....	3444	13 12.2	−10 01	7.2	A8s	+ 6.0	1.2	3
115539*.....	+14°2593	13 12.7	+14 18	7.3	G4	− 8.9	1.8	3
116010.....	3455	13 15.8	+40 41	5.7	K1	− 21.2	0.7	3
116175.....	3460	13 16.8	−12 03	7.1	M1	− 32.5	0.8	3
116365.....	3467	13 18.1	−04 24	5.9	K3	+ 10.3	0.7	3
116459.....	3470	13 18.6	+85 17	7.4	F7	+ 11.9	1.8	4
117267.....	3490	13 24.1	−00 51	6.4	Ko	+ 39.9	1.5	3
117246.....	3489	13 24.1	−18 13	7.0	K2	+ 19.8	1.5	3
117304‡.....	3492	13 24.3	+11 20	5.8	G9	− 4.4	1.9	3
117789.....	3503A	13 27.5	−14 51	5.6	K2	− 39.0	1.6	6
117818.....	3504	13 27.7	− 9 39	5.4	G5	− 1.5	0.2	3
117878.....	3505	13 28.2	− 7 07	7.1	A4n	− 17.1	3.2	3
118036*.....	+0°3075	13 29.2	+ 0 12	7.7	K1	− 1.7	0.6	3
118219.....	3510	13 30.3	− 4 53	5.8	G6	− 7.7	0.8	3
118330*.....	−0°2710	13 31.1	− 0 25	7.0	F6	+ 16.8	0.6	4
118328†.....	ADS 8959A	13 31.2	+68 17	8.9	G2	+ 19.8	1.6	4
118742.....	3522A	13 33.7	+39 41	7.9	G2	− 21.6	2.3	3
119461.....	3538A	13 38.3	−03 46	7.0	K4	+ 5.2	1.6	6
120164.....	3559	13 42.7	+39 03	5.6	G9	− 10.1	1.0	3
120565‡.....	3574	13 45.2	+83 15	6.2	G6	− 49.6	2.4	3
121107.....	3588	13 48.4	+18 26	5.7	G4	− 11.8	1.7	3
121825*‡.....	+44°2312	13 52.8	+44 46	7.6	F9	+ 22 3	2.1	3
122106.....	3608	13 54.6	− 3 04	6.3	F5	− 8.2	1.2	3
122430.....	3614	13 56.7	−26 57	5.7	K3	+ 0.5	0.2	3
122442*.....	+29°2483	13 56.8	+28 53	7.9	A7s	− 2.8	1.3	3
122992*.....	+29°2486	14 00.0	+29 37	8.2	M4	− 16.1	1.5	3
123255.....	3625	14 01.4	−08 50	5.5	A8n	− 36.5	2.9	4

TABLE 1—*Continued*

HD	Star	α (1900)	δ (1900)	Mag.	Sp.	Vel.	P.E.	No.
123409*	+29°2493	14^h02^m4	+28° 54′	7.0	G6	− 54.6	0.7	3
124674	3652B	14 09.9	+52 15	6.9	F1	− 17.5	1.1	7
125180*	+15°2690	14 12.7	+15 44	6.0	M_3	− 7.8	1.1	3
126218	3695	14 19.1	−24 21	5.4	G8	− 22.7	1.4	3
127168	3714A	14 24.8	− 3 48	7.0	F1	− 27.5	0.5	4
128902	3740	14 34.5	+44 04	5.9	K_2	− 49.6	1.3	3
128941	3741AB	14 34.7	+52 01	7.6	F_4	− 23.8	1.6	3
129230*	+0°3223	14 36.3	+ 0 32	8.1	G_7	+ 23.1	1.8	3
	ADS 9352A	14 38.0	+19 56	9.9	Mo	− 16.0	2.3	3
129798	3762A	14 39.6	+61 41	6.3	F_4	− 6.8	1.1	3
129926B	3766B	14 40.2	−25 01	6.9	F_9	− 20.4	0.6	3
129978	3768	14 40.4	−15 02	6.6	K_2	− 39.3	0.8	3
129980	3769	14 40.5	−20 45	6.4	F_9	− 0.7	1.3	4
130144	+15°2758	14 41.4	+15 33	6.1	M_5	− 21.8	0.5	3
130157	3773	14 41.5	−20 54	6.1	K_5	− 23.6	2.1	4
130741*	+44°2393	14 44.8	+44 39	9.4	F_5	− 1.6	2.6	3
130945	3789	14 45.7	+46 32	5.8	F_4	− 5.4	1.7	3
130948	+24°2786	14 45.8	+24 20	5.8	G_2	− 6.7	0.1	3
131027	3792	14 46.2	−17 57	6.8	G_7	− 21.4	1.8	4
131041A	3793A	14 46.3	+49 07	6.1	F_6	− 34.0	0.6	3
131315*	+45°2229	14 47.8	+45 20	8.5	Go	− 25.6	0.8	3
131507	3803	14 48.9	+59 42	5.7	K_4	+ 12.6	1.2	4
131530	3804	14 49.0	−11 29	5.8	G_7	− 23.3	1.5	3
132683†	C 1989	14 55.3	−10 44	9.3	Mo	+ 14.3	2.1	4
133544*	+29°2618	15 00.0	+29 26	7.8	A2n	− 18.1	0.3	3
133670	−21°4030	15 00.6	−21 39	6.1	Ko	+ 5.2	1.0	3
133872	3851	15 01.7	+84 20	7.1	K_3	− 11.5	1.6	4
134066A	ADS 9507A	15 02.7	+ 9 37	6.7	Go	− 35.0	1.0	4
134066B	9507B	15 02.7	+ 9 37	7.0	Go	− 34.7	0.5	3
134323	+13°2901	15 04.1	+13 37	6.1	G_6	− 47.1	1.7	4
135208	3873A	15 08.8	−18 03	6.7	F_3	− 24.9	0.8	4
135244*	+59°1632	15 09.0	+59 26	7.6	K_5	− 10.8	0.3	3
135534	3884	15 10.6	−22 02	5.7	K_5	− 4.8	1.9	4
136479	3904	15 15.8	− 5 28	5.6	K_1	− 32.5	1.7	7
136512	3908	15 16.0	+29 59	5.6	G_7	− 53.3	1.0	4
136801	3913	15 17.5	−14 47	6.7	Mo	+ 14.2	1.0	3
136956	3917	15 18.4	−12 01	5.8	G_6	− 25.5	1.2	4
137949	3941	15 23.9	−17 06	7.2	F1p	− 31.6	1.2	5
138562	3948	15 27.8	− 0 51	5.8	G_9	− 15.6	0.5	3
138852	3958	15 29.5	+64 33	5.9	G_5	+ 10.6	1.2	3
139087	+11°2826	15 31.1	+11 35	6.1	G_9	− 26.7	1.9	3
139225	3970	15 31.9	+16 27	5.9	A6n	− 0.4	2.6	4
139254	3971	15 31.9	−22 49	5.8	Ko	+ 7.6	1.8	3
139446	3974	15 33.1	−18 58	5.5	G_2	+ 46.6	0.4	3
139457	+10°2886	15 33.2	+10 35	7.0	F_6	+ 38.1	1.4	3

TABLE 1—*Continued*

HD	Star	α (1900)	δ (1900)	Mag.	Sp.	Vel.	P.E.	No.
139460	3975B	15^h33^m3	−08° 28′	6.6	F6	+ 3.0	1.0	4
139569A‖	ADS 9727A	15 33.8	+30 26	8.8	F6	− 24.4	1.6	3
139569B‖	ADS 9727B	15 33.8	+30 26	9.0	G1	− 27.7	2.2	3
139590	+ 0°3387	15 33.9	+ 0 01	7.6	F9	− 28.0	1.1	3
139641	3979	15 34.2	+60 41	5.4	G5	− 8.3	0.9	4
139778	+54°1758	15 35.0	+54 51	6.0	K0	− 22.3	0.8	3
139892	3988B	15 35.6	+36 58	5.1	B7s	− 19.1	2.3	5
140301	3996	15 37.8	−14 43	6.4	K0	+ 21.0	1.1	3
140538	4000A	15 39.0	+02 50	5.8	G5	+ 18.9	1.4	4
141353	+14°2940	15 43.6	+14 06	6.1	K0	− 50.5	1.0	3
143393*	+29°2748	15 55.0	+29 44	7.2	K3	+ 18.3	0.8	4
143803	4079	15 57.4	+75 52	6.9	G5	− 18.4	0.5	3
143807*	4080	15 57.4	+30 07	4.9	A0s	− 24.3	1.1	3
	+35°2774	16 02.9	+34 55	10.5	M0	+ 8.7	1.4	3
145085	+ 3°3132	16 04.0	+ 3 43	6.1	K5	+ 9.8	0.9	3
145772	βGC 7542A	16 07.6	+14 49	8.1	K4	+ 35.2	1.8	4
145809	4127	16 07.8	−21 09	6.7	G0	+ 16.2	0.1	3
146169	4136	16 09.9	+ 8 07	6.8	K4	− 19.8	0.6	3
146388	4139	16 11.0	+19 04	5.9	K3	− 17.3	0.7	6
146436	4140	16 11.1	−19 51	6.6	G8	− 32.8	1.1	3
147142*	4157	16 15.0	+75 28	6.5	K3	− 25.3	1.1	5
148374	4191A	16 22.5	+61 55	5.9	G7	− 24.3	1.2	3
150117	4232A	16 33.9	+53 08	5.6	A0n	− 12.0	2.0	4
150118	4232B	16 33.9	+53 08	6.6	A0n	− 18.0	0.6	4
150449‡	4240	16 36.0	+56 13	5.4	K0	− 20.1	2.4	3
151415	4267A	16 42.1	−24 21	7.5	M0	− 74.5	1.5	3
151837	4275	16 44.8	+55 35	7.0	K5	− 6.5	0.9	5
152173‡	4286	16 46.7	+29 59	5.9	M1	− 8.0	1.9	5
152534	4298	16 48.8	−23 21	7.0	G7	− 26.0	1.2	3
153166	4314	16 52.7	+60 31	7.2	K3	− 41.7	1.8	3
154084	+25°3183	16 58.2	+25 40	6.0	G7	− 50.6	1.1	3
154127*	+29°2924	16 58.5	+29 26	7.5	A3n	− 27.0	1.5	3
154212	4339	16 59.0	−10 57	7.1	K2	− 23.7	1.1	3
154227*	+29°2927	16 59.1	+29 38	8.0	K3	− 2.6	0.6	3
154779	4352	17 02.4	−17 29	6.1	K0	− 13.2	1.9	3
155967*	+14°3206	17 09.7	+14 42	8.1	F2	− 16.7	1.9	3
156115*	−15°4502	17 10.6	−15 06	6.8	M0	− 7.7	0.4	3
156164B	4376B	17 10.9	+24 57	8.3	G4	+ 5.0	2.5	3
156350	4383B	17 11.9	−24 11	6.9	F5	− 28.9	1.3	4
156365	4385	17 12.0	−23 58	6.7	G3	− 15.2	0.6	3
157089	+ 1°3421	17 16.1	+01 32	7.0	F5	−161.1	2.4	4
157498	4412	17 18.5	− 9 16	7.8	G1	− 38.2	0.7	3
158974	4440	17 27.1	+31 14	5.8	G8	− 25.9	1.5	3
159501	4455	17 29.9	+41 19	5.8	K1	− 28.3	1.5	4
160018	−10°4528	17 32.6	−10 52	5.9	G8	− 32.0	0.7	3

‖ Combined velocity, −26.0± 1.3.

TABLE 1—*Continued*

HD	Star	α (1900)	δ (1900)	Mag.	Sp.	Vel.	P.E.	No.
160042	4467	$17^h32^m.7$	−21° 51′	6.7	G7	+ 0.2	1.5	5
160181	4468	17 33.4	+24 22	5.7	A0	+ 1.0	0.9	6
160290	4471	17 34.0	+48 39	5.5	K1	+ 31.5	1.6	3
160315	4472A	17 34.1	+ 2 05	6.4	K0	+ 3.2	1.2	3
†	20C 1062	17 40.9	+43 26	10.3	M3	− 21.5	1.7	4
162757	4515	17 47.5	−10 53	6.3	K1	− 34.2	1.3	3
162989	4518	17 48.8	+40 00	6.1	K4	− 61.6	1.6	4
163532	4529	17 51.5	− 4 04	5.6	G9	− 35.4	0.7	3
163589*‡	+45°2620	17 51.8	+45 33	8.2	G3	− 37.6	2.5	3
163608*	+45°2621	17 51.9	+45 13	8.0	A2n	− 25.6	1.9	5
163966*	+45°2626	17 53.8	+45 01	6.8	A0n	− 21.9	0.9	3
163990*	+45°2627	17 53.9	+45 28	6.2	M6	+ 16.5	1.6	3
164031	4540	17 54.1	−24 17	6.7	K0	− 25.4	0.7	3
164253*	+30°3096	17 55.2	+30 03	7.3	G4	− 20.3	0.9	4
164595*	+29°3165	17 56.8	+29 34	7.2	G1	+ 6.7	1.2	3
164755*	+30°3106	17 57.6	+30 39	7.1	K4	− 28.6	1.0	3
165281	+30°3113	18 0.1	+30 24	6.7	F7	+ 1.2	0.9	3
165438	4574	18 0.9	− 4 46	5.9	K1	− 18.4	1.7	3
165687	4579	18 2.0	−17 10	5.7	K1	− 31.9	1.5	3
166460	4597	18 5.7	+ 3 18	5.7	K2	+ 10.0	1.0	3
167027	4608	18 8.3	+56 15	7.5	K3	− 51.8	0.9	3
167036	4607	18 8.3	−21 44	5.7	K3	− 58.4	1.9	4
167570	4616	18 10.6	−20 35	7.1	G2	− 16.6	1.7	4
167720	−17°5112	18 11.4	−17 24	6.0	K3	− 6.7	0.3	3
168432	ADS 11257A	18 14.3	− 5 0	7.8	F6	− 10.9	0.8	3
169028	4647	18 17.6	+51 18	6.5	K1	− 9.8	1.3	6
169191	4651	18 18.4	+17 47	5.5	K2	− 19.2	1.2	4
169666	4659	18 20.7	+71 28	7.8	F2	− 40.9	0.2	3
170433	4676	18 24.3	−18 48	5.8	K0	− 0.9	1.0	3
170657	4684	18 25.5	−18 58	7.0	K0	− 47.7	1.1	3
170975	4694	18 27.0	−14 56	5.9	cK5	+ 1.6	0.6	3
171237	4700	18 28.4	−24 18	6.4	cF3	+ 9.2	0.6	3
171746A	ADS 11483A	18 31.4	+16 51	6.2	F9	+ 8.6	1.1	3
171746B	ADS 11483B	18 31.4	+16 51	7.2	G0	+ 1.6	0.2	3
172085‡†	C 2446	18 33.1	+24 21	7.4	F9	− 37.2	2.0	6
173399	4741A	18 40.0	+44 50	7.1	G2	− 35.6	0.9	4
173666*	+44°2983	18 41.4	+44 47	7.8	F4	− 35.2	0.6	3
174504*	+45°2777	18 45.7	+45 09	6.8	A9s	− 15.5	1.2	3
175317	4791	18 49.8	−16 30	5.6	F5	− 42.3	1.3	3
175466	4795	18 50.3	+42 47	6.9	K5	− 14.8	1.8	3
175515	4798	18 50.6	+ 6 29	6.0	G9	− 23.0	0.7	3
175751	4808	18 51.7	− 5 59	5.0	K2	− 91.1	0.5	3
172232	4818	18 54.2	+13 46	5.9	A6sp	+ 13.8	0.3	3
176408	4822	18 55.1	+57 41	5.7	K3	− 33.5	1.5	3
176593	4828	18 55.8	−15 25	6.4	G6	+ 20.8	1.0	3

TABLE 1—*Continued*

HD	Star	α (1900)	δ (1900)	Mag.	Sp.	Vel.	P.E.	No.
176598	4829	18^h56^m0	+65° 07′	5.8	G5	− 4.1	1.4	4
230409†	+18°3991	18 56.4	+18 57	10.0	G4	− 19.4	2.2	4
177463	4853A	18 59.7	− 4 11	5.5	K1	− 17.2	0.8	4
177809*‡	+30°3409	19 1.1	+30 35	6.4	M2	− 15.7	2.1	5
178003*	+29°3472	19 1.9	+29 46	6.6	Mo	− 27.7	1.0	3
179130‡	4879	19 6.3	−14 45	7.4	K3	− 37.6	3.2	4
179484BC	ADS 12145 BC	19 7.8	+38 37	8.7	G4	+ 25.3	1.0	6
179785*	+14°3830	19 8.8	+14 46	7.4	K4	− 32.1	1.1	3
180006	4894	19 9.8	+56 41	5.2	G7	− 12.9	0.9	3
180928*	4915	19 13.3	−15 43	6.3	K4	− 17.3	1.2	6
181645‡	4935	19 16.0	−18 30	6.0	G9	− 12.2	1.8	5
182416	4944	19 19.4	−24 10	5.6	K4	+ 40.0	1.9	4
182998	4968	19 22.3	−18 34	6.9	K5	− 31.6	0.9	3
183968*	+59°2038	19 27.0	+59 34	7.8	K4	− 24.9	1.0	3
184835	5001	19 31.3	−18 27	5.9	K3	− 6.8	1.9	3
184985	5006	19 31.9	−14 31	5.6	F6	− 14.7	0.5	3
185128	5008	19 32.5	− 4 52	5.5	F1	− 37.8	1.4	3
185194	5010A	19 32.8	+16 14	5.7	G8	− 33.6	1.4	3
185394	5013	19 33.7	+63 13	6.6	K4	+ 9.2	1.8	3
185467	5016	19 34.1	−23 39	6.1	K1	− 27.6	1.0	3
187810*	+44°3265	19 46.8	+44 54	8.3	Ko	− 20.1	1.4	3
189231	5114	19 53.8	+64 27	6.9	K1	+ 0.7	0.3	3
190403*	+29°3873	19 59.7	+29 42	6.8	G5	− 11.6	1.3	3
191067	5159	20 2.9	− 0 58	6.0	K1	− 2.6	1.0	3
191277	5165	20 4.0	+61 42	5.6	K3	+ 6.0	0.2	3
191753	5174	20 6.4	−12 41	6.4	G9	+ 1.4	0.4	3
192107	5179	20 8.1	− 1 19	5.6	K5	− 27.7	1.8	5
192145*	+15°4089	20 8.2	+15 47	7.6	F4	+ 3.7	1.8	3
192781	5194	20 11.6	+60 20	6.2	K5	0.0	1.4	3
192879	5198	20 12.1	−22 17	6.0	G8	− 17.3	0.8	3
194577	5238	20 21.3	+21 05	5.8	Go	− 21.1	0.3	3
194765‡	5242A	20 22.3	− 2 26	6.6	F2	− 16.7	1.7	5
194959	5246	20 23.3	−17 46	6.8	F8	− 14.9	1.6	4
194960	5247D	20 23.3	−18 12	6.7	G8	+ 4.4	1.8	4
195019	+18°4505	20 23.7	+18 28	6.8	G2	− 93.2	0.7	3
196348	5285	20 31.7	−15 30	6.9	K2	+ 19.0	0.5	3
196565	5293	20 33.2	+81 06	6.9	G9	− 3.6	0.2	3
197039	5314	20 36.0	+15 17	6.8	F6	− 31.6	0.9	3
198237*	+45°3275	20 43.9	+45 13	6.7	Mo	− 5.4	0.8	3
198390	5358A	20 44.9	+12 10	6.0	F4	+ 0.8	0.4	3
198431‡	5360	20 45.2	−12 55	6.0	K1	− 43.6	2.5	3
198802	5372	20 47.6	−11 57	6.4	G1	− 1.3	0.9	5
199012	5374	20 49.1	−18 18	5.9	Ko	− 38.4	1.5	5
199098*	5376	20 49.8	+44 48	5.6	G8	− 26.5	0.7	4
199101	5378	20 49.8	+33 03	5.7	K5	− 7.5	1.5	5

TABLE 1—*Continued*

HD	Star	α (1900)	δ (1900)	Mag.	Sp.	Vel.	P.E.	No.
199191	5381	20^h50^m4	+54° 08′	7.2	G6	−195.0	0.5	6
199223	5382A	20 50.7	+ 4 09	6.2	G6	− 30.5	2.0	6
199665	5395	20 53.6	+10 27	5.6	G6	+ 3.7	1.3	3
199870	5401	20 54.7	+44 05	5.8	G7	− 19.4	1.6	5
199960	5406	20 55.3	− 5 07	6.3	G1	− 17.9	1.1	3
200256	5413A	20 57.3	+ 6 47	7.4	F3	− 5.2	1.4	3
200465	5416A	20 58.5	+39 07	6.5	K3	− 7.4	1.3	3
200497	5418A	20 58.8	− 6 13	6.2	G4	+ 2.0	1.6	3
201194*	+30°4322	21 2.9	+30 12	7.5	B3n	− 15.6	0.4	3
202403	5459A	21 10.5	+40 44	7.8	G5	− 12.5	0.9	4
203364	5483	21 16.6	− 9 45	6.9	K3	− 51.2	1.9	4
203380A	5485A	21 16.8	+52 33	6.9	F6	+ 33.1	1.0	4
203380B	5485B	21 16.8	+52 33	6.9	G5	+ 33.5	1.1	3
203638	5494	21 18.5	−21 17	5.5	K2	+ 23.0	1.4	3
†	+41°4115	21 18.7	+41 26	9.1	K4	+ 23.5	2.4	4
203926	5503	21 20.1	− 3 59	5.7	K4	− 24.0	0.4	3
204692	5521	21 25.2	−14 44	6.8	K2	+ 3.7	0.5	3
205072	5533	21 27.8	+80 05	6.1	G6	+ 3.8	0.9	3
206078	5561	21 34.5	+61 51	7.7	G6	− 74.4	0.5	3
207489	5612	21 44.9	+38 29	7.2	cGo	− 58.1	1.5	3
207920	5622	21 47.5	− 4 28	6.7	G5	+ 7.4	1.6	4
207978	5625	21 48.0	+28 20	5.6	Fo	+ 16.3	1.3	3
208111	5631	21 49.0	− 4 45	5.9	K2	− 36.8	0.9	3
209964*	+29°4585	22 2.0	+30 05	8.7	F3	+ 13.0	1.0	3
210060*	+29°4586	22 2.6	+29 49	7.4	K2	− 9.0	2.6	3
211800*	+14°4772	22 14.6	+15 03	7.2	M1	0.0	0.5	3
*	+15°4622	22 15.0	+15 20	9.3	K3	− 21.1	0.2	3
212271	5768	22 17.9	−25 16	5.6	G9	− 10.0	1.5	3
212790	5788	22 21.9	+53 18	7.4	K2	− 33.8	1.6	3
213022‡	5792	22 23.4	+70 16	5.7	K2	− 16.3	2.7	4
213042†	C 2920	22 23.6	−30 30	7.8	K6	+ 5.8	1.2	3
213179	5798	22 24.5	+26 15	6.0	K2	− 45.3	1.6	6
214128‡	5830	22 31.0	+19 46	6.7	K2	− 32.3	2.8	4
214567	5840	22 34.0	+19 00	5.8	G7	− 21.3	1.2	3
216174	5887	22 45.6	+55 22	5.6	Ko	− 35.8	0.4	3
216380	5896A	22 47.5	+61 10	6.1	G3	+ 1.3	1.0	3
216777†	20C 1391	22 50.5	− 8 21	8.9	G1	− 24.2	1.3	4
217264	5924A	22 54.3	+ 0 26	5.6	K1	− 10.6	1.5	3
217303	5925	22 54.7	−25 42	5.8	Ko	− 34.4	0.5	3
218043*	+30°4869	22 59.8	+30 45	6.8	F2	− 8.9	1.9	3
218300*	+30°4875	23 01.8	+30 29	8.4	Ko	− 3.6	1.5	3
218527	5959	23 03.6	+ 1 35	5.6	G4	− 18.3	1.0	3
219945	6001	23 14.8	+48 05	5.4	Ko	+ 11.3	0.6	3
220088‡	6006	23 15.9	+29 52	5.8	Mo	− 18.7	2.0	6
220102*	+59°2701	23 16.0	+59 44	6.7	cF3	− 21.9	1.0	3

TABLE 1—*Continued*

HD	Star	α (1900)	δ (1900)	Mag.	Sp.	Vel.	P.E.	No.
220363.....	6015AB	23^h18^m0	+11°46′	5.3	K4	− 1.5	0.4	3
220766.....	6028A	23 21.3	−22 17	6.6	Ko	+ 11.6	1.1	3
221146.....	6043	23 24.4	−01 35	7.1	Go	− 14.9	1.1	3
221409.....	6051	23 26.8	−01 38	6.5	K1	− 22.0	0.4	3
221438*.....	+59°2740	23 27.1	+59 59	9.2	A4s	− 5.6	1.3	3
221639*.....	+59°2744	23 28.7	+59 52	7.3	G9	+ 0.8	0.6	3
221758.....	6061	23 29.7	+32 57	5.7	Ko	− 2.3	0.7	3
*.....	+60°2582	23 30.8	+60 22	8.9	B8	− 64.2	3.1	3
222455*.....	− 0°4547	23 35.6	− 0 08	7.7	K4	− 1.7	0.1	3
223096*.....	− 0°4566	23 41.5	− 0 01	7.4	G7	+ 1.3	0.2	3
223170.....	6104	23 42.1	−12 28	5.9	K1	+ 11.7	0.4	3
223238†.....	C 3121	23 42.7	+ 3 36	8.2	G2	− 16.5	1.4	3
223252.....	6107A	23 42.8	− 3 19	5.6	G8	− 6.4	1.9	3
223792.....	6130	23 47.6	+21 11	6.8	G6	− 2.7	0.4	4
224103.....	6139	23 50.0	+ 6 31	6.1	A1	+ 18.3	1.2	4
224152.....	6141	23 50.5	+52 11	6.8	K3	− 1.4	1.9	3
224402*.....	+ 75°901	23 52.5	+75 45	7.7	Aon	+ 6.8	1.4	3
224661.....	6159	23 54.5	− 6 27	6.8	G7	+ 13.7	0.9	3
225010.....	6177	23 57.5	+65 33	7.5	A1	− 6.7	1.3	3
225197.....	6181	23 59.2	−17 05	5.8	K2	+ 26.4	0.2	3

TABLE 2

MEASURES OF 69 SPECTROSCOPIC BINARIES

HD	Star	α (1900)	δ (1900)	Mag.	Sp.	Range	No.
1210Ft....	ADS 218A	0^h11^m4	+54° 07′	8.1	A6n	+ 41, − 1	4
6114*.....	ADS 862A	0 57.3	+46 50	7.2	A3n	+ 50, −69	5
8909.....	+29° 243	1 22.7	+30 02	6.9	F4	− 10, −31	4
10783.....	+ 7° 275	1 40.4	+ 8 04	6.6	A3sp	+ 31, + 3	3
12558.....	470A	1 50.0	+25 27	5.9	F4	+ 24, +13	3
14044.....	516A	2 11.3	−10 17	7.2	G0	+ 42, +20	5
14597†.....	+14° 383	2 16.3	+15 04	7.9	A0	+ 65, +16	4
16663†.....	+44° 558	2 35.2	+45 41	8.4	F8	+ 30, + 4	3
‡.....	+48° 740	2 36.4	+48 35	9.0	K3	+ 16, −47	5
18538.....	678Ft	2 53.7	+51 37	6.8	A1n	+ 16, −10	4
19926§.....	720	3 07.1	+ 6 17	6.1	cG2	+ 19, −12	5
‡.....	C 431	3 10.8	+30 40	9.7	K5	+ 52, +19	4
20631.....	753A	3 14.1	−18 55	6.1	F2	+ 44, + 2	7
23643*.....	+23° 539	3 41.5	+23 24	8.1	A3n	+123, −26	4
25202*.....	919	3 55.0	+17 55	6.3	A9n	+138, −43	8
27429*.....	+18° 624	4 14.6	+18 29	6.0	F0	+ 88, −64	2
27483*.....	+13° 665	4 15.2	+13 38	6.8	F2	+118, −28	3
29678.....	1100	4 35.4	+75 46	6.3	A6n	+ 7, −30	5
30021.....	1113A	4 38.8	− 8 59	7.0	G6	+ 66, +23	3
37013.....	ADS 4200A	5 30.4	+21 56	7.2	F7	+ 41, + 7	6
40535.....	1491	5 54.3	− 9 23	6.3	F2	+ 29, + 4	4
41547*.....	1519	6 00.7	−10 14	5.8	F4	+ 73, − 9	3
42398.....	1541	6 05.4	+24 27	5.9	K0	+ 43, +11	4
43246.....	+28°1062	6 10.1	+28 54	7.3	A2p	+ 43, −67	5
48767.....	1726	6 39.9	+55 49	6.6	F6	+ 24, − 3	3
57049†.....	+15°1541	7 14.5	+15 21	6.5	A1n	+ 13, −19	3
58579.....	1941	7 21.0	+20 27	5.9	F0	+ 32, − 4	6
66751.....	2139	8 00.0	+70 01	6.5	F8	0, −16	4
69479.....	+ 4°1945	8 12.1	+04 31	7.0	F8	+ 12, −20	4
70442–3....	2212	8 16.9	−19 50	5.9	G0	+ 1, −28	6
71663‖.....	2254	8 23.4	−02 11	7.0	F0	+ 23, −70	16
78668.....	2453	9 04.4	−11 57	5.8	G6	0, −22	6
91106.....	2796A	10 26.0	− 7 07	6.4	M0	+ 17, −12	5
91706.....	2818	10 30.2	−22 40	6.2	F5	+ 33, +10	3
93526.....	βGC 5563A	10 42.7	−14 44	6.5	A2s	+ 15, −44	3
94671.....	2914	10 50.6	+18 41	7.6	G4	+ 2, −20	6
95976.....	2941	10 59.2	+38 47	7.4	F5	+ 14, − 1	5
97140†.....	+59°1353	11 05.8	+59 27	7.3	F9	− 4, −38	3
100238.....	3034	11 26.9	− 5 55	7.3	K1	+ 4, −30	3
105590.....	ADS 8440A	12 04.3	−11 18	6.8	G2	+ 15, − 7	4

* Double lines.

† Selected Area star.

‡ Proper-motion star.

§ The spectrum is veiled by that of companion.

‖ Double lines?

TABLE 2—*Continued*

HD	Star	α (1900)	δ (1900)	Mag.	Sp.	Range	No.
107642†.....	−14°3500	12h17m1	−15° 00′	6.7	K2	+ 14, −12	3
109944.....	3295A	12 33.6	− 3 49	7.2	Mo	+ 26, 0	4
115559.....	−17°3811	13 12.8	−17 47	9.2	G1	+ 34, −11	5
115903.....	3454	13 15.1	−10 47	7.1	Ko	+ 60, +35	4
135775¶.....	+10°2818	15 11.8	+10 04	6.6	F4	+ 1, −22	7
137629.....	3932	15 21.9	+47 25	7.2	F9	− 7, −31	5
139137†.....	3966	15 31.4	− 0 14	6.8	F5	− 5, −42	5
139461.....	3976A	15 33.3	− 8 28	6.5	F6	+ 14, −16	6
139813.....	3986Ft	15 35.2	+80 47	7.6	Ko	− 8, −42	8
140122†.....	+ 0°3389	15 36.9	+ 0 46	8.1	A7s	+ 17, −14	4
144208.....	4088	15 59.6	+36 54	5.9	F3	+ 22, −18	8
146604**....	4142	16 12.0	+23 22	6.6	G9	+ 19, + 5	6
146850†.....	−14°4398	16 13.3	−14 38	6.1	K4	− 24, −51	3
150937.....	4254	16 39.1	−23 00	6.9	F3	− 17, −49	4
161083.....	4485	17 38.4	−22 09	7.1	A5n	+ 30, −19	3
165590.....	ADS 11060A	18 01.6	+21 26	7.9	G1	+ 17, − 9	5
172712.....	4728A	18 36.6	+52 15	7.5	A1n	+ 72, − 7	4
175035.....	4801A	18 51.2	+33 50	6.4	G2	+ 1, −25	9
189379†.....	+29°3829	19 54.6	+29 40	7.4	F8	+ 40, −49	4
196925.....	5312	20 35.3	+80 44	6.1	G8	− 4, −20	3
197433*†....	+75° 752	20 38.7	+75 14	8.3	G4p	.....	3
198345††....	5355A	20 44.5	+47 28	5.6	K5	− 44, −17	8
204964†.....	+59°2387	21 27.0	+59 56	7.5	B2s	− 10, −31	4
206482.....	5571A	21 37.3	+57 08	7.1	F4	− 13, −32	4
212474.....	5775	22 19.4	− 1 42	7.1	G6	− 19, −48	7
213930.....	5821	22 29.8	+56 06	5.8	G6	0, −19	6
217888†.....	+30°4867	22 58.8	+30 32	8.1	A2s	+ 50, −75	4
221670‡‡†...	+59°2746	23 29.0	+59 54	7.7	G6	+ 13, − 4	4
221833§§....	6064	23 30.4	+ 0 46	6.6	K2	+ 15, + 3	4

¶ Victoria, −7.6± 1.4.
** Victoria, +15.0± 0.2.
†† Victoria, −29.5± 0.3.
‡‡ Victoria, +9, one plate.
§§ Probably binary with small range; Victoria, +7.8± 1.9.

CARNEGIE INSTITUTION OF WASHINGTON
MOUNT WILSON OBSERVATORY
March 1938

PHYSICAL PROCESSES IN GASEOUS NEBULAE

III. THE BALMER DECREMENT

JAMES G. BAKER[1] AND DONALD H. MENZEL

ABSTRACT

This paper contains a numerical solution of the equations derived and formally solved in two earlier papers of the series. Various tables of general interest, including those of functions $X_n = hR/n^2kT_e$ and $-[Ei(-X_n)]$, for useful astrophysical ranges of n and T_e are given. The Balmer decrement, computed under two alternative hypotheses—**A** for a nebula transparent to Lyman line radiation, and **B** for an opaque nebula—is tabulated. The latter hypothesis agrees better with the observed data. The conclusion is reached that the electron temperature, T_e, of the nebular gas cannot be effectively determined from observed Balmer decrement data, because the decrement is insensitive to temperature. In view of the extreme physical conditions that exist in nebulae, the partition of atoms among the various excited levels approaches surprisingly close to the thermodynamic value.

In papers I and II[2] of this series the fundamental equations for calculating the relative intensities of lines of the Balmer series were set up and formally solved. The present paper gives the numerical results and the comparison of theory with observation.

For the benefit of those whose interest is chiefly in the final results, we shall briefly recapitulate the theory and fundamental hypotheses on which the calculations were based. The energy emitted in a given Balmer line, say in the transition from level n to level 2, is given by

$$E_{n2} = N_n A_{n2} h\nu \,, \tag{1}$$

where N_n is the number of atoms per cubic centimeter in level n, A_{n2} is the Einstein spontaneous probability coefficient, and ν is the frequency. Outside of thermodynamic equilibrium, N_n must be calculated by balancing the number of atoms leaving a given quantum level against those entering, by all possible routes. We thus have an infinite set of simultaneous equations to solve, one equation for each level. The method of solving these equations, for certain specified physical conditions, was given in II. The results are most con-

[1] Society of Fellows, Harvard University.

[2] Menzel, *Ap. J.*, **85**, 330; **86**, 70, 1937.

veniently expressed in terms of a dimensionless parameter, b_n, defined by

$$N_n = b_n N_{nT} = b_n N_i N_e \frac{h^3}{(2\pi mkT_e)^{3/2}} n^2 e^{X_n}, \tag{2}$$

(II, Eq. [4]), where

$$X_n = \frac{hRZ^2}{n^2 KT_e}. \tag{3}$$

b_n gives the departure from thermodynamic equilibrium. For thermodynamic equilibrium, $b_n = 1$.

We have calculated the Balmer decrement on two alternative hypotheses about the nature of nebular excitation. Under **A** we assume that an electron enters quantum level n of an atom either by capture from the free state or by cascade from a higher discrete level. We neglect the radiation field of the star and assume that there is no reabsorption of Lyman line radiation. For **A** we distinguish two cases: $\mathbf{A}_1$, where an idealized hydrogen atom with the Gaunt g factor equal to unity was employed, and $\mathbf{A}_2$, where the exact g values were introduced. Comparison of the results indicates how far calculations based on the simpler assumptions may be trusted and in what directions the deviations will tend. In a nebula that is very opaque to Lyman line radiation, we may take account of the nebular radiation field, but not of the stellar, by assuming that absorptions from level 1 to level n are exactly balanced by the inverse spontaneous transitions. Zanstra has based his theoretical calculations on this assumption, which we shall designate as **B**. In II the radiation field was entirely neglected. We may allow for it, under **B,** by redefining the quantity t_n as

$$t_n = \sum_{2}^{n-1} - u_{n'n} \tag{4}$$

instead of

$$t_n = \sum_{1}^{n-1} - u_{n'n}. \tag{5}$$

The remaining terms of the previous equations are unaltered, and the solution is carried out as before.

The numerical calculations were laborious, and various intermediate results of astrophysical interest have been tabulated with the hope that they may prove useful to others. The tables cover a large range of temperatures and quantum numbers. A sufficient number of figures was carried in the calculations to insure the correctness of the values as tabulated.

TABLE 1

$X_n \times 10^{-p}$

n	5,000°	p	10,000°	p	20,000°	p	40,000°	p	80,000°	p	160,000°	p	320,000°	p
1	3.141	1	1.570	1	7.851	0	3.926	0	1.963	0	9.814	−1	4.907	
2	7.851	0	3.926	0	1.963		9.814	−1	4.907	−1	2.454		1.227	
3	3.490		1.745		8.724	−1	4.362		2.181		1.090		5.450	−2
4	1.963		9.814	−1	4.907		2.454		1.227		6.140	−2	3.070	
5	1.256		6.281		3.141		1.570		7.851	−2	3.930		1.970	
6	8.724	−1	4.362	−1	2.181	−1	1.091	−1	5.453	−2	2.727	−2	1.36	−2
7	6.409		3.205		1.602		8.012	−2	4.006		2.003		1.00	
8	4.907		2.454		1.227		6.134		3.067		1.533		7.67	−3
9	3.877		1.939		9.693	−2	4.847		2.423		1.212		6.06	
10	3.141		1.570		7.851		3.926		1.963		9.815	−3	4.91	
11	2.596	−1	1.298	−1	6.489	−2	3.244	−2	1.622	−2	8.11	−3	4.06	−3
12	2.181		1.091		5.452		2.726		1.363		6.82		3.41	
13	1.858		9.292	−2	4.646		2.323		1.161		5.81		2.90	
14	1.602		8.012		4.006		2.003		1.001		5.01		2.50	
15	1.396		6.979		3.490		1.745		8.725	−3	4.36		2.18	
16	1.227	−1	6.134	−2	3.067	−2	1.534	−2	7.670	−3	3.83	−3	1.92	−3
17	1.087		5.434		2.717		1.358		6.790		3.40		1.70	
18	9.693	−2	4.847		2.423		1.212		6.058		3.03		1.52	
19	8.700		4.350		2.175		1.087		5.437		2.72		1.36	
20	7.851		3.926		1.963		9.814	−3	4.907		2.45		1.23	
21	7.121	−2	3.561	−2	1.780	−2	8.902	−3	4.45	−3	2.23	−3	1.11	−3
22	6.489		3.244		1.622		8.111		4.06		2.03		1.01	
23	5.937		2.968		1.484		7.421		3.71		1.86		9.28	−4
24	5.452		2.726		1.363		6.815		3.41		1.70		8.52	
25	5.025		2.512		1.256		6.281		3.14		1.57		7.85	
26	4.646	−2	2.323	−2	1.161	−2	5.807	−3	2.90	−3	1.45	−3	7.26	−4
27	4.308		2.154		1.077		5.385		2.69		1.35		6.73	
28	4.006		2.003		1.002		5.007		2.50		1.25		6.26	
29	3.734		1.867		9.336	−3	4.668		2.33		1.17		5.83	
30	3.490		1.745		8.724		4.362		2.18		1.09		5.45	

Table 1 contains values of X_n, equation (3), with Z set equal to unity. When Z is not unity, as for ionized helium, the tabulated temperatures must be multiplied by Z^2, to correspond with the true

TABLE 2

$g_{nn'}$

n'	n													
	2	3	4	5	6	7	8	9	10	11	12	13	14	15
1	.717	.765	.780	.786	.790	.792	.793	.794	.795	.795	.795	.796	.796	.796
2	....	.757	.822	.844	.855	.861	.865	.867	.869	.870	.871	.872	.872	.873
3	....	....	.768	.839	.865	.878	.886	.891	.895	.897	.899	.900	.901	.902
4	....	....	....	.772	.847	.874	.890	.898	.903	.908	.911	.914	.915	.916
5	....	....	....	....	.774	.851	.881	.896	.905	.912	.916	.919	.922	.924
6	....	....	....	....	....	.776	.853	.884	.899	.910	.917	.922	.926	.929
7	....	....	....	....	....	....	.777	.852	.887	.904	.915	.922	.926	.930
8	....	....	....	....	....	....	....	.779	.856	.888	.905	.916	.925	.929
9	....	....	....	....	....	....	....	....	.779	.856	.889	.906	.917	.925
10	....	....	....	....	....	....	....	....	....	.780	.858	.888	.907	.919
11	....	....	....	....	....	....	....	....	....	....	.781	.854	.890	.908
12	....	....	....	....	....	....	....	....	....	....	....	.781	.860	.891
13	....	....	....	....	....	....	....	....	....	....	....	....	.781	.861
....	....	....	....	....	....	....	....	....	....	....	....	....	....	.781

n'	n														
	16	17	18	19	20	21	22	23	24	25	26	27	28	29	30
1	.796	.796	.796	.796	.796	.797	.797	.797	.797	.797	.797	.797	.797	.797	.797
2	.873	.874	.874	.874	.874	.875	.875	.875	.875	.875	.875	.875	.875	.875	.875
3	.902	.903	.904	.904	.904	.904	.905	.905	.905	.905	.906	.906	.906	.906	.906
4	.917	.918	.919	.920	.920	.921	.921	.921	.922	.922	.922	.922	.922	.923	.923
5	.926	.927	.928	.929	.930	.930	.931	.931	.932	.932	.932	.933	.933	.933	.933
6	.931	.933	.934	.936	.937	.937	.938	.939	.939	.940	.940	.940	.941	.941	.941
7	.933	.935	.937	.939	.940	.941	.942	.943	.943	.944	.945	.945	.945	.946	.946
8	.933	.937	.939	.941	.943	.944	.945	.946	.947	.948	.948	.949	.949	.950	.950
9	.930	.934	.938	.940	.942	.944	.945	.947	.948	.948	.949	.950	.950	.951	.952
10	.927	.932	.936	.940	.942	.944	.946	.948	.949	.950	.951	.952	.953	.953	.954
11	.919	.927	.933	.937	.940	.943	.945	.947	.949	.950	.951	.952	.953	.954	.955
12	.909	.920	.928	.933	.938	.941	.944	.946	.948	.950	.951	.952	.953	.954	.955
13	.892	.910	.921	.929	.935	.939	.943	.946	.948	.950	.952	.953	.954	.955	.956
14	.862	.894	.911	.923	.931	.936	.941	.945	.947	.950	.952	.954	.955	.956	.957
15	.782	.864	.894	.912	.923	.931	.937	.941	.945	.948	.950	.953	.954	.956	.957
16	....	.782	.866	.894	.912	.923	.931	.937	.942	.946	.949	.951	.953	.955	.956
17	....	....	.782	.868	.894	.912	.924	.932	.938	.942	.946	.950	.951	.954	.955
18	....	....	....	.782	.862	.894	.912	.924	.932	.938	.942	.946	.949	.952	.954
19	....	....	....	....	.782	.862	.894	.912	.924	.932	.938	.943	.947	.950	.952
20	....	....	....	....	....	.782	.862	.895	.912	.924	.932	.938	.943	.947	.950
21	....	....	....	....	....	....	.782	.862	.895	.913	.924	.932	.939	.943	.947
22	....	....	....	....	....	....	....	.782	.862	.895	.913	.924	.933	.939	.943
23	....	....	....	....	....	....	....	....	.782	.862	.895	.913	.924	.933	.939
24	....	....	....	....	....	....	....	....	....	.782	.863	.895	.913	.924	.933
25	....	....	....	....	....	....	....	....	....	....	.782	.863	.895	.913	.925
26	....	....	....	....	....	....	....	....	....	....	....	.782	.863	.895	.913
27	....	....	....	....	....	....	....	....	....	....	....	....	.782	.863	.895
28	....	....	....	....	....	....	....	....	....	....	....	....	....	.782	.863
29	....	....	....	....	....	....	....	....	....	....	....	....	....	....	.782

temperatures. For example, the solution for He^+ at $T_e = 40{,}000°$ is equivalent to that for hydrogen at $T_e = 10{,}000°$.

The Kramer-Gaunt factors for the discrete-discrete transitions are given in Table 2. The functional form of this factor, $g_{nn'}$, is

TABLE 3*a*

$[-E_i(-X_n)]$

n	T_e						
	5,000°	10,000°	20,000°	40,000°	80,000°	160,000°	320,000°
2.....	0.0000	0.0041	0.0525	0.2264	0.5712	1.0590	1.6399
3.....	0.0071	0.0700	0.2727	0.6453	1.1524	1.7449	2.3857
4.....	0.0525	0.2264	0.5712	1.0590	1.6399	2.2746	2.9377
5.....	0.1451	0.4296	0.8720	1.4252	2.0443	2.6993	3.3731
6.....	0.2727	0.6453	1.1524	1.7449	2.3857	3.0521	3.7318
7.....	0.4188	0.8574	1.4080	2.0256	2.6799	3.3533	4.0365
8.....	0.5712	1.0590	1.6400	2.2746	2.9377	3.6167	4.3012
9.....	0.7235	1.2483	1.8512	2.4976	3.1669	3.8481	4.5352
10.....	0.8720	1.4252	2.0443	2.6993	3.3731	4.0565	4.7448
11.....	1.0252	1.5905	2.2217	2.8832	3.5703	4.2454	4.9345
12.....	1.1524	1.7449	2.3857	3.0521	3.7318	4.4182	5.1079
13.....	1.2832	1.8896	2.5379	3.2082	3.8899	4.5772	5.2675
14.....	1.4080	2.0256	2.6799	3.3533	4.0365	4.7246	5.4153
15.....	1.5268	2.1537	2.8128	3.4888	4.1732	4.8620	5.5530
16.....	1.6400	2.2745	2.9377	3.6157	4.3012	4.9906	5.6818
17.....	1.7480	2.3890	3.0555	3.7352	4.4216	5.1114	5.8028
18.....	1.8512	2.4976	3.1669	3.8481	4.5352	5.2253	5.9170
19.....	1.9498	2.6009	3.2726	3.9550	4.6427	5.3331	6.0249
20.....	2.0443	2.6993	3.3731	4.0565	4.7448	5.4355	6.1274
21.....	2.1348	2.7933	3.4689	4.1532	4.8419	5.5328	6.2249
22.....	2.2217	2.8832	3.5703	4.2454	4.9345	5.6257	6.3178
23.....	2.3053	2.9694	3.6529	4.3337	5.0231	5.7144	6.4066
24.....	2.3857	3.0521	3.7318	4.4182	5.1079	5.7994	6.4917
25.....	2.4632	3.1318	3.8124	4.4993	5.1893	5.8809	6.5732
26.....	2.5379	3.2082	3.8899	4.5772	5.2675	5.9592	6.6516
27.....	2.6101	3.2820	3.9645	4.6523	5.3428	6.0346	6.7270
28.....	2.6799	3.3533	4.0365	4.7247	5.4153	6.1072	6.7997
29.....	2.7474	3.4221	4.1061	4.7945	5.4853	6.1773	6.8699
30.....	2.8128	3.4887	4.1732	4.8620	5.5530	6.2450	6.9376

given by Menzel and Pekeris.[3] For n' from 1 to 6, and for n from 2 to 30, the accurate expressions were employed; for all other values, the asymptotic expression

$$g_{nn'} = 1 - \frac{0.1728\left(1 + \frac{n'^2}{n^2}\right)}{\left(1 - \frac{n'^2}{n^2}\right)^{2/3}(n^2)^{2/3}} \qquad (6)$$

[3] *M.N.*, **96**, 77, 1935.

was used. This expression differs from the exact one for n' equal to 6 by a small number in the third decimal place. Consequently, an adjustment was made to the asymptotic values in order to remove the discrepancy. It is evident that this factor converges only very slowly to unity as n becomes infinite.

TABLE 3*b*

$\bar{g}[-E_i(-X_n)]$

n	T_e						
	5,000°	10,000°	20,000°	40,000°	80,000°	160,000°	320,000°
2	0.000	0.004	0.053	0.229	0.578	1.374	1.884
3	0.007	0.071	0.279	0.662	1.185	1.808	2.483
4	0.053	0.231	0.588	1.093	1.699	2.374	3.081
5	0.148	0.440	0.900	1.479	2.130	2.832	3.556
6	0.278	0.663	1.193	1.816	2.496	3.213	3.946
7	0.427	0.882	1.459	2.112	2.811	3.535	4.276
8	0.583	1.091	1.702	2.377	3.088	3.822	4.564
9	0.739	1.287	1.922	2.611	3.331	4.071	4.816
10	0.891	1.470	2.124	2.824	3.550	4.295	5.043
11	1.048	1.641	2.309	3.018	3.760	4.498	5.249
12	1.178	1.800	2.480	3.196	3.933	4.684	5.437
13	1.312	1.950	2.640	3.362	4.102	4.856	5.611
14	1.440	2.091	2.788	3.515	4.259	5.016	5.773
15	1.562	2.224	2.928	3.659	4.406	5.166	5.924
16	1.678	2.349	3.059	3.794	4.544	5.306	6.065
17	1.789	2.468	3.182	3.921	4.674	5.437	6.199
18	1.895	2.581	3.299	4.041	4.797	5.562	6.325
19	1.996	2.688	3.410	4.155	4.913	5.680	6.445
20	2.093	2.790	3.516	4.263	5.023	5.792	6.558
21	2.186	2.888	3.617	4.366	5.128	5.899	6.667
22	2.275	2.981	3.723	4.465	5.229	6.001	6.770
23	2.361	3.071	3.810	4.559	5.325	6.099	6.869
24	2.443	3.157	3.894	4.649	5.417	6.192	6.964
25	2.523	3.240	3.979	4.736	5.505	6.282	7.055
26	2.600	3.319	4.060	4.820	5.590	6.368	7.142
27	2.675	3.396	4.139	4.900	5.672	6.451	7.226
28	2.746	3.470	4.215	4.977	5.751	6.531	7.307
29	2.815	3.542	4.288	5.052	5.827	6.608	7.385
30	2.882	3.611	4.359	5.125	5.900	6.682	7.461

The familiar exponential integral function

$$[-E_i(-X_n)] = \int_{X_n}^{\infty} \frac{e^{-\zeta}}{\zeta}\, d\zeta \qquad (7)$$

is given in Table 3*a* as a function of n and T_e. In the computations we made use of formulae (12) and (13) of paper II, and of Jahnke

and Emden's tables. The ordinary tables, with uniformly spaced argument, are somewhat difficult to use because of the involved interpolation.

The expression

$$\bar{g}[-Ei(-X_n)] = \int_{X_n}^{\infty} \frac{e^{-\zeta}}{\zeta} g_{\kappa n} d\zeta \tag{8}$$

is given in Table 3*b*. The Kramer-Gaunt factor for the bound-free transitions, $g_{\kappa n}$, was obtained from the formulae of Menzel and Pekeris. The integration was carried out by numerical integration formulae. Tables 3*a* and 3*b*, by multiplication with e^{X_n}, are convertible immediately into the functions S_n and $\bar{g}S_n$, which are given in paper II, equations (11) and (12).

Table 4*a* gives the expression

$$t_n = \sum_{1}^{n-1} \frac{2n^2}{n'(n^2 - n'^2)} \tag{9}$$

and Table 4*b*,

$$t_n = \sum_{1}^{n-1} \frac{2n^2 g_{nn'}}{n'(n^2 - n'^2)} . \tag{10}$$

The first four tables of this paper give directly and indirectly all the functions of n and T_e necessary in the evaluation of b_n by equation (17) of paper II, both for **A** and for **B**. Since the function V_n is only very slowly convergent, the calculations proved to be lengthy. An expression of the form

$$\sum_{i=31}^{\infty} \frac{S_i u_{in}}{t_i} = a + bn + cn^2 \tag{11}$$

was developed to complete the first summation accurately. This summation is the kernel of the succeeding double summation, which reduces, therefore, to a single summation. The first three terms of V_n were computed directly. The contribution of the remaining terms was obtained graphically by careful asymptotic extrapolation based on the plot of S_n and of the first three terms of V_n against position in the sequence. The b_n's for the two cases $\mathbf{A}_1$ and $\mathbf{A}_2$, which

were smoothed in the last figure to take out slight numerical inaccuracies, are tabulated in Tables 5*a* and 5*b*.

In Table 6, under the column headed b_n, are given the values, computed on hypothesis **B**, for an atom with an infinite number of

TABLE 4*a*

l_n (CASE $\mathbf{A}_1$)

2.....2.6667	11.....8.1614	21.....10.1363
3.....4.0500	12.....8.4285	22.....10.2775
4.....4.9905	13.....8.6738	23.....10.4124
5.....5.7044	14.....8.9005	24.....10.5415
6.....6.2801	15.....9.1112	25.....10.6653
7.....6.7627	16.....9.3082	26.....10.7841
8.....7.1782	17.....9.4929	27.....10.8984
9.....7.5430	18.....9.6670	28.....11.0086
10.....7.8682	19.....9.8321	29.....11.1148
	20.....9.9881	30.....11.2174

TABLE 4*b*

l_n (CASE $\mathbf{A}_2$)

2.....1.911	11.....6.943	21.....8.886
3.....3.084	12.....7.205	22.....9.026
4.....3.929	13.....7.442	23.....9.160
5.....4.589	14.....7.668	24.....9.287
6.....5.132	15.....7.876	25.....9.410
7.....5.590	16.....8.070	26.....9.528
8.....5.989	17.....8.253	27.....9.641
9.....6.339	18.....8.426	28.....9.750
10.....6.657	19.....8.589	29.....9.859
	20.....8.740	30.....9.956

levels. For purposes of comparison, we also give values of b_n derived from the work of Cillié.[4] Cillié based his calculations on assumption **B,** but he made two approximations to facilitate the numerical work. A model atom consisting of only fourteen levels was assumed, and the higher discrete states were neglected. For the fourteen levels, accurate values of the Einstein A's were taken; but for the electron captures, the g factor was set equal to unity. For purposes of comparison, we have also given the b_n for a fourteen-state atom at $T_e =$

[4] *Ibid.*, **96**, 771, 1936.

TABLE 5*a*

b_n (CASE $\mathbf{A}_1$)

n	T_e						
	5,000°	10,000°	20,000°	40,000°	80,000°	160,000°	320,000°
2.....	0.000034	0.002893	0.03365	0.1377	0.3306	0.5873	0.8809
3.....	.003273	.02945	.1097	.2447	.4251	.6237	.8303
4.....	.01824	.07359	.1781	.3182	.4843	.6558	.8268
5.....	.04280	.1180	.2330	.3705	.5264	.6801	.8293
6.....	.07199	.1588	.2764	.4115	.5538	.6994	.8335
7.....	.09926	.1937	.3116	.4431	.5780	.7141	.8472
8.....	.1259	.2237	.3387	.4663	.5978	.7260	.8532
9.....	.1499	.2486	.3629	.4888	.6161	.7358	.8555
10.....	.1710	.2714	.3836	.5062	.6281	.7439	.8604
11.....	.1912	.2903	.4002	.5190	.6381	.7509	.8632
12.....	.2074	.3072	.4147	.5302	.6449	.7568	.8657
13.....	.2233	.3223	.4275	.5399	.6525	.7622	.8697
14.....	.2376	.3358	.4388	.5485	.6595	.7667	.8699
15.....	.2507	.3478	.4489	.5561	.6657	.7708	.8718
20.....	.3016	.3931	.4891	.5899	.6889	.7852	.8780
25.....	.3359	.4269	.5203	.6121	.7033	.7912	.8801
30.....	0.3581	0.4487	0.5400	0.6237	0.7085	0.7936	0.8818

TABLE 5*b*

b_n (CASE $\mathbf{A}_2$)

n	T_e						
	5,000°	10,000°	20,000°	40,000°	80,000°	160,000°	320,000°
3.....	0.00434	0.0393	0.146	0.296	0.576	0.843	1.136
4.....	.0234	.0961	.233	.420	.639	.861	1.103
5.....	.0540	.150	.296	.478	.685	.877	1.089
6.....	.0905	.202	.350	.528	.714	.888	1.079
7.....	.123	.242	.391	.561	.736	.898	1.068
8.....	.154	.277	.422	.586	.753	.905	1.061
9.....	.182	.311	.448	.609	.770	.910	1.058
10.....	.206	.340	.470	.626	.780	.918	1.056
11.....	.228	.359	.488	.641	.790	.921	1.054
12.....	.248	.376	.503	.651	.800	.925	1.052
13.....	.266	.392	.517	.663	.808	.928	1.050
14.....	.281	.406	.528	.673	.813	.930	1.048
15.....	.296	.419	.539	.680	.818	.933	1.046
20.....	.350	.467	.583	.712	.842	.943	1.041
25.....	.385	.498	.611	.732	.858	.952	1.037
30.....	0.408	0.519	0.630	0.750	0.871	0.962	1.031

20,000°, with the capture g factor taken into account. The effect of the neglected higher levels is clearly exhibited by the actual crossing of the true b_n's by Cillié's b_n's at quantum number 6.

It is to be noted that b_n can be greater than unity. Referring to paper II, equation (17), we see that S_n and V_n must increase with T_e. For any T_e, as we have shown in II, $b_n \to 1$ as $n \to \infty$. There must,

TABLE 6

b_n (CASE B)

n	T_e								
	5,000°		10,000°		20,000°			40,000°	80,000°
	b_n	b_n (Cillié)	b_n	b_n (Cillié)	b_n	b_n (Cillié)	14-State b_n	b_n	b_n
3.....	0.0098	0.0120	0.089	0.111	0.330	0.409	0.420	0.670	1.304
4.....	.0406	.0448	.166	.188	.404	.453	.466	.729	1.108
5.....	.0840	.0878	.233	.251	.460	.494	.510	.743	1.065
6.....	.132	.131	.296	.298	.512	.520	.538	.773	1.045
7.....	.173	.166	.341	.333	.550	.538	.558	.789	1.036
8.....	.211	.195	.379	.357	.577	.547	.568	.802	1.032
9.....	.244	.218	.417	.373	.600	.549	.570	.816	1.031
10.....	.271	0.236	.448	0.383	.620	0.545	0.565	.825	1.030
15.....	.371		.526		.676			.853	1.027
20.....	.428		.571		.713			.871	1.025
25.....	.464		.600		.736			.882	1.024
30.....	0.486		0.618		0.750			0.893	1.024

then, be a temperature for which $b_n \sim 1$, when the conditions of thermodynamic equilibrium are closely approximated by the nebula. For assumption $\mathbf{A}_2$, the temperature at which the pseudo-thermodynamic equilibrium occurs is about 235,000°. For **B** it occurs near 71,000°.

The relative intensities I_n of the Balmer lines, referred, as is customary, to $H\beta$ as unity, are listed in Tables 7*a*, 7*b*, and 8 for the assumptions $\mathbf{A}_1$, $\mathbf{A}_2$, and **B**, respectively. In the last table are given, also, the values of I_n as derived by Cillié. The intensities are calculated from the formula

$$I_n = \left(\frac{b_n}{b_4}\right) e^{X_n - X_4} \frac{(4)^3}{n^3} \frac{g_{n2}}{g_{42}} = \left(\frac{b_n}{b_4}\right) I_{nT} , \qquad (12)$$

TABLE 7*a*

I_n (CASE A_1)

n	T_e						
	5,000°	10,000°	20,000°	40,000°	80,000°	160,000°	320,000°
3	1.953	2.035	2.118	2.205	2.289	2.364	2.438
4	1.000	1.000	1.000	1.000	1.000	1.000	1.000
5	0.592	0.576	0.561	0.546	0.533	0.519	0.508
6	0.389	0.368	0.350	0.334	0.317	0.305	0.294
7	0.271	0.252	0.235	0.220	0.205	0.195	0.187
8	0.198	0.180	0.165	0.152	0.141	0.132	0.126
9	0.149	0.135	0.121	0.111	0.101	0.094	0.089
10	0.115	0.104	0.091	0.083	0.075	0.069	0.066
11	0.092	0.081	0.071	0.063	0.057	0.052	0.049
12	0.074	0.065	0.056	0.050	0.044	0.040	0.038
13	0.060	0.052	0.045	0.040	0.035	0.032	0.030
14	0.050	0.043	0.037	0.032	0.028	0.026	0.024
15	0.042	0.036	0.030	0.026	0.023	0.021	0.019
20	0.020	0.017	0.014	0.012	0.010	0.009	0.008
25	0.011	0.009	0.007	0.006	0.005	0.005	0.004
30	0.007	0.005	0.004	0.004	0.003	0.003	0.002

TABLE 7*b*

I_n (CASE A_2)

n	T_e						
	5,000°	10,000°	20,000°	40,000°	80,000°	160,000°	320,000°
3	1.859	1.915	1.984	2.073	2.165	2.241	2.302
4	1.000	1.000	1.000	1.000	1.000	1.000	1.000
5	0.598	0.576	0.560	0.548	0.539	0.524	0.513
6	0.396	0.374	0.353	0.338	0.321	0.307	0.296
7	0.274	0.255	0.236	0.221	0.207	0.196	0.185
8	0.199	0.182	0.165	0.153	0.141	0.132	0.124
9	0.149	0.136	0.120	0.111	0.101	0.093	0.086
10	0.114	0.105	0.091	0.082	0.075	0.069	0.063
11	0.090	0.081	0.070	0.062	0.056	0.052	0.048
12	0.073	0.065	0.055	0.050	0.045	0.040	0.036
13	0.059	0.052	0.043	0.039	0.035	0.032	0.029
14	0.049	0.042	0.036	0.032	0.029	0.025	0.023
15	0.041	0.035	0.030	0.025	0.023	0.020	0.019
20	0.019	0.016	0.014	0.012	0.010	0.009	0.007
25	0.011	0.009	0.007	0.006	0.005	0.004	0.004
30	0.006	0.005	0.004	0.003	0.003	0.003	0.003

where I_{nT} is the value of the relative intensity for thermodynamic equilibrium. Because of the approximations, the decrements calculated by Cillié for a given temperature actually correspond to those for a temperature much higher.

In Table 8, under the heading I_n (Obs.), are given the means of the observed data for 17 nebulae, as determined by Berman.[5] The

TABLE 8

I_n (CASE B)

n	T_e									
	5,000°		10,000°		20,000°		40,000°		80,000°	160,000°
	I_n	I_n (Cillié)	I_n	I_n (Cillié)	I_n	I_n (Cillié)	I_n	I_n (Obs.)	I_n	I_n
3	2.43	2.70	2.50	2.78	2.59	2.88	2.71	2.77	2.83	2.93
4	1.00	1.00	1.00	1.00	1.00	1.00	1.00	1.00	1.00	1.00
5	0.53	0.51	0.51	0.50	0.50	0.48	0.49	0.50	0.48	0.47
6	0.33	0.30	0.31	0.29	0.30	0.27	0.29	0.26	0.27	0.26
7	0.223	0.193	0.206	0.180	0.192	0.168	0.179	0.18	0.169	0.159
8	0.157	0.134	0.143	0.120	0.130	0.110	0.120	0.12	0.112	0.104
9	0.115	0.094	0.105	0.084	0.093	0.076	0.085	0.09	0.078	0.072
10	0.087	0.069	0.079	0.061	0.069	0.054	0.062		0.057	0.052
15	0.030		0.025		0.021		0.018		0.017	0.015
20	0.014		0.012		0.010		0.009		0.006	0.006
25	0.007		0.006		0.005		0.004		0.003	0.003
30	0.004		0.003		0.003		0.002		0.002	0.001

means are set between T_e equal to 40,000° and to 80,000°, because the correspondence is closest for these temperatures. We draw attention to the fact that the observations seem to agree best with theory in the same region where thermodynamic equilibrium nearly prevails, although we attach no especial significance to this result. The Balmer decrement shows only a very slow change with temperature. Observations of extreme accuracy will be required if electron temperatures are to be determined from line intensities. Selective interstellar absorption, as discussed by Page[6] and by Berman,[5] only adds to the difficulties. Furthermore, as a comparison of Tables

[5] *Ibid.*, p. 890.

[6] *Ibid.*, p. 604.

7*b* and 8 shows, the decrement is much more sensitive to the mode of excitation than it is to electron temperature.

We conclude, therefore, that measures of the Balmer decrement are unsuited to determinations of the temperatures of the electron gas. The result, disappointing at first sight, proves to be fortunate, after all. The observed Balmer decrement can be used to indicate the physical nature of the excitation. For example, the general agreement of the observational data with the entries of Table 8 probably signifies that assumption **B** lies nearer to the truth than **A**.

Attention is also drawn to the close numerical agreement of Tables 7*a* and 7*b* for quantum numbers greater than 4. For the higher series members, the introduction of the Gaunt factors does little to change the relative intensities, although the absolute intensities change by as much as 20 per cent.

One advantage of the present type of solution, aside from its numerical accuracy, is the fact that the absolute intensities of both low and high series members, and even of the continuum beyond the Balmer limit, are determinate. The emission intensity, depending secondarily upon the temperatures, can be used to evaluate nebular densities to a high degree of astrophysical accuracy. Further discussion of the point is deferred until a later paper of the series. We may conclude the present contribution with the remark that perhaps the most surprising result of our investigation is that the individual b_n's fall as close to unity as they do, under conditions apparently far from those of thermodynamic equilibrium.

HARVARD OBSERVATORY
December 9, 1937

A MULTIPLET CALIBRATION OF THE ARCTURUS SPECTRUM

SIDNEY G. HACKER

ABSTRACT

An independent multiplet calibration of the writer's intensity scale of the Arcturus spectrum (λλ 4119–6743) is effected after the method used by Russell, Adams, and Moore in their calibration of Rowland's solar intensities. Certain data of astrophysical importance about the atmosphere of the star are then obtained from the atomic lines identified in its spectrum.

The calibration of the intensity scale is given in Table 2. Its general reliability is examined in Tables 3–6, and the errors involved in the calibration are discussed.

Assuming the stellar atmosphere to be in thermodynamic equilibrium, the linear relationship between $Y = \log (N_x^i/N_x)$ and E_x demanded by equation (1) is found to represent the data satisfactorily; the "quadratic effect" found by Adams and Russell is not observed. The corresponding lines for the seven best represented elements are shown in Figure 1. Their slopes, S, were found by least-squares solutions from the data given in Table 7, and the weighted mean slope (Table 9) gives $3925° \pm 75°$ K as the effective photospheric temperature of Arcturus, taking the sun's as 5740° K. The mean electron pressure in the star's atmosphere is found to be 3.9×10^{-8} atm, and the "level of ionization" is 7.7 volts. Incidentally, with the values used in this paper, the degree of ionization in the sunspot corresponds roughly to the mean between that in the solar disk and in Arcturus, decreased by a factor of 1/12. For the sake of completeness, the relative abundance of the atoms of different elements present in the star is indicated in Tables 11 and 12.

The writer has previously made a study of the spectrum of Arcturus (α Boötis), Draper class gKo, in the region λλ 4119–6743, on spectrograms taken with the 15-foot autocollimating spectrograph of the 100-inch Mount Wilson reflector, which were very kindly made available for measurement through the co-operation of the Mount Wilson and Princeton University observatories.[1] At the time of measurement of the plates the intensities of the lines were estimated visually on an arbitrary scale. In the present paper an independent multiplet calibration of this intensity scale is given, and with its aid certain data of astrophysical importance about the atmosphere of the star are obtained from the atomic lines identified in its spectrum.

The method of calibration employed here is the same as that used by Russell, Adams, and Moore[2] in their well-known study of Rowland's solar-intensity scale. The details of the method are described

[1] *Contr., Princeton Univ. Obs.*, No. 16, 1935; *Ap. J.*, **83**, 140, 1936.

[2] *Ap. J.*, **68**, 1, 1928.

in their paper, and only a brief summary will suffice to show what has been done here. The theoretical intensities for the relative strengths of the lines in normal multiplets are assumed to be proportional to the relative number of atoms N in the stellar atmosphere, which are producing the observed absorption lines. Differences (ΔI) of the visually estimated intensities (I) of the lines and the corresponding differences of the logarithms of their theoretical intensities ($\Delta \log N$) are obtained between groups of the unblended *diagonal and satellite* lines in normal multiplets. The mean value of the esti-

TABLE 1

NUMBER OF MULTIPLETS, LINES, AND DIFFERENCES AVAILABLE FOR THE CALIBRATION

Element	Multiplets	Lines	ΔI and $\Delta \log N$	Element	Multiplets	Lines	ΔI and $\Delta \log N$
Fe	22	104	25	*Na*	1	2	1
Ti	19	66	21	Fe^+	4	15	4
V	8	33	9	Ti^+	7	17	7
Cr	5	21	6	Sc^+	2	5	2
Ni	4	23	6	Y^+	1	4	1
Ca	4	13	5				
Mn	3	13	4	Total	80	316	91

mated intensities is found for each pair of these differences, and the corresponding average values of ΔI and $\Delta \log N$ are obtained, in order to diminish the effect of the admittedly large accidental errors made in the original estimation of the intensities. Using these average values of $\Delta \log N$, ΔI, and I, the ratios $\Delta \log N/\Delta I$ are plotted against I, and a "calibration curve" is drawn. From it the value of $\log N$ corresponding to a given intensity estimate I can be determined.

Table 1 gives the elements and the number of multiplets, lines, and differences ΔI and $\Delta \log N$ which are available from the previous work[1] for the construction of the calibration curve, which is not reproduced here.

The values[3] of $\log N$ obtained from this curve for the writer's estimated intensities I are given in Table 2. At the time the spectrograms were studied, the faintest lines just visible on the plates were

[3] Throughout logarithms are to the base 10.

assigned intensity 0, and the corresponding value of log N has here been taken equal to zero. It is clear that the true zero point of the scale is therefore undetermined, so that only the relative, and not the absolute, "number of atoms" N over unit area of the star's photosphere is represented.

Using Table 2, the calibrated log N can be found for the intensities of all the lines of Table 1, and hence the average calibrated Δ log N for each group that was used in finding the average values of the theoretical Δ log N may be obtained. Ideally, the ratio of these two

TABLE 2

CALIBRATION TABLE

I	log N	I	log N	I	log N
0	0.00	12	3.31	24	4.31
1	0.45	13	3.46	25	4.34
2	0.80	14	3.59	26	4.37
3	1.06	15	3.70	27	4.39
4	1.31	16	3.80	28	4.41
5	1.59	17	3.89	29	4.43
6	1.88	18	3.98	30	4.45
7	2.17	19	4.05	35	4.55
8	2.44	20	4.11	40	4.65
9	2.69	21	4.17	50	4.85
10	2.92	22	4.22	60	5.05
11	3.13	23	4.27	70	5.25

should be everywhere equal to unity, but the errors of observation necessarily enter. The approximation of the ratios to unity for groupings of various kinds, shown in Tables 3–6, serve to indicate the general validity of the calibration. In Table 6 the individual values of the theoretical and calibrated Δ log N are given, but elsewhere the values of the ratios (theoretical/calibrated) suffice. The number of differences which were used in finding the various average Δ log N is given in the column headed "No.," and low weight is to be attached to the values of those ratios where this number is small.

In Table 3 the differences are grouped according to the mean values of the intensities of the lines used, and each entry of the first column is inclusive of the upper limit. The satisfactory distribution in the number of available differences over the whole range of the intensity scale may also be seen from this table. The ratios are shown

in Table 4 according to range in wave length of the lines. This table is of particular importance because there may have been a systematic variation with wave length in the original estimation of the in-

TABLE 3

GROUPING BY INTENSITY

Range of Intensity	No.	Mean *I*	Ratio
0–2	6	1.7	0.91
2–3	10	2.6	1.20
3–4	13	3.8	1.07
4–5	14	4.7	0.95
5–7	13	6.1	0.94
7–10	16	8.7	1.13
10–15	11	12.6	0.92
>15	8	25.0	0.87

tensities, as was the case in the Rowland scale.[4] The ranges in wave length have been so chosen that the number of differences used in each case would be sufficiently large to have significance. The absence of any systematic variation in the values of the ratios indicates that the calibration needs no correction for wave length. However,

TABLE 4

GROUPING BY WAVE LENGTH

λ	No.	Ratio	λ	No.	Ratio
4119–4500	25	1.00	4900–5500	22	0.95
4500–4900	22	1.01	5500–6743	22	1.06

of the plates which were used to map the stellar spectrum, some were taken with two-prism and others with four-prism dispersion, at different times and with different exposures,[1] so that it is worth while to check this last result by grouping the differences according to the plates on which the lines used in finding them occur. This is done in Table 5, and the conclusion is confirmed. There are fifteen lines, in two multiplets, which occur on Plate 507[1], and these yield only two differences; this row has been bracketed off because of the low

[4] Cf. n. 2. It is of interest to compare the corresponding results obtained by Mulders in his work on the equivalent breadths of the solar lines, *Zs. f. Ap.*, **10**, 297, 1935.

weight which is therefore to be attached to it, but it has been included in finding the general average for "all low-dispersion plates." Finally, the differences are grouped in the first part of Table 6 according to the elements from whose multiplets they have been found. Again the ratios are satisfactory, although, of course, the most weight should be given to the values for *Fe* and *Ti*.

The general validity of the calibration being thus examined, it is now possible to find the probable error in log N corresponding to a given intensity I. For this purpose the completely unforced values

TABLE 5

GROUPING BY PLATES

Plate No.	Range in λ	No.	Ratio
*76[1]	4245–4522	25	0.99
*76[2]	4526–4974	24	1.11
†507[2]	4974–5620	20	0.87
†519[3]	5622–5896	6	0.93
†507[3]	5896–6743	14	1.13
†(507[1])	.....	(2)	(0.59)
*All high-dispersion plates	.....	49	1.05
†All low-dispersion plates	.....	42	0.95

in Table 6 may be used. Here the outstanding discordances (i.e., neglecting those for *Fe*, *Cr*, *Ca*, and *Na*) average 16 per cent of the theoretical values, or ±0.13 in log N. On the average there are about twelve differences in intensity for each of the groups in the various tables, and these are found from multiplets averaging 3.75 lines in number. The discordance between calibration and theory for the value of log N derived from a single line will therefore be ±0.62 (P.E. ±0.53). The writer previously reported,[1] from a study of two independent estimates of the intensities of a thousand lines on the various plates, that the accidental error of an estimate is about one unit of the scale. Ninety-five per cent of the lines which were used in that determination have intensities from 0 to 11. From Table 2 we see that for this range log N changes, on the average, by ±0.28 per unit of intensity. The probable error in the intensity scale as derived from the present work is therefore ±1.9 unit of the scale, or just twice as large as the error reported before.

It would be of interest to know whether the magnitude of the error in log N, which will reappear in the applications of the calibration, is due entirely to the raggedness in the original intensity estimates, which are admittedly rough, or whether it is induced to some appreciable extent by the limitations in the amount of material that has been available for calibration. Fortunately, there is a way in which the answer to this question can be sought. On the basis of the

TABLE 6

GROUPING BY ELEMENTS

Element	No.	Theoretical Δ log N	Stellar Lines		Solar Lines	
			Cal. Δ log N	Ratio	Cal.* Δ log N	Ratio
Fe	25	0.84	0.85	1.01	0.70	0.83
Ti	21	0.86	0.96	1.12	0.99†	1.27†
V	9	0.72	0.85	1.18	0.88	1.22
Cr	6	0.55	0.56	1.02	0.64	1.16
Ni	6	0.73	0.84	1.15	0.79	1.08
Ca	5	1.05	1.05	1.00	1.21	1.15
Mn	4	0.68	0.88	1.30	0.68	1.00
Na	1	0.30	0.31	1.03	0.23	0.77
Fe^+	4	0.57	0.54	0.95	0.61	1.07
Ti^+	7	1.05	0.76	0.72	0.68	0.65
Sc^+	2	0.93	0.73	0.79	1.09	1.17
Y^+	1	1.04	0.88	0.85	1.11	1.07

* Calibration of the Rowland scale by Russell, Adams, and Moore, *Ap. J.*, **68**, 1, 1928.

† For *Ti*, in the case of the solar lines, there are 17 differences, with theoretical Δ log N = 0.78, instead of the 21 differences, with theoretical Δ log N = 0.86, for the stellar lines.

extensive material which was used in the calibration[2] of Rowland's solar intensities (228 multiplets, 1288 lines, 312 differences), the probable error in log N was there calculated to be ± 0.32; and since the calibration material was so complete, this error could be attributed principally to the roughness in the visual intensity estimates. It so happens that, with the single exception of five lines due to *Ti*, there is an unblended line in the spectrum of the solar disk corresponding to each of those stellar lines in Table 1 which have been used in this calibration of the stellar spectrum. If we assign to the intensities of these solar lines the proper values of log N as already given in the calibration of the Rowland scale, we can find the corresponding calibrated Δ log N for those multiplet differences which

have been used in the present work. In this way it will be possible to compare the *already calibrated* $\Delta \log N$ of the Rowland lines with the theoretical $\Delta \log N$ *on the basis of the present material*, and this comparison will help to show how clearly the determinations are of a definitely statistical nature and are dependent on the extent of the calibration data. The results are given in the last columns of Table 6, where the basic data are, therefore, the same as that for the stellar lines, with the exception of *Ti*, for which now, in the case of the solar lines, only seventeen differences of the original twenty-one used in the stellar calibration can be found. The outstanding discordances (neglecting that for *Mn*) between the theoretical and calibrated $\Delta \log N$ average 20 per cent of the theoretical values or ± 0.16 in $\log N$. The discordance between theory and the Rowland calibration for the value of $\log N$ derived from a single line on the basis of the present material is therefore ± 0.76, with the corresponding probable error of ± 0.65. But this is just twice as large as the known error in $\log N$ for the Rowland scale, as obtained on the basis of the wealth of material which was available in its own calibration. Accordingly, the relatively large errors making their appearance in the present work appear to be due not only to the raggedness in the original intensity estimates but also in some part to the limitations in the data available for the calibration.

The Russell-Adams-Moore calibration method which is used here proceeds by finding differences between the groups of diagonal and satellite lines of the multiplets. It has been suggested by various investigators in the recent literature that the Rowland scale might profitably be re-examined, giving closer attention to certain important finer distinctions between the different kinds of lines (principal and subordinate, etc.). Aside from such considerations, however, it is clear that practical difficulties will arise in applying the method, even as it stands, independently to stellar spectra in general: the number of differences which can be found from the unblended diagonal and satellite lines in normal multiplets of a stellar spectrum may be so small and so badly distributed over the range of the intensity scale that no reliable calibration curve can be drawn. In such cases one could follow the method which Adams and Russell[5] used in their

[5] *Ap. J.*, **68**, 9, 1928.

great pioneer work of 1928. Spectrograms of seven stars representing different spectral classes and of the sun were taken with the same instrument, and by a comparison of each stellar spectrum with the solar spectrum the intensities of the unblended stellar lines were estimated upon the previously calibrated Rowland scale. However, this procedure involves the further assumption that the calibration by multiplet intensities for the individual spectra of different stars (regardless of spectral type, etc.) would be the same as for the sun. This clearly involves questions worthy of serious study in their own right. But in being free from this assumption an independent multiplet calibration of a stellar spectrum has a distinct advantage.

ASTROPHYSICAL DATA

The intensity scale having been calibrated, certain data of astrophysical importance about the atmosphere of Arcturus can now be obtained.[5] For a gas in thermodynamic equilibrium and of known composition the methods of statistical mechanics permit the derivation of well-known expressions[6] giving the relative number of atoms of the gas which are in different energy states of excitation and ionization. These results can be used if it is assumed that the stellar atmosphere is in thermodynamic equilibrium and that atoms at different depths in the atmosphere are equally effective in producing a given spectral line. If N'_x/N_x denotes the ratio of the relative number of atoms of a particular element in the xth state of excitation which are producing a given arc line in the spectra of any two stars, and N'_0/N_0 the corresponding ratio of the neutral atoms of the element, considered above equal areas of the photospheres, then, by an application of Boltzmann's principle,

$$\log \frac{N'_x}{N_x} = \log \frac{N'_0}{N_0} + 5040E_x\left(\frac{1}{T} - \frac{1}{T'}\right), \qquad (1)$$

where E_x is the excitation potential of the line in volts and T and T' are the effective photospheric temperatures of the two stars in absolute units. If the primed letters refer to Arcturus and the unprimed ones to the solar disk, the values of $\log (N'_x/N_x)$ can be de-

[6] R. H. Fowler, *Phil. Mag.*, 7th ser., **1**, 845, 1926. Also Fowler's *Statistical Mechanics*, Cambridge University Press.

termined from the foregoing and from the Rowland calibrations for those elements which have been observed in both spectra. For convenience let

$$Y = \log \frac{N'_x}{N_x}, \qquad Y_0 = \log \frac{N'_0}{N_0}, \qquad S = 5040\left(\frac{1}{T} - \frac{1}{T'}\right),$$

TABLE 7

ELEMENTS USED IN DETERMINING SLOPE*

Element	E_x	No.	Y	Element	E_x	No.	Y
Fe	0.06	19	2.27	*Cr*	0.98	25	1.42
	0.95	26	1.05		2.62	16	1.31
	1.54	26	1.26		2.88	8	1.34
	2.22	36	0.83		3.02	15	0.85
	2.43	19	0.71		3.42	9	1.00
	2.63	16	0.47				
	2.84	41	0.78		.....	73	±0.61
	2.99	37	1.20				
	3.24	19	0.25	*Ni*	1.67	15	0.95
	3.38	36	0.64		1.92	6	.81
	3.63	27	0.27		3.37	9	.75
	3.94	29	0.25		3.56	14	.31
	4.21	33	0.41		3.67	16	.26
	4.40	17	0.13		3.84	17	.60
	4.57	12	−0.66		4.12	12	0.03
	4.75	7	−0.92				
	.....	400	±0.58		.....	89	±0.55
				Mn	0.00	1	1.68
Ti	0.03	18	2.32		2.30	2	0.66
	0.83	42	2.23		2.91	14	1.10
	1.05	19	1.78		3.07	6	0.16
	1.44	16	1.73		3.84	1	0.30
	1.83	27	1.68				
	2.10	14	2.01		.....	24	±0.63
	2.25	16	1.62				
	2.36	13	1.71	*Co*	0.39	5	2.66
	2.51	6	1.50		1.83	7	1.88
	2.75	2	0.85		3.04	9	1.29
	3.30	2	1.18		3.66	5	0.60
	.....	175	±0.58		.....	26	±0.65
V	0.03	12	3.02				
	0.28	16	2.48				
	1.06	17	1.83				
	1.24	4	1.42				
	1.47	6	1.54				
	2.15	5	1.46				
	.....	60	±0.53				

* All values in this table are positive unless preceded by a minus sign.

and write equation (1) in the form

$$Y = Y_0 + S \cdot E_x . \qquad (2)$$

Likewise, for ionized atoms we have the corresponding equation

$$Y = Y_1 + S \cdot E_x , \qquad (2a)$$

where $Y_1 = \log (N_1'/N_1)$ is the relative number of singly ionized atoms in the normal state.

TABLE 8

Element	Ex	No.	Y	Element	Ex	No.	Y
Na.....	0.00	2	0.99	Cr^+.....	3.85	1	0.26
	2.09	6	0.07		4.06	5	−0.03
	.....	8	±0.49		.....	6	±0.43
Mg.....	2.70	1	0.66	Fe^+.....	2.57	3	1.19
	4.33	6	0.81		2.76	5	0.40
	.....	7	±0.58		2.83	8	−0.09
					2.88	6	−0.31
Ca.....	1.88	9	0.99		3.21	4	0.20
	2.51	17	.14		.....	26	±0.49
	2.70	4	.47				
	2.92	5	0.20	Y^+.....	0.15	2	2.74
	.....	35	±0.78		0.41	2	2.08
					1.03	5	0.95
Sc.....	0.01	3	2.56		.....	9	±0.49
	1.44	3	2.39				
	.....	6	±0.50	*Zr*.....	0.63	4	1.58
					.....	4	±0.38
Sc^+.....	0.55	6	2.03				
	1.47	9	0.69	Zr^+.....	0.63	2	2.28
	.....	15	±0.39		1.48	1	1.31
					2.41	1	0.59
Ti^+.....	1.15	34	1.62		.....	4	±0.21
	1.57	5	1.07				
	2.08	7	1.59	Ba^+.....	0.40	3	0.27
	.....	46	±0.60		2.61	2	0.87
					.....	5	±0.43
V^+.....	1.68	2	1.40				
	2.02	1	1.06	La^+.....	0.16	3	1.44
	.....	3	±0.22		0.36	2	0.79
					.....	5	±0.27

The values of Y and E_x for the various elements identified in both sun and star are collected in Tables 7 and 8. For each element, lines

of about the same excitation potential have been averaged; and the different columns of the two tables give the element, the mean E_x in volts, the number of lines involved, and the corresponding values for Y. The total number of lines and the average residual in the individual values of Y from the mean for each group are placed at the end of the respective columns.

The size of these Y-residuals may be profitably compared with those in the well-known work[7] of Dr. Charlotte E. Moore, where the sunspot temperature is determined (as 4720° ± 40° K) by the same methods as those employed here but using, of course, the calibration of the Rowland scale for the intensities of the spot lines, and with those in the Adams-Russell study[5] of selected stellar spectra, which included Arcturus:[8]

Study	Intensity Scale	Y-Residual
I. C. E. Moore: Sunspot	Rowland scale only	±0.31
II. Adams-Russell:		
a) All selected stars	Rowland scale *and* Independent estimates of the stellar intensities on the Rowland scale	± .43
b) Arcturus		± .41
III. This paper: Arcturus	Independent scale, independently calibrated, *and* The Rowland scale	±0.59

This same corresponding increase in the Y-residuals exists for the individual elements. For example, the results for the *Fe* lines alone are:

Study	Y-Residual	Study	Y-Residual
I	±0.21	II*b*	±0.29
II*a*	±0.34	III	±0.58

[7] *Ap. J.*, **75**, 222–273 and 298–336, 1932. In particular, sec. 5.

[8] The residuals have been computed from those elements which are represented by some twenty-five or more lines; those for the Adams-Russell study are taken from their paper.

It is noteworthy that the errors in Y are of the same order as the discordances in log N for a single line as obtained in the calibrations of the respective intensity scales, ± 0.37 in the Rowland calibration, ± 0.62 in the present one.

If equation (2), which assumes the stellar atmosphere to be in thermodynamic equilibrium, is valid, the values of Y, when plotted against the corresponding values of E_x for each element, should lie

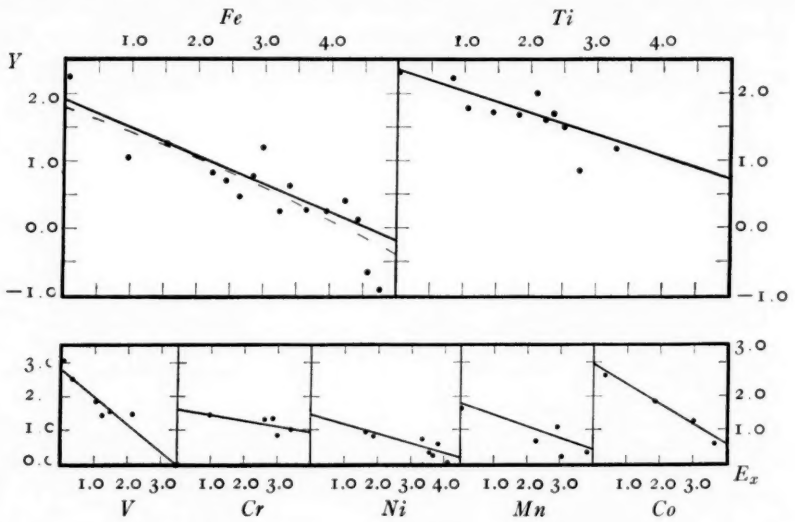

FIG. 1

within observational errors on a straight line of slope S. Given the value of T, the star's effective photospheric temperature T' can then be readily obtained from the value of S. The data are better determined for the seven elements listed in Table 7, and for these the corresponding plots of Y against E_x are shown in Figure 1.

It is clear, upon inspection, that the data are satisfactorily represented by a linear relationship, although, as we have just pointed out, the residuals in the ordinates Y are comparatively large here. The actual lines which are drawn in Figure 1 were found by least-squares solutions with weight for each point equal to the number of spectral lines used in determining its co-ordinates.

It is well known that Adams and Russell[5] found their values for Y to depend on E_x quadratically rather than linearly; and in view of

this apparent breakdown in the validity of equation (2), they provisionally attributed the quadratic deviation to a departure in the stellar atmosphere from thermodynamic equilibrium. Many interesting attempts have been made recently to explain away this effect,[9] although its complete understanding remains an outstanding astrophysical problem whose solution may have to wait until details of the method of calibration, and the data, can be more thoroughly looked into. This quadratic effect, however, does not appear in the

TABLE 9

VALUES AND WEIGHTS FOR SLOPE S

Element	S	n	r	Wt
Fe	−0.422	400	4.69	88
Ti	.323	175	3.27	19
V	.818	60	2.12	3
Cr	.177	73	2.44	4
Ni	.285	89	2.45	5
Mn	.342	24	3.84	4
Co	−0.586	26	3.27	3

present work. If, for example, in the case of the extensive *Fe* data, we assume a quadratic dependence of Y on E_x, a least-squares solution with the same weights as before gives

$$Y = +1.81 - 0.34E_x - 0.02E_x^2,$$

which is shown by the dashed curve in Figure 1.[10]

The numerical values of the slopes of the straight lines found from the least-squares solutions are given in Table 9. Although theoretically the slopes of these lines should be the same, observational errors enter and it is necessary to find a weighted mean value of S. If n is the number of spectral lines and r is the range in E_x for each element, the weights may be taken[5] proportional to $n \cdot r^2$.

[9] In a recent paper, *Ap. J.*, **84**, 481, 1936, Pannekoek has discussed the results for Sirius, α Orionis, and α Scorpii when the values of Y are multiplied by the respective continuous absorption coefficients of the lines.

[10] It may be noted, in passing, that by reason of the negative coefficient of E_x^2 the curvature of this parabolic arc is, in fact, opposite to the one found by Adams and Russell for Arcturus (*loc. cit.*, p. 23).

Taking the temperature T of the sun's photosphere at Milne's value of 5740° K, the mean value of the effective photospheric temperature of Arcturus T' is readily obtained: (1) with the weights listed in Table 9:

$$S = -0.405 \pm 0.025\,, \qquad T' = 3928° \pm 77° \text{ K}\,;$$

(2) giving the same weight 3 to the other elements, but keeping those for *Fe* and *Ti* as 88 and 19, respectively,

$$S = -0.409 \pm 0.024\,, \qquad T' = 3916° \pm 73° \text{ K}\,;$$

(3) using only the slopes for *Fe* (weight 88) and for *Ti* (weight 19):

$$S = -0.404 \pm 0.026\,, \qquad T' = 3931° \pm 80° \text{ K}\,.$$

The value of T' which will be adopted here is the convenient mean of these three values, namely, $T' = 3925° \pm 75°$ K. Had the solar temperature been taken at the round value of 6000°, the corresponding value of T' would have been 4050° K.

If a stellar atmosphere be considered as a gas composed of neutral and ionized atoms and free electrons in thermodynamic equilibrium, the degree of ionization is given by Saha's classical equation. As corrected by Pannekoek,[11] in particular for the dominating role played by the photospheric radiation of effective temperature T, this equation states that the ratio N_1/N_0 of the number of ionized and neutral atoms of a given element above the photosphere is given by

$$\log \frac{N_1}{N_0} = -\frac{5040\,I}{T} + \tfrac{5}{2} \log T - \log P_e + \log \frac{B_1(T)}{B_0(T)} - 6.59\,, \quad (3)$$

where the ionization potential I is in volts and the mean electron pressure of the gas P_e is in atmospheres. The quantities $B_0(T)$ and $B_1(T)$ are the partition functions for the neutral and singly ionized atoms.[6]

In order to compare the behavior of an element which occurs in

[11] *Handb. d. Ap.*, **3**, Part 1, 256, 1930.

both the neutral and ionized states in Arcturus and in the solar disk, we obtain from (3)

$$Y_1 - Y_0 = S \cdot I + \tfrac{5}{2} \log \frac{T'}{T} + B - \log \frac{P_e'}{P_e}, \qquad (4)$$

where

$$B = \log \frac{B_1(T')}{B_0(T')} - \log \frac{B_1(T)}{B_0(T)},$$

and the other letters have the same meanings as before. By means of the data for the six elements *Sc*, *Ti*, *V*, *Cr*, *Fe*, and *Zr*, for which values of both Y_1 and Y_0 are available, the mean value of the electron pressure of the star's atmosphere, P_e', can be calculated from equation (4). The pertinent data are collected in Table 10. Assigning

TABLE 10

DETERMINATION OF THE EFFECTIVE ELECTRON PRESSURE

Element	I	Y_0	Y_1	B	log P_e'/P_e	Wt
Sc	6.57	2.77	1.67	−0.05	−2.03	1
Ti	6.80	2.48	2.10	+ .02	2.77	2
V	6.76	2.47	2.01	− .04	2.73	1
Cr	6.74	2.14	1.65	+ .10	2.56	1
Fe	7.83	1.86	1.31	− .01	3.05	2
Zr	6.92	1.84	2.14	−0.02	−3.54	1

greater weight, as shown, to the values of log (P_e'/P_e) for *Ti* and *Fe* because of the more extensive material upon which they are based, the weighted mean value from all six elements is

$$\log \frac{P_e'}{P_e} = -2.81 \pm 0.12.$$

Using Russell's value[12] for P_e, namely, 2.5×10^{-5} atm, we find

$$P_e' = 1.55 \times 10^{-3} P_e = 3.9 \times 10^{-8} \text{ atm}.$$

The "level of ionization," I_0, in a stellar atmosphere may be defined[12] as the ionization potential of an element 50 per cent of whose atoms would be ionized under the stellar conditions. Putting $B_1(T')$

[12] *Ap. J.*, **70**, 54, 1929.

$= B_0(T')$, $N_1' = N_0'$, $T' = 3925°$, and $P_e' = 3.9 \times 10^{-8}$ atm in equation (3), the level of ionization in the atmosphere of Arcturus is found to be $I_0' = 7.7$ volts.

The relative behavior of the different elements present in the sunspot (Ko), the solar disk (Go), and Arcturus (gKo) is of considerable interest. Throughout the stellar spectrum the relative intensities of the arc lines are strikingly similar to those in the sunspot spectrum, while the enhanced lines are stronger.[1] The relative behavior of the line intensities can be understood in large part from the accompanying data, all of which, it is interesting to note, has been obtained by the Russell-Adams-Moore calibration methods, after taking $T = 5740°$ for the disk. With these data the general correspondence in the

Spectrum	T	P_e	I_0
Solar disk*	5740	2.5×10^{-5}	8.5
Sunspot†	4720	1.5×10^{-5}	7.0
Arcturus	3925	3.9×10^{-8}	7.7

* *Ap. J.*, **70**, 54, 1929.
† *Ibid.*, **75**, 222–273 and 298–336, 1932. In particular, sec. 5.

relative degree of ionization between the three spectra can be indicated graphically by plotting the following equations, which are readily obtained from (3) if the partition functions be neglected:

Solar disk	$y = -0.88I + 7.41$	(D)
Sunspot	$y = -1.07I + 7.41$	(S)
Arcturus	$y = -1.28I + 9.80$	(A)

where $y = \log (N_1/N_0)$. Although it is unnecessary to reproduce the graphs of these lines here, two rather interesting things about them may be mentioned. Lines (D) and (A) intersect at $y = +2.15$ and $I = 5.98$, which is nearly the ionization potential of Ca (6.09), the enhanced lines of which are well known to be by far the strongest in the whole spectrum of both the sun and the star. The equation of the bisector of the angle between (D) and (A) is readily found to be

$$y = -1.06I + 8.50,$$

and this is parallel to (S), so that, for the data given above, the relative ionization in the sunspot corresponds to the mean between that

in the disk and in Arcturus decreased uniformly for values of I by an amount equal to $-\log (N_1/N_0) = 1.09$, that is, by a factor of 1/12.

The values of the relative abundance of the different elements in the star to that in the solar disk, Y_0 and Y_1, may now be calculated from the data given in Tables 7 and 8, using equations (2) and (2*a*). It is well to emphasize the fact that a zero point which would permit the determination of the actual concentration of the elements cannot

TABLE 11

RELATIVE ABUNDANCE OF ELEMENTS IN ARCTURUS

Element	Y_0	Y_1	Element	Y_0	Y_1
H	5.01:	.....	*Cu*	1.50:	.....
Na	0.94	.....	*Zn*	1.14:	.....
Mg	2.45	.....	*Sr*	1.04:	?
Al	1.27:	.....	*Y*	.....	2.42
Si	1.75:	.....	*Zr*	1.84	2.14
Ca	1.39	?	*Cb*	2.23:	.....
Sc	2.77	1.67	*Ru*	2.91:	.....
Ti	2.48	2.10	*Ba*	.....	1.03
V	2.47	2.01	*La*	.....	1.28
Cr	2.14	1.65	*Ce*	.....	?
Mn	1.96	?	*Nd*	.....	?
Fe	1.86	1.31	*Sa*	.....	?
Co	2.52	.....	*Eu*	.....	?
Ni	1.83	.....	*Gd*	.....	?

be determined by this calibration method alone, either for Arcturus or for the sun. These "abundance" factors indicate, therefore, only the relative number of atoms above the stellar photosphere as compared with the relative number over the solar disk. Without further information which would lead to a knowledge of the absolute abundance of the atoms in the stellar atmosphere, they do not, in the strict sense, constitute an astrophysical datum of the star.[13] They are, nevertheless, of interest and are given in Table 11. The value for *H* is calculated from the three Balmer lines which appear in the spectral region studied, but the intensities of these lines are really too large for reliable calibration here. For certain of the other elements as well, the data for which have been omitted from Table 8, the

[13] Cf. Pannekoek's remarks on "The Number of Atoms above the Photosphere." *Observatory*, **58**, 322, 1935.

values are of relatively low reliability, and these are marked with colons, indicating their uncertainty. A question mark(?) is used for those elements for which no value at all is available although the element is known[1] to be present in the star, as well as for Ca^+, the H and K lines of which are unfortunately beyond the violet limit of the spectrograms which were studied.

TABLE 12

LOG N'/N

Element	I	Neutral Atom		Ionized Atom	
		$\log \frac{N'}{N}$	Wt.	$\log \frac{N'}{N}$	Wt.
Ca	6.09	1.34	1	.....	.....
Sc	6.57	2.49	0	1.68	1
Ti	6.80	2.18	4	2.11	2
V	6.76	2.09	2	1.99	0
Cr	6.74	1.94	2	1.67	0
Mn	7.40	1.50	1	.....	.....
Fe	7.83	2.08	8	1.26	1
Co	7.81	2.31	1	.....	.....
Ni	7.64	1.55	2	.....	.....

If the fractions of the neutral and ionized atoms of an element over unit area of the star's photosphere be denoted by $1 - x'$ and x', and over unit area of the sun's photosphere by $1 - x$ and x, and N' and N represent the relative values of the total number of atoms of each element over unit area of the two photospheres, then

$$N_0 = N(1 - x) \quad \text{and} \quad N_1 = Nx\,,$$

so that

$$Y_0 = \log \frac{N'(1 - x')}{N(1 - x)} \quad \text{and} \quad Y_1 = \log \frac{N'x'}{Nx}\,.$$

From equation (3)

$$\log \frac{x}{1 - x} = -\frac{5040}{T}(I - I_0) + \log \frac{B_1(T)}{B_0(T)}\,.$$

Hence, the value of $\log (N'/N)$ for a given element may be determined. Those elements which are best represented by the data in

Tables 7 and 8 are *Ca* and the eight members of the *Fe* group: *Sc*, *Ti*, *V*, *Cr*, *Mn*, *Fe*, *Co*, and *Ni;* and for them the values of log (N'/N) are shown in Table 12. The values are fairly constant, indicating that the relative distribution of these nine important elements is approximately the same over the stellar and solar photospheres. With the suggested weights the mean value of log (N'/N), determined from the different values for both neutral and ionized atoms, is 1.95 ± 0.06; but the interpretation of this number depends upon the fundamental zero points in the calibration of the intensity scales of the star and the sun, as yet undetermined.

The writer desires to thank Professor Henry Norris Russell for several very helpful suggestions regarding the preparation of this paper.

STATE COLLEGE OF WASHINGTON
PULLMAN, WASHINGTON
October 1, 1937

THE EXCITATION OF ABSORPTION LINES IN OUTER ATMOSPHERIC SHELLS OF STARS

O. STRUVE AND K. WURM

ABSTRACT

I. The *He* I lines show abnormal intensities in the outer shells of peculiar B stars. In ζ Tauri and φ Persei *He* I λ 3965 (2^1S-4^1P) is narrow and sharp, while all lines arising from the levels 2^1P and 2^3P are broad and diffuse. This is attributed to the dilution of the radiation from the B star in the shell. The anomalous intensities of *He* I are investigated in the entire sequence of B stars having outer shells.

II. The theory of the excitation of absorption lines in a field of diluted radiation is developed and applied to six levels of *He* I: 1^1S, 2^1S, 2^1P, 2^3S, 2^3P, and the state of ionization. The populations in the various states have been computed for dilution factors 0.1, 0.02, and 0.01, and for temperatures of 10^4 and 2.5×10^4 degrees.

III. The theoretical populations for a dilution factor of the order of 0.01 agree with the observations. Accordingly, the radius of the shell is approximately five times the radius of the star. The entire *He* I anomaly is accounted for by the theory.

IV. The absence of rotational broadening in lines produced in the shells shows that these shells do not rotate as solid bodies with the photospheres. The latter are rotating rapidly in most of the stars investigated. Some lines, such as *Si* II in ζ Tauri, show broadening intermediate between the normal *He* I lines in the deepest layers and the λ 3965 line of *He* I in the shell. Hence, the elements are stratified. The ionization decreases outward in all stars investigated except β Lyrae. The strength of the *H* cores in the shells is explained by the metastability of the 2S-level. The weakness of *Mg* II 4481 is explained by the fact that the lower level has strong transitions downward.

V. The *He* I anomaly in ordinary giants and dwarfs of class B bears a strong resemblance to the anomaly in the shells. The explanation is doubtless similar, but there are complications due to Stark effect, collisional damping, etc.

I. THE HELIUM ANOMALY IN THE OUTER SHELLS OF PECULIAR B STARS

ζ Tauri.—This star is representative of a small group of B stars which have extremely sharp and deep absorption lines of hydrogen, between symmetrically spaced emission components of relatively low intensity. These emission components are conspicuous in *H*α and *H*β; they are weak in *H*γ and are absent in *H*δ as well as in all higher members of the Balmer series. The hydrogen lines show also fairly conspicuous broad absorption wings, suggestive of the normal Stark effect in early-type stars. The *He* I lines $\lambda\lambda$ 4472, 4388, 4144, 4121, 4026, and 4009 are broad and very diffuse. They suggest rapid axial rotation—of the order of 200 km/sec at the equator, for $v_{\text{rot}} \sin i$.

The star is a well-known spectroscopic binary, having been dis-

covered to be such by Frost and Adams[1] in 1903. The period is 138 days according to Adams,[2] or 133 days according to Miss Losh.[3] The total range in velocity is 22 km/sec, but the results from different lines are not entirely consistent.[3] Miss Losh concludes: ". . . . the velocity or wave length variations of ζ Tauri can not be explained fully by orbital motion alone. While these curves undoubtedly result largely from orbital motion, clearly there are other factors involved which can not now be identified. . . . ."

The rotational explanation of the great widths of the *He* I lines listed above is so well supported by their contours that it can be safely trusted in our discussion, despite the fact that the absorption lines of *Fe* II, *Ni* II, *Si* II, and the cores of the Balmer lines are very much narrower. In order to strengthen this conclusion we have examined the spectra of all B-type stars for which spectrograms are available at the Yerkes Observatory. In all normal stars—several hundred in number—the dish-shaped rotational contours are observed in all lines of all elements. This rule is violated only in a small group of stars—all of peculiar spectrum—which have emission lines of hydrogen, narrow absorption cores between the double emission components of hydrogen, narrow lines of *Fe* II, which sometimes lie between double emission components, strong narrow lines of *Ni* II and weak ones of *Si* II, occasionally very faint narrow *Mg* II 4481, but always broad and diffuse lines of *He* I, $\lambda\lambda$ 4472, 4388, 4026, 4009, etc. The best-known representatives of this group of stars are ζ Tauri, φ Persei, 48 Librae, ϵ Capricorni, *o* Aquarii, $+47^{\circ}3985$, and β Monoceratis A.

Since the presence of emission lines demonstrates the existence of a large outer shell, the simultaneous appearance of narrow absorption lines of *Fe* II, *Ni* II, *H*, etc., with broad *He* I lines raises no serious difficulty in regard to the rotational interpretation of the broad *He* I lines. The broad lines are believed to come from the true reversing layer of the star, while the narrow lines originate in the outer shells.

However, the spectrum of ζ Tauri reveals a phenomenon of very

[1] *Ap. J.*, **17**, 151, 1903.

[2] *Ibid.*, **22**, 115, 1905.

[3] *Pub. Obs. U. Michigan*, **4**, 21, 1932.

great interest. While all other *He* I lines which we are able to observe on our plates between λ 3900 and λ 5000 are rotationally broadened, the line *He* I 3965 is exceedingly narrow and sharp (Pl. II). Since we cannot reasonably question the rotational theory of the broad *He* I lines, we are compelled to attribute the origin of the sharp λ 3965 to the same outer shell which gives rise to the narrow cores of the hydrogen lines.

A clue to the explanation of this phenomenon is found in the metastability of the 2^1S-level of the *He* I atom from which the line λ 3965 arises. It is due to the transition $2^1S - 4^1P$. An inspection of the Grotrian diagram for *He* I shows that the only other member of the series $2^1S - n^1P$ which can be observed with our spectrograph, λ 5016, is in the green part of the spectrum, where our photographic emulsion was not sensitive. It is, however, quite certain from evidence supplied by other stars that all members of the series $2^1S - n^1P$ behave in substantially the same manner as λ 3965.

It is evident that the relatively greater strength of λ 3965 in the shell than in the normal reversing layer is caused by the effect of dilution of radiant energy. The interpretation is thus substantially similar to that which Bowen has advanced for the explanation of large populations in metastable levels in gaseous nebulae. In the shell the dilution of the radiation is quite pronounced and the Rosseland cycle goes into operation. If the radiation is sufficiently diluted, the atoms accumulate in the metastable level 2^1S. Hence, in the shell λ 3965 is strong. In the star proper, where rotation is large, λ 3965 is weak because we have essentially conditions of thermodynamic equilibrium.

The spectrum of *He* I possesses another metastable level, namely, 2^3S. Of the series $2^3S - n^3P$, only λ 3889 falls in the region which can be photographed with our spectrograph, and this line is hopelessly blended with $H\zeta$. It is, however, probable from evidence supplied by other stars (β Lyrae) that this line behaves substantially as does λ 3965. A detailed study is impossible.[4]

The *He* I series ($2^1P - n^1S$) and ($2^1P - n^1D$) contain many observable lines. In ζ Tauri all of them belong to the reversing layer

[4] It is suggestive that O. C. Wilson has found *He* I 3889 as a moderately strong absorption line in the Orion nebula (*Pub. A.S.P.*, **49**, 338, 1937).

PLATE II

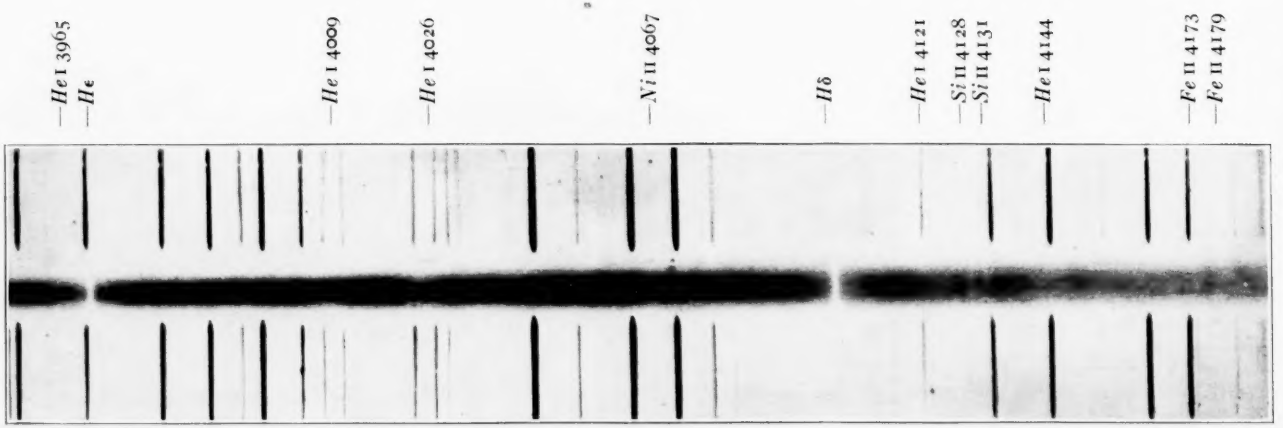

THE SPECTRUM OF ζ TAURI

(1937 Sept. 21; 11^h03^m G.C.T.)

The *He* I line λ 3965 is sharp and narrow, while the other lines of *He* I are very broad and diffuse

of the star, not to the shell. The triplet series ($2^3P - n^3S$) and ($2^3P - n^3D$) in ζ Tauri also belong to the reversing layer.

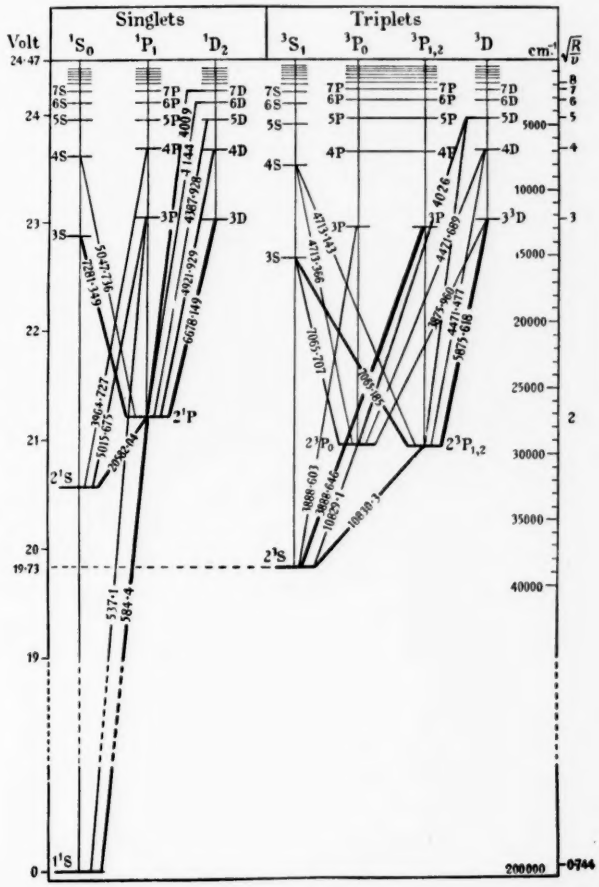

FIG. 1.—Grotrian diagram of *He* I

It is obvious that the population of the level 2^1S is greatly increased in the shell with respect to the levels 2^1P and 2^3P. How much this increase amounts to cannot be ascertained from ζ Tauri alone, since the shell shows no lines originating from levels 2^1P and 2^3P, while the reversing layer shows no line originating from 2^1S. In the following discussion we shall supply additional information from other stars.

The unusual interest of this problem is enhanced by the fact that the metastable *He* I levels lie very high: 2^1S at 20.5 volts and 2^3S at 19.7 volts. The ionization potential of *He* I is 24.5 volts. In this respect the case under consideration differs materially from Bowen's case of the nebular lines of [*O* III]: there the metastable levels are close to the ground-level, and their populations are largely produced by collisions.

If we consider in our *He* problem only three states, namely, the ground state, the metastable state, and a third state which combines directly with the ground state (this may be the 2^1P-level or the state of ionization), then Rosseland's formula may be used to compute the relative populations. Disregarding for the moment the statistical weights, we have

$$\frac{n_2}{n_1} = e^{-h\nu_{12}/kT}\left[\frac{1-(1-W)e^{-h\nu_{23}/kT}}{1-(1-W)e^{-h\nu_{13}/kT}}\right],$$

where W is the dilution factor $R^2/4r^2$.

This formula is exact. If the metastable-level is close to the ground-level, $\nu_{23} \approx \nu_{13}$ and the expression in square brackets drops out. We then have pure Boltzmann distribution for n_2. In our case, $h\nu_{23} \neq h\nu_{13}$, and the expression in brackets must be retained. However, for moderately large dilutions, W is so close to zero that it affects the expression very little. In our case, for $T = 20{,}000°$ we have approximately

$$\left[\frac{1-(1-W)e^{-h\nu_{23}/kT}}{1-(1-W)e^{-h\nu_{13}/kT}}\right] = 0.68\,.$$

On the other hand, the ratio

$$\frac{n_3}{n_1} = We^{-h\nu_{13}/kT}\left[\frac{1}{1-(1-W)e^{-h\nu_{13}/kT}}\right] \approx \frac{1}{0.999}\,We^{-h\nu_{13}/kT}\,.$$

It is obvious that if we can obtain from the observations satisfactory estimates of n_3/n_1 and n_2/n_1, we should, in principle, be able to determine W. In practice we shall use the following observed quantities

$$\frac{\text{Int. 3965 (shell)}}{\text{Int. 3965 (star)}} \cdot \frac{\text{Int. 4009 (star)}}{\text{Int. 4009 (shell)}}\,.$$

PLATE III

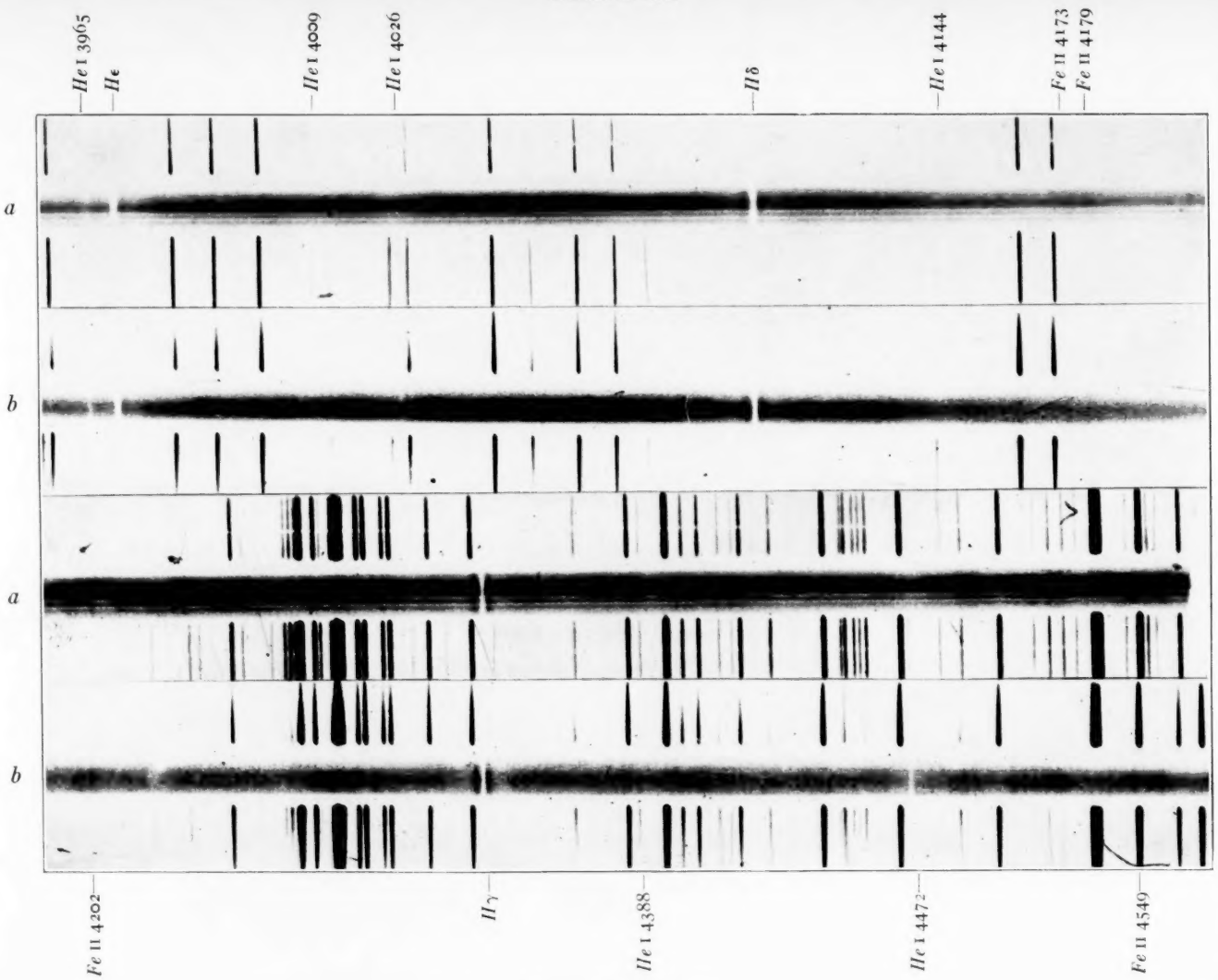

SPECTRA OF φ PERSEI

a) 1934 Dec. 11; 4^h20^m G.C.T. *b*) 1935 Jan. 24; 3^h21^m G.C.T.

Within the precision of the three-cycle theory this quantity should be equal to (disregarding the statistical weights)

$$\frac{n_0\,(\text{shell})\;0.68\;e^{-h\nu_{12}/kT}}{n_0\,(\text{star})\;e^{-h\nu_{12}/kT}} \times \frac{n_0\,(\text{star})\;e^{-h\nu_{13}/kT}}{n_0\,(\text{shell})\;\frac{1}{0.999}\;We^{-\frac{h\nu_{13}}{kT}}}.$$

It is clear that all values of n_0 and $e^{-h\nu/kT}$ drop out, leaving only a numerical constant close to one and $1/W$.

However, in view of the fact that the three-cycle theory of Rosseland does not allow us to investigate the simultaneous behavior of the singlets and triplets, we have, in Section II, analyzed the corresponding problem of six states: the ground-level 1^1S, the singlet levels 2^1S and 2^1P, the triplet levels 2^3S and 2^3P, and the state of ionization.

φ Persei.—A star which resembles ζ Tauri to a surprising degree is φ Persei. It, too, is a spectroscopic binary of fairly long period—126.6 days. The spectral features, which are variable, have been described by several astronomers.[5] The emission lines of *H* and *Fe* II are stronger than in ζ Tauri, and so are also the central absorption cores. The *He* I lines λλ 4472, 4388, 4144, 4026, and 4009 are almost always exceedingly broad and diffuse, suggesting an equatorial component in the line of sight of the rotational velocity amounting to about 250 km/sec. The *He* I line λ 3965 is strong and sharp—as in ζ Tauri. It may possibly be superposed over a background of a broad and diffuse line, but this line is too faint to be identified with certainty.

A striking peculiarity of the spectrum of φ Persei is the variation of the *He* I absorption lines. While λ 3965 is always sharp, the other *He* I lines are broad and diffuse, except at certain phases—especially from 20 to 40 days after maximum positive velocity.[6] Plate III shows at the top (*a*) the normal spectrum, at the bottom (*b*) the spectrum taken during the interval of phase stated in the foregoing. The *He* I lines in (*b*) show sharp cores for the triplets λλ 4472 and 4026 but no cores for the singlets λλ 4388 and 4009. The singlets remain per-

[5] See H. F. Schiefer, *Ap. J.*, **84**, 568, 1936, where complete references to other papers are given. See also Struve and Swings, *ibid.*, **75**, 161, 1932.

[6] This feature was detected by F. C. Jordan, *Pub. Alleghany Obs.*, **3**, 34, 1913.

SPECTRA OF φ PERSEI
a) 1934 Dec. 11; 4^{h}20^m G.C.T. *b*) 1935 Jan. 24; 3^{h}21^m G.C.T.

fectly normal while the triplets develop cores which are superposed over the broad rotational lines. At the same time the singlet λ 3965 is strengthened.

It is not yet possible to advance a complete physical interpretation of the spectrum of φ Persei. But the phenomenon resembles in a striking manner the variation of the *He* I lines in μ Sagittarii discovered by Morgan.[7] There, too, the strengthening of the lines is limited to the *He* I triplets, and the entire phenomenon takes place within a short interval of time, on the descending branch of the velocity curve, not far from the place where an eclipse would occur if the inclination were suitable.

There is also a distinct resemblance between the phenomena in these two stars and the spectroscopic features of ζ Aurigae, ε Aurigae, and VV Cephei immediately preceding and following eclipse. It would be profitable to pursue this matter and to investigate whether eclipses by the atmospheres of spectroscopic components are really responsible for the phenomenon.[8]

It is sufficient for our present purpose to assume, as seems reasonable, that in the phase interval of 20–40 days after maximum the amount of *He* I gas in a field of diluted radiation is greater than normal. We conclude that although λ 3965 ($2^1S - 4^1P$) is, among the observable lines, the one that is most enhanced in the presence of diluted radiation, the triplet lines λ 4472 ($2^3P - 4^3D$) and λ 4026 ($2^3P - 5^3D$) are also enhanced relative to the singlet lines λ 4388 ($2^1P - 5^1D$), λ 4144 ($2^1P - 6^1D$), and λ 4009 ($2^1P - 7^1D$).

The other triplet lines are not suitable for a comparison; λ 4121 ($2^3P - 5^3S$) may be present, but it is very weak. The normal spectrum of φ Persei reveals, upon close inspection, an exceedingly faint core in λ 4026 and perhaps also in λ 4472. This would, if real, show that the phenomenon is naturally present in the outer shell.

Other stars having outer shells.—It is evident that the spectral type of ζ Tauri and φ Persei is composite. Normal B stars do not show the absorption lines of *Ni* II and *Fe* II, except in the latest

[7] *Ap. J.*, **75**, 407, 1932.

[8] We are indebted to Dr. W. W. Morgan for having called our attention to this possibility in the case of μ Sagittarii. At his suggestion Dr. C. T. Elvey is now observing μ Sagittarii with the photoelectric photometer at the McDonald Observatory.

PLATE IV

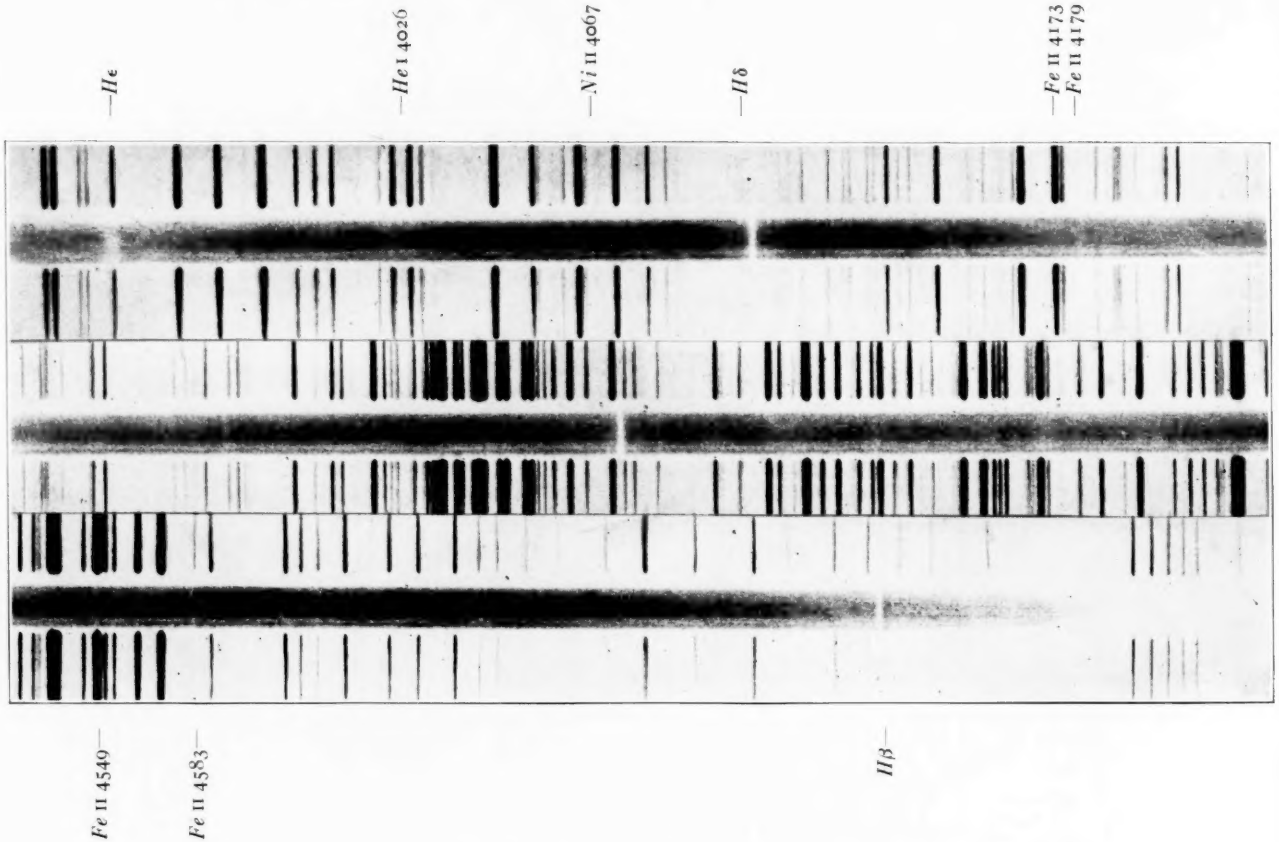

THE SPECTRUM OF 48 LIBRAE (BS5941)
(1935 June 8; $4^{h}02^{m}$ G.C.T.)

subdivisions where the *He* I lines are weak and the Stark wings of the *H* lines are strong. For purposes of classification it will be best to treat separately the normal rotational reversing layer and the outer shell. Although such a division is somewhat arbitrary—the two types of structure doubtless merge into one another—the classification becomes more consistent. The spectral type of φ Persei is given as Bope by Schiefer,[5] and that of ζ Tauri is given as B3p in the *Henry Draper Catalogue*. From the fairly large intensities of the rotational *He* I lines in ζ Tauri it would appear that the spectral class is about B3. In φ Persei the rotational *He* I lines are somewhat weaker than in ζ Tauri, but the characteristic stellar lines of the early subdivisions of class B, such as *Si* III, *Si* IV, *O* II, etc., are not visible, perhaps because of the large rotational broadening. Neither is there any indication of a broad *Mg* II 4481, which should be present if the spectrum were B5 or later. The Stark wings of *H* are fairly well pronounced, however, and it seems reasonable to attribute class B3 to the reversing layer of φ Persei.

It will be of interest to consider several other stars of similar character. ϵ Capricorni[9] (Pl. IV) has strong rotational lines of *He* I, variable sharp lines of *Fe* II in absorption, and strong cores of *H* superposed over fairly strong Stark wings. *Mg* II 4481 is present as a faint absorption line of intermediate width, probably variable in intensity. The spectral class from the broad *He* I lines may be B5. The line *He* I 3965 is not visible, but our plates are not quite conclusive in this respect. It is fairly certain, however, that λ 3965 is not as strong as in φ Persei. The spectral type of the shell is definitely later than that of φ Persei.

The spectrum of 48 Librae resembles that of ϵ Capricorni. The broad *He* I lines are very weak, while the sharp *Fe* II lines are quite strong. There is probably a very weak broad line of *Mg* II 4481 (but its width seems to be less than that of *He* I 4472). The *Ni* II line λ 4067 is sharp. The *Si* II lines 4128.0 and 4131.9 are moderately sharp and very faint. The wings of the *H* lines are faint. There is a slight suggestion of a faint, narrow line of *He* I 3965, but

[9] *Ap. J.*, **75**, 176, 1932. Numerous other stars of similar character are known from the work of Merrill, Harper, and others. We shall confine ourselves here to a few typical stars for which spectrograms have been secured at the Yerkes Observatory.

the evidence is not conclusive. The spectral class of the reversing layer is about B5.

The sequence of peculiar stars with large outer shells continues to cooler objects such as 17 Leporis[10] and the I component of ϵ Aurigae.[11] The former possesses a rotationally broadened line of *Mg* II 4481 but fails to show the lines of *He* I. The wings of the *H* lines are strong. Accordingly, the spectral type of the reversing layer is A. The I component of ϵ Aurigae shows the spectrum of its outer shell several months prior to the first contact of the eclipse and a similar length of time following the last contact of the eclipse. Its spectral type is F.

On the hot side of ζ Tauri our information concerning the absorption spectra of shells is limited to the B5 component of β Lyrae[12] and the expanding shell of P Cygni.[13] The latter shows only the spectrum of the shell. There is no indication of Stark wings of *H*, or of normal, broadened *He* I lines. The so-called B5 component of β Lyrae is produced by absorption in the expanding shell which surrounds the binary system composed of the strong B8 component and the hypothetical A component. The expanding shells of both stars show very strong *He* I 3965 and strong triplet *He* I lines; the singlet lines $\lambda\lambda$ 4009, 4144, and 4388 are also present, and are moderately strong in absorption but are weak in emission. Both shells correspond to much earlier types than the shell of ζ Tauri. Hence, it would appear that at least on the hot side of the sequence the normal *He* I singlet level 2^1P is fairly well populated, although there is a deficiency as compared with the populations of the corresponding triplet levels.

Summarizing our observations concerning the *He* lines, we establish the following properties:

1. In the cooler stars, λ 3965 ($2^1S - 4^1P$) is the first line to appear in the shell.

2. The triplet lines ($2^3P - n^3D$) appear in the shell when (ζ Tauri

[10] *Ap. J.*, **76**, 85, 1932. [11] *Ibid.*, **86**, 570, 1937.

[12] Struve, *Observatory*, **57**, 265, 1934; Baxandall-Stratton, *Annals Solar Phys. Obs.* (Cambridge), **2**, Part 1, 1930.

[13] *Ap. J.*, **81**, 66, 1935.

and abnormal stage of φ Persei) the number of atoms is large, but for the cooler stars λ 3965 is stronger than λ 4026.

3. When the excitation of the shell is larger, so that *Fe* II no longer appears in absorption, the singlet lines ($2^1P - n^1D$) begin to appear faintly in the spectrum of the shell. In β Lyrae[14] the estimated intensities of three lines are: λ 3965, 10; λ 4009, 2; λ 4026, 8. In a normal B5 giant, 67 Ophiuchi, the corresponding intensities are: λ 3965, 8; λ 4009, 9; λ 4026, 12. In the shell of β Lyrae, λ 3965 remains the strongest of the three lines.

4. When the excitation in the shell is very high, the triplet lines become relatively stronger and λ 4026 surpasses λ 3965. The intensities in P Cygni[15] are: λ 3965, 10; λ 4009, 8; λ 4026, 15. Although the singlet lines ($2^1P - n^1D$) remain considerably weaker than the triplets ($2^3P - n^3D$), the difference is less striking than in shells of lower excitation.

II. POPULATIONS OF THE SINGLET AND TRIPLET LEVELS

In regard to the variation of the absorption lines from star to star, as described in the preceding part of this paper, it is quite reasonable to seek the causes in a variation of the relative populations of the states involved. We may expect that in passing within the absorbing layer to greater distances from the photospheric region there will be more or less marked deviations from thermodynamical equilibrium, which may give a distribution of the atoms over the various states that is very different from a Boltzmann distribution for any temperature. As is well known, there exists no adequate theoretical formula for such conditions by means of which we can compute the ionization and excitation. It is not to be expected that such a general formula can be derived. It is not difficult to see that the excitation properties, especially the relative populations of the energy levels, will depend strongly on the arrangement of these levels within the individual atom. Therefore, every atom must be treated more or less separately, even though we have some general rules which have been derived to explain the appearance of bright lines, especially forbidden lines in stars with extended atmospheres of low pressure. But in our case such a general rule cannot

[14] Pillans, *ibid.*, **80**, 57, 1934.

[15] *Ibid.*, **81**, 69, 1935.

give a satisfactory explanation of the different features of the observations, and we shall therefore try to obtain more accurate information.

Since approximate values of the transition probabilities for the strongest *He* I transitions are known from a quantum-mechanical computation of Hylleraas,[16] it is possible to carry out at least an approximate computation of the relative populations of the most important *He* I levels, if we can neglect the influence of collisions. To carry through this computation we shall use a method suggested by Rosseland (theory of cycles) and worked out in detail by Woolley[17] in connection with the fluorescence in $H\alpha$ and $H\beta$ in an atmosphere of diluted radiation; for this problem Woolley took into account the simplest possible transition schemes involving only four levels in each case. Our problem is somewhat more complicated because we are interested in the two *He* I systems (singlets and triplets). We shall, therefore, take into consideration six states, namely, 1^1S, 2^1S, 2^1P, 2^3S, 2^3P, and the ground state of *He* II. The limitation to these six states naturally disregards higher quantum states in both systems from which strong transitions start toward the lower levels. But we may expect that these higher transitions do not appreciably change the relative properties for singlets and triplets, especially in view of the fact that the two systems are arranged in an entirely similar manner. We shall discuss the influence of collisions later. It is possible to predict approximately how these, if they are present at all, will change the distribution created by radiation alone.

The population of a particular state will be determined by certain coefficients A_{ik} and A_{ki}, which are the expressions for the probability that an atom makes a transition per second, as indicated by the subscripts. Using the notation of Woolley's paper, which is identical with that of Eddington in his *Internal Constitution of the Stars*, we have $(i < k)$:

$$A_{ik} = a_{ik}\rho(\nu) \; ; \qquad A_{ki} = b_{ki} + a_{ki}\rho(\nu) \, , \tag{1}$$

where $\rho(\nu)$ is the energy density of radiation, b_{ki} is the probability coefficient for spontaneous transitions, and a_{ik} and a_{ki} are the coef-

[16] *Zs. f. Phys.*, **106**, 395, 1937.

[17] *M.N.*, **94**, 631, 1934.

ficients for absorption and for induced emission. The a's and the b's are connected by the well-known relations

$$a_{ik}\rho(\nu) = \frac{q_k}{q_i} \times \frac{b_{ki}}{e^{h\nu/kT} - 1} \quad \text{and} \quad a_{ki}\rho(\nu) = \frac{b_{ki}}{e^{h\nu/kT} - 1}, \qquad (2)$$

where q designates the statistical weight of the term and $\rho(\nu)$ is now the equilibrium value at the temperature T. If we deal with diluted radiation, the equilibrium value of $\rho(\nu)$ has to be replaced by $\rho'(\nu) = W\rho(\nu)$, where W is the dilution factor.

TABLE 1

	1^1S	2^1S	2^1P		2^3S	2^3P
2^1P.....	0.349	0.39	.....	2^3P.....	0.55	.....
Cont.....	1.55	1.38	0.19	Cont.....	1.36	0.19

With the exception of A_{6i}, the index 6 referring to the ionized state, all A_{ik} and A_{ki} can be computed with the use of the values of the oscillator strength, f, which were computed by Hylleraas and are listed in Table 1.

The values of b_{ik} can be computed with the aid of the relation

$$f_{ik} = \frac{1}{3} \times \frac{q_k}{q_i} \times \frac{b_{ki}}{\omega}, \qquad (3)$$

where ω is the classical damping constant equal to $8\pi^2e^2\nu^2/3mc^3$. The probability coefficients for transitions into the ionized state can be evaluated from

$$A_{i6} = \frac{3f_{i6}\omega}{e^{h\nu/kT} - 1}\left[= \frac{\pi e^2}{mh\nu} \times f\rho(\nu)\right]. \qquad (4)$$

The probability coefficients for the opposite jumps, A_{6k}, cannot be determined directly. But we require only their relative values, which can be found by applying the principle of detailed balancing in the thermodynamical equilibrium, where the following relation must hold:

$$A_{61} : A_{62} : A_{63} \ldots = n_1A_{16} : n_2A_{26} : n_3A_{36} \ldots . \qquad (5)$$

The values of n are here given by the Boltzmann formula.

With respect to the recombination, we must take into account the fact that the temperature of the recombining electrons may be different from the temperature T which we assume for the radiation. But the values of A_{6k} in Table 3 show that over a large range of temperature there is no strong dependence of the values of A_{6k} upon temperature.

In a steady state we have

$$\sum_k n_i A_{ik} = \sum_k n_k A_{ki} , \tag{6}$$

which means that the number of transitions ending in a state is equal to the number which start from it. As was pointed out by Woolley, we can include in the states considered in (6) the ionized state, without specifying a definite electron pressure, if we do not wish to determine n_6/n_k.

If we have to deal with r different states, including the ionized state, then, according to (6), we have r different equations with $r - 1$ unknowns: $n_2/n_1, n_3/n_1, \ldots, n_r/n_1$. In our case r is equal to six. Using the abbreviations

$$\left.\begin{aligned} A_{11} &= -(A_{12} + A_{13} + \ldots . A_{1r}) , \\ A_{22} &= -(A_{21} + A_{23} + \ldots . A_{2r}) , \end{aligned}\right\} \tag{7}$$
$$\ldots \ldots \ldots \ldots \ldots \ldots$$

the determinant

$$D = \begin{vmatrix} A_{11} \ldots . A_{r1} \\ A_{12} \ldots . A_{r2} \\ \ldots \ldots \ldots \\ \ldots \ldots \ldots \\ A_{1r} \ldots . A_{rr} \end{vmatrix} \tag{8}$$

vanishes and the values of $n_1, n_2, n_3, \ldots$, must be proportional to the minors $A_{1i}, A_{2i}, A_{3i}, \ldots$.

We have evaluated the minors A_{21}, A_{31}, A_{41}, and A_{51} for the levels 2^1S, 2^1P, 2^3S, and 2^3P, in which we are interested, for two different temperature values, $T = 10^4$ and $T = 2.5 \times 10^4$, and for the dilution factors $W = 1$, $1/10$, $1/50$, and $1/100$. The constants used are listed in Tables 2 and 3. The values of A_{ik} and A_{ki} between singlets

and triplets are all set equal to zero because these intercombinations are forbidden or are extremely weak. Table 4 gives the results of

TABLE 2

LINE TRANSITIONS

TRANSITION	VOLTS	$e^{h\nu/kT}$		f_{ik}	q_i/q_k	ω	b_{ki}
		$T=10^4$	$T=2.5\times10^4$				
$1^1S\rightarrow2^1P$	21.13	4.37×10^{10}	1.80×10^4	0.349	1/3	6.44×10^9	2.25×10^9
$2^1S\rightarrow2^1P$	0.60	2.01	1.32	0.390	1/3	5.19×10^6	2.02×10^6
$2^3S\rightarrow2^3P$	1.14	3.74	1.70	0.550	3/9	1.88×10^7	1.03×10^7

	A_{ik}; $W=1$		A_{ik}; $W=1/10$		A_{ik}; $W=1/50$		A_{ik}; $W=1/100$	
	$T=10^4$	$T=2.5\times10^4$	$T=10^4$	$T=2.5\times10^4$	$T=10^4$	$T=2.5\times10^4$	$T=10^4$	$T=2.5\times10^4$
$1^1S\rightarrow2^1P$	1.54×10^{-1}	3.75×10^5	1.54×10^{-2}	3.75×10^4	3.08×10^{-3}	7.50×10^3	1.54×10^{-3}	3.75×10^3
$2^1S\rightarrow2^1P$	6.00×10^6	1.89×10^7	6.00×10^5	1.89×10^6	1.20×10^5	3.78×10^5	6.00×10^4	1.89×10^5
$2^3S\rightarrow2^3P$	1.13×10^7	4.41×10^7	1.13×10^6	4.41×10^6	2.26×10^5	8.82×10^5	1.13×10^5	4.41×10^5

	A_{ki}; $W=1$		A_{ki}; $W=1/10$		a_{ki}; $W=1/50$		A_{ki}; $W=1/100$	
	$T=10^4$	$T=2.5\times10^4$	$T=10^4$	$T=2.5\times10^4$	$T=10^4$	$T=2.5\times10^4$	$T=10^4$	$T=2.5\times10^4$
$1^1S\rightarrow2^1P$	2.25×10^9	2.25×10^9	2.25×10^9	2.25×10^9	2.25×10^9	2.25×10^9	2.25×10^9	2.25×10^9
$2^1S\rightarrow2^1P$	4.02×10^6	8.33×10^6	2.22×10^6	2.64×10^6	2.06×10^6	2.14×10^6	2.03×10^6	2.08×10^6
$2^3S\rightarrow2^3P$	1.41×10^7	2.60×10^7	1.07×10^7	1.17×10^7	1.03×10^7	1.06×10^7	1.03×10^7	1.05×10^7

TABLE 3

TRANSITIONS INTO CONTINUUM

TRANSITION	VOLTS	$e^{h\nu/kT}$		f_{ik}	q	ω	A_{i6}; $W=1$	
		$T=10^4$	$T=2.5\times10^4$				$T=10^4$	$T=2.5\times10^4$
$1^1S\rightarrow$Cont.	24.47	2.11×10^{10}	8.50×10^4	1.55	1	8.66×10^9	1.91×10^{-2}	4.74×10^5
$2^1S\rightarrow$Cont.	3.94	9.56×10^1	6.17	1.38	1	2.26×10^8	9.90×10^6	1.81×10^8
$2^1P\rightarrow$Cont.	3.36	4.94×10^1	4.76	0.9	3	1.63×10^8	1.92×10^6	2.47×10^7
$2^3S\rightarrow$Cont.	4.73	2.42×10^2	9.02	1.36	3	3.26×10^8	4.79×10^6	1.66×10^8
$2^3P\rightarrow$Cont.	3.60	6.46×10^1	5.31	0.19	9	1.88×10^8	1.70×10^6	2.46×10^7

	A_{i6}; $W=1/10$		A_{i6}; $W=1/50$		A_{i6}; $W=1/100$		A_{6k}	
	$T=10^4$	$T=2.5\times10^4$	$T=10^4$	$T=2.5\times10^4$	$T=10^4$	$T=2.5\times10^4$	$T=10^4$	$T=2.5\times10^4$
$1^1S\rightarrow$Cont.	1.91×10^{-3}	4.74×10^4	3.82×10^{-4}	9.48×10^3	1.91×10^{-4}	4.74×10^3	1000.00	1000.00
$2^1S\rightarrow$Cont.	9.90×10^5	1.81×10^7	1.98×10^5	3.62×10^6	9.90×10^4	1.81×10^6	23.30	28.10
$2^1P\rightarrow$Cont.	1.92×10^5	2.47×10^6	3.84×10^4	5.94×10^5	1.92×10^4	2.47×10^5	6.89	8.68
$2^3P\rightarrow$Cont.	4.79×10^5	1.66×10^7	9.58×10^4	3.32×10^6	4.79×10^4	1.66×10^6	86.20	111.11
$2^3P\rightarrow$Cont.	1.70×10^5	2.46×10^6	3.40×10^4	4.92×10^5	1.70×10^4	2.46×10^5	24.80	29.40

our computation. Judging from the numerical values of the differences appearing in the members of the minors, the accuracy of the

computation is of the order of 5 per cent. To obtain a higher accuracy, three decimals in the A_{ik} and A_{ki} should be used instead of only the two used here.

As is to be expected, for $W = 1$ we obtain a Boltzmann distribution. This computation was carried out for the purpose of checking our results. What is demonstrated most strikingly in Table 4 is the

TABLE 4

RELATIVE POPULATIONS IN FOUR LEVELS OF *He* I

$T = 10^4$

	Boltzmann Distribution at $T = 10^4$	$W = 1$	$W = 1/10$	$W = 1/50$	$W = 1/100$	Term
n_2	100	100	100	100	100	2^1S
n_3	150	152	11	5	2	2^1P
n_4	753	756	814	1140	1150	2^3S
n_5	610	602	75	30	15	2^3P

$T = 2.5 \times 10^4$

	Boltzmann Distribution at $T = 2.5 \times 10^4$	$W = 1$	$W = 1/10$	$W = 1/50$	$W = 1/100$	Term
n_2	100	100	100	100	100	2^1S
n_3	226	227	45	5	3	2^1P
n_4	428	420	501	545	538	2^3S
n_5	703	710	321	70	40	2^3P

preference of the metastable states for higher dilutions. But the two metastable levels 2^1S and 2^3S behave in a slightly different manner: the relative population of the 2^3S state increases somewhat more strongly than that of the 2^1S state. This may be expressed by saying that the metastability of the 2^3S-level is somewhat higher than that of the 2^1S-level. This is explained by the fact that the depopulation of the former can go in only one direction, namely, over the ionized state, while for the 2^1S-level the atoms can also escape over the very short-lived 2^1P-level to the ground state. That the 2^1P term shows the strongest decrease is quite consistent with the general rule hereinbefore mentioned. The table shows a number of other interesting

features which we shall discuss in connection with the observational data in Section III.

We shall now discuss the influence of collisions. Since the atmosphere which we are considering is in a high state of ionization, we can neglect the atomic and ionic collisions and direct our attention only to electron collisions. Analogous to our A_{ik} and A_{ki} for the radiation jumps, we define certain coefficients a_{ik} and a_{ki} for collision transitions, which designate the probability that an atom will make, per second, a transition, as indicated by the subscripts. Naturally, our a_{ik} and a_{ki} depend on the electron density n_e, as well as on the velocity distribution of the electrons (temperature) and the excitation and de-excitation cross-sections σ^2_{ik} and σ^2_{ki}. Strictly speaking, our a_{ik} and a_{ki} would be determined by [18]

$$a_{ik} = n_e \int_{\eta=\eta_0}^{\infty} S_i^k(\eta) \left(\frac{2\eta}{m}\right)^{1/2} \mu(\eta) d\eta \; ; \qquad \left[\mu(\eta)d\eta = \frac{2\pi}{(\pi kT)^{3/2}} e^{-\eta/kT} \eta^{1/2} d\eta\right] , \tag{9a}$$

$$a_{ki} = n_e \int_{0}^{\infty} S_k^i(\eta) \left(\frac{2\eta}{m}\right)^{1/2} \mu(\eta) d\eta \, , \tag{9b}$$

where η is the energy of the relative motion of atom and electron, η_0 is equal to the excitation energy of the level, S_i^k and S_k^i are the excitation and de-excitation cross-sections, n_e is the electron density, and m is the mass of the electron.

Since we do not have any information on the functions $S(\eta)$, the best we can do is to replace them by an average value of the excitation cross-section σ^2_{ik}. Even concerning σ^2_{ik} we have very little information. From the experimental results on the determination of σ^2 for different elements, we can only conclude that it varies from 10^{-16} to 10^{-18} cm^2 and to even smaller values. Assuming a constant σ^2, equation (9) gives, after integration,[19]

$$a_{ik} = n_e \sigma^2_{ik} 2 \left\{\frac{2\pi kT}{m}\right\}^{1/2} e^{-\eta_0/kT} \, , \tag{10a}$$

$$a_{ki} = n_e \sigma^2_{ki} 2 \left\{\frac{2\pi kT}{m}\right\}^{1/2} . \tag{10b}$$

[18] See R. H. Fowler, *Statistical Mechanics*, 2d ed., p. 680, Cambridge, 1936.

[19] *Ibid.*, pp. 703–706.

There are some indications that for higher values of the excitation energy, σ^2 is nearer to 10^{-18} than to 10^{-16} cm^2. Assuming $\sigma^2 = 10^{-18}$, we find for the deepest upper level, 2^3S,

$$a_{14} = \left\{ \begin{array}{ll} n_e \times 10^{-18} & \text{for} \quad T = 10^4 , \\ n_e \times 10^{-12} & \text{for} \quad T = 2.5 \times 10^4 . \end{array} \right\} \tag{11}$$

These values of a_{14} we compare with our A_{ik} in Tables 2 and 3 for transitions to 2^1P and to the continuum. Regarding the case $W = 1$, we have $A_{13} = 1.5 \times 10^{-1}$ and $A_{16} = 2 \times 10^{-2}$ for $T = 10^4$ and $A_{13} = 4 \times 10^5$ and $A_{16} = 5 \times 10^5$ for $T = 2.5 \times 10^4$. There will be an appreciable additional population by collisions from the ground state only if a_{14} becomes of the same order as the values of A_{ik}. This means that the electron density must be

$$n_e \gtrsim 10^{18} \text{ cm}^{-3} \quad \text{for} \quad T = 10^4 \text{ and } T = 2.5 \times 10^4 . \tag{12}$$

Even if we should assume the higher value of σ^2 ($= 10^{-16}$), which gives $n_e \gtrsim 10^{16}$, it is evident that collisions can play no role because we cannot expect such electron densities to exist in our shells. The analysis of stellar atmospheres points to an electron pressure of between 1 to 100 bar for normal layers, which corresponds to values of n_e between 10^{12} and 10^{14}.

For higher dilutions there will be no difference if the density decreases in the same proportion as the dilution increases ($W\rho =$ const.); this condition may be approximately fulfilled in most cases. If the density decreases much more slowly than the radiation density, we may arrive at a stage where collisions begin to have a slight influence. But there is another point to take into consideration which has already been mentioned in connection with the recombination processes. In carrying out our estimates we have assumed that the temperature of the electrons is identical with the radiation temperature T. This will probably not always be the case, as is evident from the following consideration: the average velocity of the photoelectrons after leaving the atoms will have a temperature distribution which is identical with the radiation temperature (color temperature), as has been pointed out by Eddington. The distribution will be preserved if the electrons, before recombination, have no oppor-

tunity to give off energy in collisions. But this will strongly depend on the atomic composition of the atmosphere. Independently of the pressure the electrons will give off energy in collisions before recombining, if the atmosphere contains atoms with low-lying energy levels, because, generally, the excitation cross-sections are much larger than the recombination cross-sections. The former range from 10^{-16} to 10^{-18} cm², the latter[20] from 10^{-18} to 10^{-21} cm². The appearance of the well-known forbidden lines in the nebular spectra, the excitation of which is, according to Bowen, created by electron impact, shows that such loss of energy by the photoelectrons takes place even in stellar atmospheres of high ionization and of extremely low pressure.[21] Such a drop of the electron temperature will, even if slight, further diminish our values of α_{14} in equation (10).

Besides the collisions from the ground state, we have still to consider those collisions which can produce transitions of the atoms between the different higher levels. For these small differences in energy we may assume a value of σ^2 of the order of 10^{-16} cm². Since the factor $e^{-h\nu/kT}$ does not change appreciably for the four different levels, we may neglect it. Then we have

$$\alpha_{ik} \approx n_e \times 10^{-8} \quad \text{for} \quad T = 10^{-4} \quad \text{and} \quad T = 2.5 \times 10^{-4}. \quad (13)$$

The average values of A_{ik} (see Tables 2 and 3) for the transitions involved are of the order of 10^7, for $W = 1$. Hence, we find for the condition that the collisions will have an influence:

$$n_e \geqq 10^{15} \text{ cm}^{-3}. \qquad (W = 1) \quad (14)$$

The lower limit of n_e in (14), as compared with (12), originates chiefly from the higher assumed value of σ^2, whereby we come much nearer to the critical value of n_e (10^{12} to 10^{14}). Going to higher dilutions, the influence of collisions does not increase if we have $W\rho$ = constant. But there is a difference between the low and the high excitations if we consider the case in which ρ decreases more slowly than the dilution increases and in which we have at the same

[20] F. L. Mohler, *Rev. Mod. Phys.*, **1**, 216, 1929.

[21] Naturally, the process described is independent of pressure; but, as has already been explained, it depends strongly upon the atomic composition.

time a drop of the electron temperature. With decreasing T the factor $e^{-\eta_0/kT}$ in formula (10*a*) decreases only slightly for small values of η_0, that is, for excitation energies of 1–5 volts. But for the 20 volts of excitation from the ground state the factor $e^{-\eta_0/kT}$ decreases very much. This effect again suggests that we must at first expect an influence of collisions between closely spaced levels. Since our estimates show that we are near the critical values of n_e when an influence of collisions for the higher *He* I levels begins to appear, we may further examine how the collisions change the populations created by absorption. As was pointed out by one of the present writers,[22] the collisions in an atmosphere of diluted radiation create a very similar distribution of the atoms over the various energy levels of different lifetimes, as does the diluted radiation. In both cases there results an accumulation in metastable states. In general, the shorter the lifetime of a level, the greater must be the electron density (as in the case of absorption excitation, the greater must be the radiation density) in order to produce a similar approximation toward a Boltzmann distribution. Therefore, the first influence of collisions will express itself in a tendency to give an approach to a Boltzmann distribution (corresponding to the electron temperature T_e) for the two metastable levels 2^3S and 2^1S (but see below). The second stage will show such an approach for the 2^3P-level ($\tau = 10^{-7}$ sec) which may be reached at electron densities of $n_e = 10^{15}$, provided that $\alpha_{ik} \gtrsim A_{ik}$ for this transition.[23] To establish a Boltzmann distribution for the very short-lived 1^1P-level ($\tau = 10^{-9}$ sec), we must have at least an electron density of $n_e = 10^{17}$ cm^{-3}. To obtain more accurate information we need more knowledge concerning the differences in the cross-sections σ^2_{ik} and σ^2_{ki} of excitation and de-excitation for the different transitions $2^3\text{S} \leftrightarrow 2^1S$, 2^3P, 2^1P; $2^3\text{S} \leftrightarrow 2^1$P, 2^3P; $2^3\text{P} \leftrightarrow 2^1$P. We can expect that within a system (singlets or triplets) σ^2_{ik} is somewhat larger than for intercombination transitions. This will somewhat diminish the approach toward temperature distribution between the two systems. Since collisions from transitions $2^1\text{S} \rightarrow 2^1$P occur more frequently

[22] K. Wurm, *Zs. f. Ap.*, **14**, 321, 1937.

[23] If $\alpha_{ik} < A_{ik}$, then, naturally, the collisions cannot appreciably alter the populations created by absorption.

than transitions from 2^3S to 2^1S, there would be an additional depopulation of the singlet system as compared with the 2^1P state, and hence a stronger preference of the triplet levels. This condition we may expect when the influence of collisions first appears.

In concluding this section it may be pointed out that for levels which lie near the ground state, as we find them in *Fe* II, *Ti* II, *Cr* II, and other atoms, the collisions will generally act in quite the same manner as has been shown for the higher *He* I states. This problem has been already treated extensively by one of us in an earlier paper,[22] in connection with the problem of *Fe* II emission lines in stars with extended atmospheres. It was shown there that even relatively low electron densities are able to create an approximate Boltzmann distribution if the levels are metastable.

III. COMPARISON OF THE THEORY WITH OBSERVATIONS

Table 4 refers the populations of the various levels to that of state 2^1S as standard. In comparing the observations of Section I with the tabular values, the following considerations are important:

1. The theory of the transfer of radiation has been worked out so far for only three states.[24] We shall therefore follow the usual practice and assume that the intensity at any point within the line is given by $I = I_0 e^{-\sigma H}$, where σ is the absorption coefficient and H is the thickness of the shell.

2. The absorption coefficient in the shells is determined largely by turbulence. Stark effect is absent, and the characteristic bell-shaped contours of the H cores show conclusively that turbulence is effective.

3. The total absorption[25] within a line is equal to

$$A = 2\int_0^\infty (1 - e^{-ae^{-x^2/b^2}})dx = \sqrt{\pi}ab\left\{1 - \frac{a}{2!\sqrt{2}} + \frac{a^2}{3!\sqrt{3}} \cdots\right\},$$

$$a = 10^{-13}Nf\frac{H}{b}, \qquad b = \lambda_0\frac{v_0}{c},$$

[24] Chandrasekhar, *Zs. f. Ap.*, **9**, 266, 1935; Ambarzumian, *Bull. Obs. Poulkovo*, **13**, No. 3, 1933; *Poulkovo Circ.*, No. 6, 10, 1933; *M.N.*, **93**, 50, 1931.

[25] *Ap. J.*, **79**, 430, 1934.

where b is the Doppler shift corresponding to the most probable turbulent velocity v_0. Thus, A is proportional to f if the former is small. We shall assume that the values of f are independent of temperature and of the degree of dilution.

4. For faint lines the total absorptions of the lines should then be directly proportional to the values of n in Table 4. For strong lines the total absorptions will vary little with n.

5. From Table 4 we predict that in all shells the triplet series ($2^3S - n^3P$) must experience the greatest enhancement. Since the only suitable line, λ 3889, is blended with $H\zeta$, we are unable to test this prediction.

6. For all shells the lines ($2^3P - n^3D$), ($2^3P - n^3S$), ($2^1P - n^1D$), and ($2^1P - n^1S$) are greatly reduced in strength.

7. This reduction is greatest for the singlet lines ($2^1P - n^1D$) and ($2^1P - n^1S$), and the degree of this reduction does not depend appreciably upon the temperature.

8. The triplet lines are reduced in intensity about half as much as the singlets in the cool shells. Thus, even in the cool shells the triplet lines λλ 4026, 4472, etc., will appear relatively stronger than the singlet lines. This is in agreement with conclusion (2) of Section I.

9. In the hotter stars the triplet lines are reduced by only a factor of 18, when W changes from 1 to 0.01, while the singlets are reduced by a factor of 76. Thus, we should expect that λλ 4026, 4472, etc., will gain in intensity relative to λ 3965, as well as relative to λλ 4009, 4144, 4388, etc. This is essentially in agreement with conclusions (3) and (4) of Section I.

10. There remains the question why in P Cygni the singlet lines ($2^1P - n^1D$) are not as faint, relatively to the triplet lines ($2^3P - n^3D$), as in shells of lower excitation (conclusion 4 of Sec. I). The answer is almost certainly found in the effect of turbulence which makes A insensitive to n when a is large. That this interpretation is correct follows from the intensities of the emission lines in P Cygni, which are very weak in series ($2^1P - n^1D$) but are strong in λ 3965 as well as in series ($2^3P - n^3D$).

PLATE V

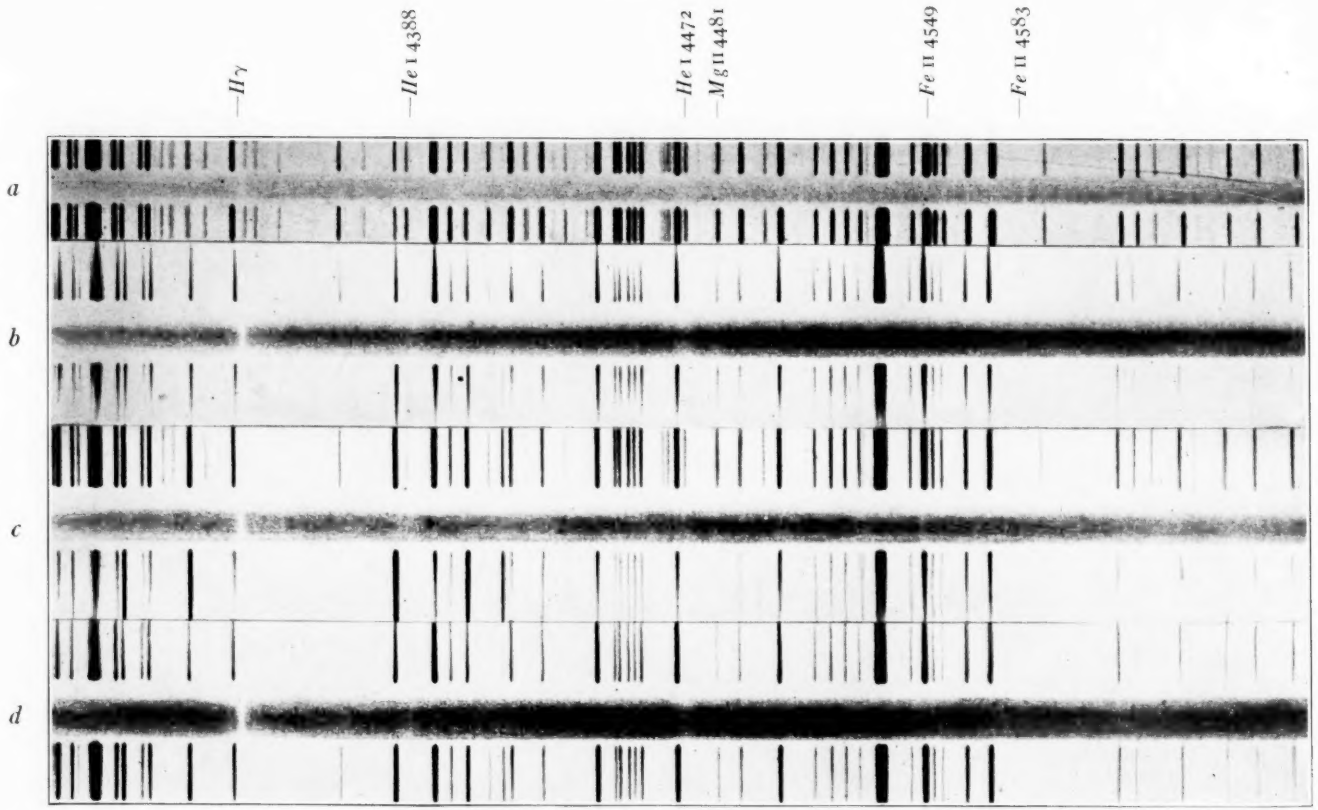

THE SPECTRUM OF ε CAPRICORNI

a) 1915, Sept. 17; 16^h02^m G.M.T.
b) 1931, May 26; 9^h13^m G.C.T.
c) 1931, June 1; 9^h07^m G.C.T.
d) 1933, June 9; 8^h50^m G.C.T.

It is of some interest to evaluate the quantity

$$\frac{\text{Int. 3965 (shell)}}{\text{Int. 3965 (normal)}} \times \frac{\text{Int. 4009 (shell)}}{\text{Int. 4009 (normal)}}.$$

Unfortunately, we cannot make an accurate evaluation because in normal B stars λ 4009 is greatly broadened by Stark effect, while λ 3965 is not sensitive to Stark broadening. Nevertheless, from the combined results of our observations we estimate that this ratio is between 10 and 100. This fixes the dilution factor at approximately $W = 0.01$. But

$$W = \frac{1}{4}\frac{R^2}{r^2} + \frac{1}{16}\frac{R^4}{r^4} + \ldots,$$

where R is the radius of the star and r is the effective radius of the shell. Accordingly,

$$r \approx 5R.$$

This gives a good estimate of the order of size of the average shell.

IV. PHYSICAL CONDITIONS IN OUTER SHELLS

The spectral lines which originate in the outermost shells of ζ Tauri, φ Persei, 48 Librae, ε Capricorni, etc., are relatively sharp. They suggest the presence of a moderate amount of turbulence (17 Leporis) but give no indication of rotation. This suggests that the shell does not rotate as a solid body with the star. Otherwise the rotational component in the line of sight would be constant and all lines would show the same broadening. We conclude that the angular velocity of rotation decreases with r.

A close inspection of Plate V shows that in ζ Tauri the *Si* II lines are appreciably broadened, and that even the *Fe* II lines are not as sharp as *He* I 3965 or *Ni* II 4067. We conclude that the atoms in the shell are stratified. The normal *He* I lines and the *H* wings are produced in the lowest levels, which we have referred to as the "reversing layer." *Si* II occurs higher in the shell, *Fe* II lies still higher, and the cores of *H*, *Ni* II, and *He* I 3965 occupy the highest levels.

A similar picture of stratification can be outlined for 48 Librae and ϵ Capricorni. The result is in harmony with the stratification formerly found in P Cygni.

The decrease in angular velocity of rotation with r is puzzling. It may be due, as Chandrasekhar suggests,[26] to the conservation of angular momentum. If rv = constant, we should find that for $r = 5R$, $v_{\text{shell}} = 0.2v_{\text{rot}}$. If the star and its shell rotated as a solid body, we should have $v_{\text{shell}} = 5v_{\text{rot}}$. A decrease in the rotational broadening by a factor of 25 would suffice to make the lines appear entirely narrow. Incidentally, this line of reasoning serves to confirm the general order of magnitude found for W.

The stage of ionization and excitation in the shells considered here (with the exception of β Lyrae) is considerably lower than in the corresponding reversing layers. Thus, the shells show lines of *Fe* II requiring an ionization energy of 7.8 volts for the ionization of *Fe* I and an additional energy of excitation amounting to 3 volts for the lower levels and 6 volts for the upper levels. For *Ni* II an ionization energy of 7.6 volts plus excitation energies of 4 and 7 volts are required. In the reversing layer we have predominantly *He* I, requiring excitation energies of over 20 volts. In terms of ordinary spectral classes we should attribute class A to the shells of ζ Tauri, φ Persei, 48 Librae, and ϵ Capricorni, and one of the intermediate subdivisions of class B to the reversing layers.

A similar result has already been obtained in the case of P Cygni,[13] where the stage of ionization decreases with the height in the reversing layer. This tendency for the ionization to decrease outward implies[27] that the pressure decreases outward less rapidly than $1/r^2$.

The spectra of the shells present one conspicuous anomaly: the line *Mg* II 4481 is either absent or very weak. Incidentally, this anomaly has already been noticed in the emission spectra of Be stars.[28] In the light of the preceding discussion the unusual weakness of λ 4481 is easily explained. This line originates between the lowest ^{2}D term and the lowest ^{2}F term of the *Mg* II atom. The ^{2}D

[26] Private communication. We are also indebted to Dr. L. H. Thomas for a discussion of this question.

[27] *Ap. J.*, **81**, 87, 1935.

[28] Struve and Swings, *ibid.*, **75**, 165, 1932.

term is not metastable, but connects with the lowest ^{2}P term, which in turn connects with the ground-level ^{2}S. By line absorption two processes are required to lift the atom from the ground-level into level ^{2}D. The population will, therefore, be proportional to W^2. This will be modified by recombinations, but even in the most favorable case the level ^{2}D will be strongly depopulated by any appreciable dilution of the radiation.

The Balmer lines are strong in all shells, their intensities bearing about the normal ratio to the intensities of the *He* I triplets. This may be due to the metastability of the 2S-level of *H*. The shell should, strictly speaking, show only the series (2S − nP) of *H*, because the 2P-level is not metastable. In principle, this should lead to an abnormal Balmer decrement, since the *f*-values of the (2S − nP) series differ from those of the combined Balmer lines.[29] But for practical purposes only the ratio $H\alpha/H\beta$ is suitable. In the shell $f\alpha/f\beta = 0.425/0.102$, while in a normal star $f\alpha/f\beta = 0.637/0.119$. No observations of $H\alpha$ are available.

Another fairly conspicuous feature is the weakness of *Si* II in most shells. This is also due to the fact that the lower level of the lines λ 4128 and λ 4131 has a strong transition toward the ground-level. We expect a similar behavior of *Si* II λ 4128 and λ 4131 and *Mg* II 4481, since these lines have not only similar excitation potentials but also nearly the same first and second ionization potentials:

	First Ionization Potential	Second Ionization Potential	Excitation Potential
Mg	7.61	14.97	8.83 *Mg* II λ 4481
Si	8.12	16.27	9.79 *Si* II λ 4128, λ 4131

On the other hand, the great relative strengths of the *Fe* II lines are caused by the metastability of all lower levels of the observable lines of ionized iron. In the case of lines like *Fe* II and *Ti* II, which arise from low levels—up to about 5 volts above the ground state—

[29] See A. Unsöld, *Physik d. Sternatmosphären*, pp. 187, 188, Berlin, 1938.

we have to take into consideration the additional population from collisions, which is then very effective (see Sec. II).

The astronomical evidence strongly suggests that the lower level of the *Ni* II line λ 4067 must also be metastable. This line is due to the transition $a^2G - z^2D^\circ$. The lower level, a^2G, is even, as is the ground level, ^2D. Since it lies lower than the lowest odd level of *Ni* II, it is metastable.

In φ Persei and in most other stars surrounded by shells, including ordinary Be stars, the broadened absorption lines of *He* I are weaker than can be accounted for by rotation alone. Although this could in part be caused by incipient emission in the lines, it does not seem probable that the shells of φ Persei, ζ Tauri, etc., give rise to strong emission in helium. In these stars even the *H* emissions are weak. It is difficult to avoid the conclusion that the shell produces a screen of continuous emission which weakens the underlying absorption lines.

V. THE *He* I ANOMALY IN NORMAL B STARS

The *He* I anomaly in the shells of peculiar B stars strongly resembles the *He* I anomaly in ordinary B stars—especially in the supergiants.[30] In stars of low luminosity the intensities are complicated by the normal Stark effect and by collisional damping.[31] Nevertheless, the decrease of the singlets ($2^1P - n^1D$) relative to the triplets ($2^3P - n^3D$) in such stars as 10 Lacertae and τ Scorpii suggests that the dilution of the radiation is already appreciable in the reversing layers of these objects.

The explanation of the *He* I anomaly in normal B stars and in supergiants proposed some time ago[30] agrees in all essential features with that presented in this paper. It is clear from Table 4 that even for relatively inappreciable dilutions the 2^1P level is greatly depopulated. Under favorable circumstances the equivalent breadths of absorption lines should easily reveal differences corresponding to a factor of 2 in the numbers of atoms. It is, therefore, entirely reasonable that departures from thermodynamic equilibrium will be observable in the supergiants. This is especially true because Stark

[30] Struve, *Ap. J.*, **82**, 256, 1935, and earlier papers.

[31] *Observatory*, **61**, 53, 1938.

effect and collisional damping are negligible in these stars. But it would be incorrect to conclude that the shells of peculiar B stars and the atmospheres of recognized supergiants of class B are identical. Not only are the departures from a Boltzmann distribution in *He* I less pronounced, but there are other important spectroscopic differences: the lines of *Mg* II 4481 and of *Si* II 4128 and 4131 are very strong in the supergiants. Evidently, the dilution is not sufficient to weaken appreciably these lines in comparison with the same lines in dwarfs. But the effect of turbulence in the supergiants makes a comparison with the dwarfs somewhat unreliable.

This difficulty is also present in the case of *He* I. It will be necessary to investigate the curves of growth for the individual lines in giants and in dwarfs before we shall be able to determine the numerical value of W.

YERKES OBSERVATORY
May 1938

NOTE

A NEW FOURTH-MAGNITUDE ECLIPSING BINARY

In an earlier investigation by one of the present authors[1] attention was called to the variation in intensity of certain lines in the spectrum of the spectroscopic binary μ Sagittarii ($P = 180^d.45$; $K = 57$ km/sec; $e = 0.40$; $\omega = 79°$; $T = 2423632.21$;[2] spectrum cB8). Examination of an early series of Yerkes spectrograms showed that near the time of periastron passage the line *He* 4471 became considerably strengthened in intensity relative to the neighboring Mg^+ 4481. At the time, it was considered that both lines contributed to the observed change in the relative intensity; Mg^+4481 was thought to grow weaker as *He* 4471 increased in intensity. A later examination of several series of spectrograms of better quality has shown, however, that the principal variation is due to *He* 4471 and that λ 4481 changes little, if at all.

There is a lag in the time of maximum of λ 4471 of about five to ten days after periastron passage; attention was called to this in 1932, but the coincidence of the phase of the spectral variations with that of superior conjunction of the primary was not noticed. The spectral changes are somewhat similar in nature to those observed in the recently discussed systems of ϵ Aurigae and ζ Aurigae; it therefore seemed likely that the observed variation in the spectral features was due to the eclipse of the primary star by a secondary having an extended gaseous envelope.

The light of the system was observed by Elvey at the McDonald Observatory during May and June, 1938; the photoelectric photometer was used with the twelve-inch refractor. The star 15 Sagittarii of spectral type Bo was used as comparison star.

An eclipse of about 0.14 mag. was observed with a duration of around twenty days; the light-curve is shown in Figure 1. The phase

[1] *Ap. J.*, **75**, 407, 1932.

[2] Kohl, *A.N.*, **246**, 426, 1932.

and duration of the observed diminution in light agree with those of the spectral variations, and the epoch of mid-eclipse corresponds

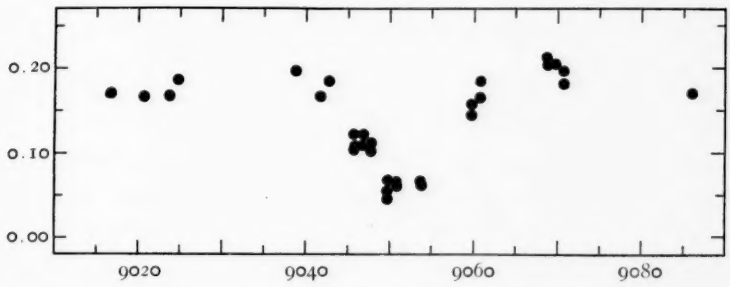

FIG. 1.—Light-curve of μ Sagittarii in 1938. Abscissas are Julian Days *minus* 2420000; ordinates are photoelectric magnitudes; the zero point of the magnitude scale is arbitrary.

to the time of superior conjunction of the brighter star. Preliminary light elements are

$$\text{Min} = \text{JD } 2429051 + 180.45 \cdot \text{E} .$$

Detailed discussion of the spectral variations and the physical characteristics of the eclipsing system will be made at a later time.

W. W. MORGAN
C. T. ELVEY

YERKES OBSERVATORY AND MCDONALD OBSERVATORY
July 6, 1938

REVIEWS

The Observational Approach to Cosmology. By EDWIN HUBBLE. Oxford University Press, 1937. Pp. vi+68. $4.00.

This short book contains the Rhodes Memorial Lectures delivered by the author at Oxford in 1936. The book gives a compact summary of the work that has been done at the Mount Wilson Observatory in the field of extra-galactic nebulae.

Following a brief historical introduction, chapter i contains an outline of the methods used for establishing the scale of distances of the nebulae and a description of the distribution of the nebulae over the observable region.

In chapter ii Hubble describes the observed relation between distance and velocity of the nebulae, together with the corrections that must be applied to the distances, depending on whether the red shifts of the nebulae are interpreted as velocity shifts or not.

The final chapter deals with the counts of faint nebulae made at the Mount Wilson and Lick observatories. After corrections due to the red shifts are applied, the resulting distributions of the nebulae are discussed and the models of the universe that best fit the observations are described.

Considered as a whole, Hubble presents in this book a condensation of the material contained in his *Realm of the Nebulae* (Yale University Press), published in 1936. The book is written in a clear style and with a minimum of mathematical formulae and technical expressions.

C. K. S.

The Physical Treatises of Pascal. Translated by I. H. B. and A. G. H. SPIERS with an Introduction by FREDERICK BARRY. New York: Columbia University Press, 1937. Pp. viii+181. $3.25.

This is Volume **28** of *Records of Civilization: Sources and Studies*, which are edited under the auspices of the department of history of Columbia University. It contains a translation of the volume *Traitez de l'équilibre des liqueurs et de la pesanteur de la masse de l'air*, which was published by Perier in 1663, a year after Pascal's death. The original publication is quite rare, and the appearance of this classic in an English translation will be of value to all students of the history of science.

S.